**Department of Precision and Microsystems Engineering**

# All-Wheel Torque Vectoring for Driver-in-the-Loop Drifting

Jeswin Koshy Cherian

Report no : 2023.061
Coach : Ir. A. Krishnakumar
Professor : Dr. S. H. Hossein Nia Kani
Specialisation : Mechatronic System Design
Type of report : Master Thesis
Date : 23 August 2023

TU Delft Delft University of Technology

Challenge the future

# All-Wheel Torque Vectoring for Driver-in-the-Loop Drifting

Master Thesis Report

Jeswin Koshy Cherian

TU Delft

# All-Wheel Torque Vectoring for Driver-in-the-Loop Drifting

by

Jeswin Koshy Cherian

to obtain the degree of Master of Science
at the Delft University of Technology,
to be defended publicly on Wednesday August 23, 2023 at 2:30 PM.


| | | |
|---|---|---|
| Student number: | 5459540 | |
| Project duration: | February 28, 2023 – August 23, 2023 | |
| Thesis committee: | Dr. S. H. Hossein Nia Kani, | TU Delft, supervisor |
| | Dr. M. Kok, | TU Delft |
| | Dr. S. P. Mulders, | TU Delft |
| | Ir. A. Krishnakumar, | Rimac Technology d.o.o. |


TU Delft

# Acknowledgements

I would like to express my deepest gratitude and appreciation to all those who have supported me throughout the journey of completing this thesis. Their encouragement, guidance, and assistance have been invaluable in shaping this work.

First and foremost, I extend my heartfelt thanks to my thesis supervisor at Rimac Technology, Ajinkya Krishnakumar whose expertise, patience, and unwavering support were instrumental in the successful completion of this research. I am truly grateful for his guidance and mentorship, which significantly contributed to the quality of this thesis.

I would also like to acknowledge the support and encouragement from my thesis supervisor at TU Delft, Dr. Hassan Hossein Nia Kani whose insightful feedback, guidance and constructive criticism have been invaluable. I would also like to thank Dr. Manon Kok and Dr. Sebastiaan Mulders for taking time out of their schedules to be part of my thesis committee.

To my friends and colleagues at my university, your companionship and camaraderie have made this academic pursuit an enjoyable and memorable experience. To my friends and teammates at Rimac Technology, I am immensely thankful for your constant support and encouragement. The camaraderie, team spirit, and shared passion for innovation have made this thesis an enriching and rewarding endeavor. Your valuable insights and diverse perspectives have been an inspiration and have contributed significantly to the depth of my research.

I would like to express my deepest gratitude to my parents and sister. Their unwavering love, support, and belief in my abilities have been the foundation of my academic journey. Their sacrifices, encouragement, and understanding have given me the strength and determination to pursue my dreams. Above all, I would like to thank God Almighty for showering His blessings upon me throughout my life.

*Thank you,*

*Jeswin Koshy Cherian*
*Delft, August 2023*

# Abstract

Drifting, a specialized form of sideslip control, involves intentionally inducing and maintaining a state of oversteer for lateral sliding of the vehicle. While previous research has primarily focused on autonomous drift control, the integration of the driver in the control loop remains largely unexplored. This thesis aims to explore how a vehicle sideslip control system can be designed and evaluated for driver-involved drifting scenarios. To this end, a seven degree-of-freedom vehicle model and a tire model calibrated on data from a test vehicle were used to develop a model-based optimization scheme, leveraging the capabilities of all-wheel torque vectoring to achieve the desired drifting behavior. Phase portrait and real data analyses during drifting maneuvers were conducted to understand drift dynamics and develop the reference generator, which calculates targets for the controller. The reference generator and controller were validated through simulations using IPG CarMaker, drifting along a constant radius circle and a section of a track. The results demonstrate that the developed control system enables stable and controllable drift behavior with a driver-in-the-loop and allows drivers to fully exploit their vehicle's capabilities.

# Contents

# 1 Introduction

As the market for performance cars continues to expand, there is a growing demand for advanced control systems that enhance safety, controllability, and the ability for drivers to fully exploit their vehicles' capabilities. Sideslip control has emerged as a crucial element in ensuring vehicle stability and handling, finding applications in electronic stability control (ESC) and drift control systems. Extensive research has been conducted on ESC systems, incorporating strategies such as Direct Yaw Moment Control (DYC), which ensure stable and controllable vehicle behavior under diverse conditions.

However, beyond the scope of safety and control, drivers also seek the ability to push their vehicles to their limits and experience the full power and performance they offer. Drifting, a specialized form of sideslip control, involves intentionally inducing and maintaining a state of oversteer, using the loss of traction in the rear wheels to enable lateral sliding of the vehicle. This is a difficult skill necessitating the driver's careful coordination of steering and throttle inputs to maintain the vehicle at an unstable equilibrium.

There is a need for a dedicated drift control system to help the driver in drifting scenarios. Although considerable research has been dedicated to autonomous drift control, the development of a driver-involved drift control system has been largely overlooked. Such a system would facilitate stable and controllable drift behavior, enabling drivers to fully exploit their vehicles' capabilities. This brings up the following research question:

*"How can a vehicle sideslip control system be designed and evaluated for driver-involved drifting scenarios?"*

Such a system should enable the integration of the driver into the control loop, considering their actions and intentions to generate target values for the controller. The controller can then take advantage of the capabilities of all-wheel torque vectoring to achieve the desired vehicle behavior during drifting maneuvers.

## 1.1. Research Objective

This thesis aims to develop an All-Wheel Torque Vectoring system for Driver-in-the-Loop Drifting. The system will rely on the steering and throttle inputs from the driver to generate references for the controller. The torque vectoring strategy will then be used to initiate drift and stabilize the vehicle at the desired equilibrium. The approach of using independent torque allocation to all four wheels enables generating additional yaw moment to stabilize the vehicle. It can also allow indirect control over the lateral force generated on both the front and rear axles by taking advantage of the coupling between the longitudinal and lateral tire forces when the tires are saturated. Using these capabilities, the controller will seek to drift at a required speed and path radius while maintaining a desired value of sideslip.

### 1.1.1. Implementation Plan

The proposed All-Wheel Torque Vectoring system for Driver-in-the-Loop Drifting would be comprised of a reference generator and a controller. The reference generator would take the driver's inputs and translate them into the desired vehicle state. The controller would then employ an optimization scheme to allocate torque to each of the four wheels to achieve the target state.

By using the errors in yaw rate, velocity and sideslip, the controller would calculate targets for longitudinal force, lateral force, and total yaw moment on the vehicle. These targets would then be met through an optimization of torque allocation to individual wheels, making use of traditional torque vectoring and also taking advantage of the coupling between longitudinal and lateral tire forces to indirectly control the lateral forces generated on the front and rear axles. This system would enable the vehicle to drift at a specified speed and radius while maintaining a desired level of sideslip, allowing for precise and accurate control over the vehicle while drifting.

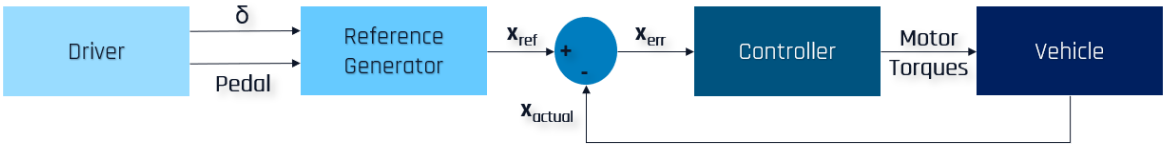


**Figure 1.1:** Block diagram of control system. "**x**" is a state vector consisting of yaw rate, sideslip and longitudinal velocity

### 1.1.2. Evaluation Plan

The evaluation plan for the proposed control system encompasses simulation-based assessments. The system's performance will be evaluated in terms of its capability to maintain predetermined target values for sideslip, velocity, and yaw rate during drift maneuvers conducted at equilibrium steering. Additionally, the system's ability to track a specified trajectory using driver inputs while maintaining a desired level of sideslip will also be examined.

## 1.2. Thesis Outline

This thesis report is structured as follows. Chapter 2 explains the basics of planar vehicle dynamics, introducing the popular single-track model of the vehicle and analyzing its dynamics. It also dives into the state-of-the-art on drift control, which has been done extensively in the context of autonomous vehicles. A review of literature on driver interactions with vehicle control systems is also presented, summarizing the human factor considerations when designing these control systems.

Chapter 3 describes the equations used to model the vehicle and tires for the control system and also outlines the process of obtaining tire data from vehicle data while drifting. Chapter 4 dives into phase plane analysis of the vehicle, studying the effects of various parameters on the drift equilibrium. These conclusions are then used to generate reference states for the controller using steering and pedal inputs from the driver.

Chapter 5 explains the design process of the controller, including the optimization problem formulation and describes the simulations used to verify performance. It also provides a theoretical basis for the controller and demonstrates robustness of the controller to noise and parameter uncertainty. Chapter 6 describes the verification and validation process using simulations performed on IPG CarMaker, a high fidelity commercial vehicle dynamics simulation package. Finally, Chapter 7 summarizes the report and provides recommendations for future work.

# 2

# Background

## 2.1. The Dynamics of a Single-Track Model of the Vehicle

The single-track model for vehicle lateral dynamics is shown in the image (2.1), with a mass point representing the center of gravity of the vehicle, and two point masses representing the front and rear wheels. The distance of the center of gravity from the front and rear axles is shown as $l_f$ and $l_r$, respectively. The tire forces generated by the front and rear wheels are denoted by $F_f$ and $F_r$, respectively. The steering angle is denoted by $\delta$. The total velocity vector of the vehicle center of gravity $V$ is shown along with the sideslip angle $\beta$, which represents the angle between the velocity vector and the longitudinal axis of the vehicle. The yaw angle $\Psi$, which represents the angle between the heading of the vehicle and the x-axis, is also shown in the image.

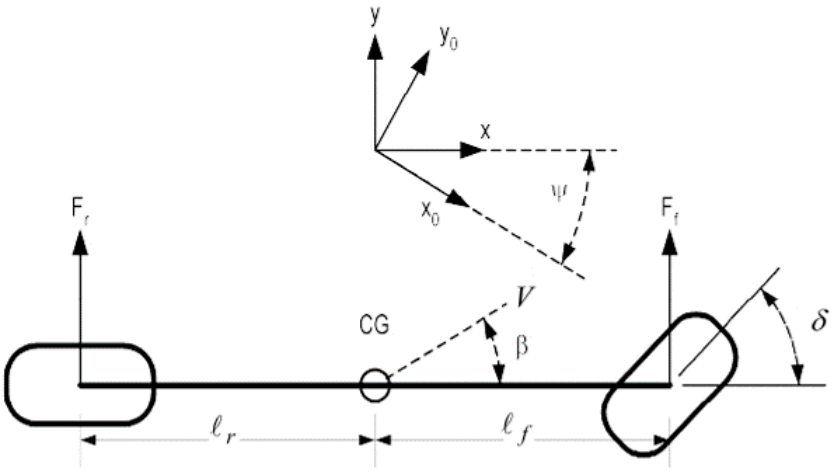


**Figure 2.1:** Single-track model for vehicle lateral dynamics [17]

The dynamics of a single-track vehicle model can be complex, involving the interplay of numerous variables and factors. To better understand its behavior, we can use phase portrait diagrams to visualize the system's trajectories and equilibrium points. By plotting the sideslip angle and yaw rate of the vehicle on orthogonal axes, we can create a two-dimensional phase portrait that provides a comprehensive view of the vehicle's dynamic behavior. Using phase portrait diagrams allows for a visual representation of the vehicle model's state variables and their interplay over time, offering insights into the system's trajectories and equilibrium points. By analyzing these portraits, it is possible to discern stability patterns, identify critical points, and assess the impact of various control inputs. In this section, we will explore the dynamics of a single-track vehicle model using phase portrait diagrams, examining the stability and behavior of the system under different conditions. This will also provide context for the

use of electronic control systems as stability systems, as well as control systems for drift, to maintain the vehicle's safety and performance.

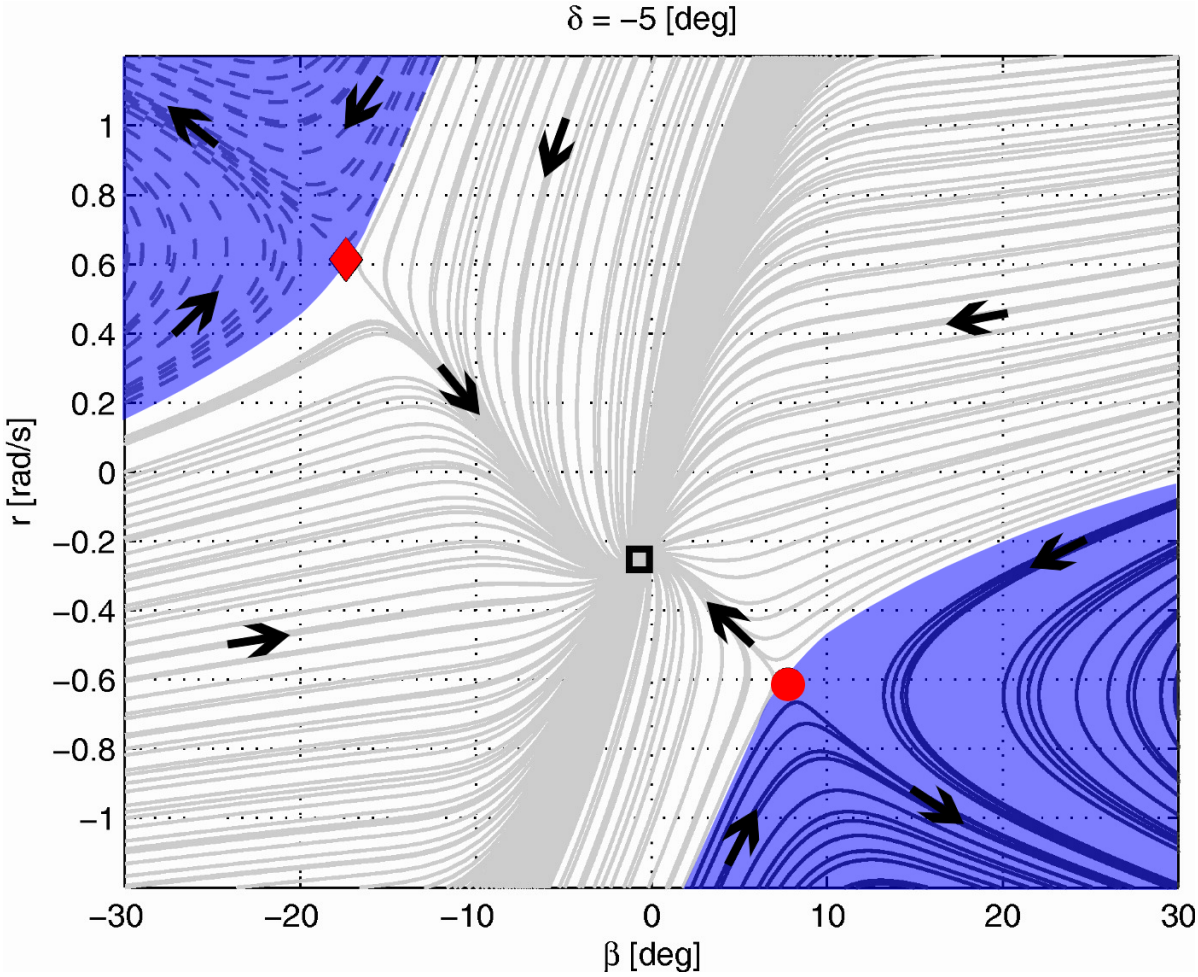


**Figure 2.2:** Phase portrait of 2 degree-of-freedom vehicle dynamic model showing the stable and unstable equilibria (adapted from [24])

Figure 2.2 displays a phase portrait depicting the dynamics of a single-track vehicle, where the x-axis represents the sideslip angle in degrees and the y-axis represents the yaw rate in radians per second. The gray rectangle marks the stable equilibrium point, while unstable equilibria are indicated by a red diamond and circle. Electronic Stability Control (ESC) systems play a pivotal role in attracting the vehicle towards the stable equilibrium point, ensuring it stays within safe and controllable limits. The blue regions depicted in the diagram signify areas of instability, leading to vehicle spin-outs. The implementation of drift control systems enables the vehicle to be deliberately maintained within this unstable regime, facilitating drivers in experiencing the limits of vehicle performance.

## 2.2. State-of-the-art Drift Control

Research on drift control has been predominantly for autonomous vehicles, with the vehicle stabilized to a pre-determined drifting equilibrium [24, 10, 8, 9, 21, 1, 2, 14, 19, 20]. Electronic control for drift assist has also been done with driver inputs used to choose setpoints for yaw rate and sideslip for the controller [23, 3].

### 2.2.1. Autonomous Drift Control

The control architecture for a typical drift controller in autonomous vehicles is illustrated in figure 2.3. The system consists of a setpoint generator that computes the desired target states, which are then attained through a controller. This controller typically comprises of a high-level controller, responsible for computing the target forces and moments at the vehicle level, and a low-level controller, which allocates the commands between the various actuators to achieve the desired motion.

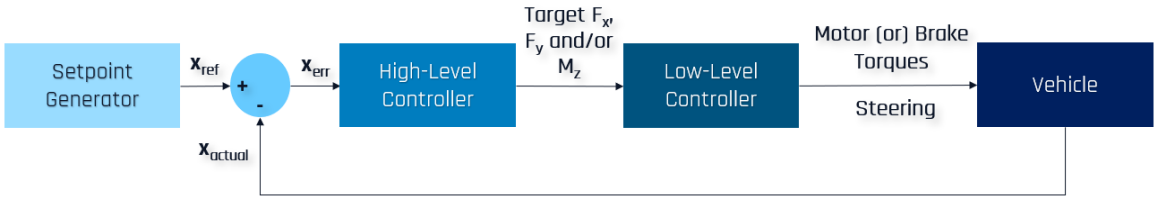


**Figure 2.3:** Block diagram of a typical drift controller. "**x**" is a state vector consisting of yaw rate, sideslip and longitudinal velocity

For autonomous drifting, longitudinal force (through motors or brakes) is used to control yaw rate along with steering [10, 8, 9, 7, 21, 1, 2, 19, 20, 23, 3]. Different control strategies have been explored in literature, with the conclusion that coordinated control over lateral and longitudinal dynamics works better than independent control, taking advantage of the coupling between lateral and longitudinal tire forces [24] when saturated.

The utilization of three actuators, namely steering, rear motors, and front brakes, offers the controller access to a broader range of drifting equilibria compared to using only two actuators. This is because the additional actuator provides independent control over the three state derivatives: yaw rate, sideslip, and vehicle speed. A study conducted by Goel et al. [7] demonstrated this advantage by executing experiments where a circular path was traversed at a constant velocity while sinusoidally varying the sideslip, and at a constant sideslip while sinusoidally varying the velocity. The results highlighted the ability of the controller to explore and maintain different drifting equilibria by effectively manipulating the three state derivatives using the three actuators (figure 2.4).

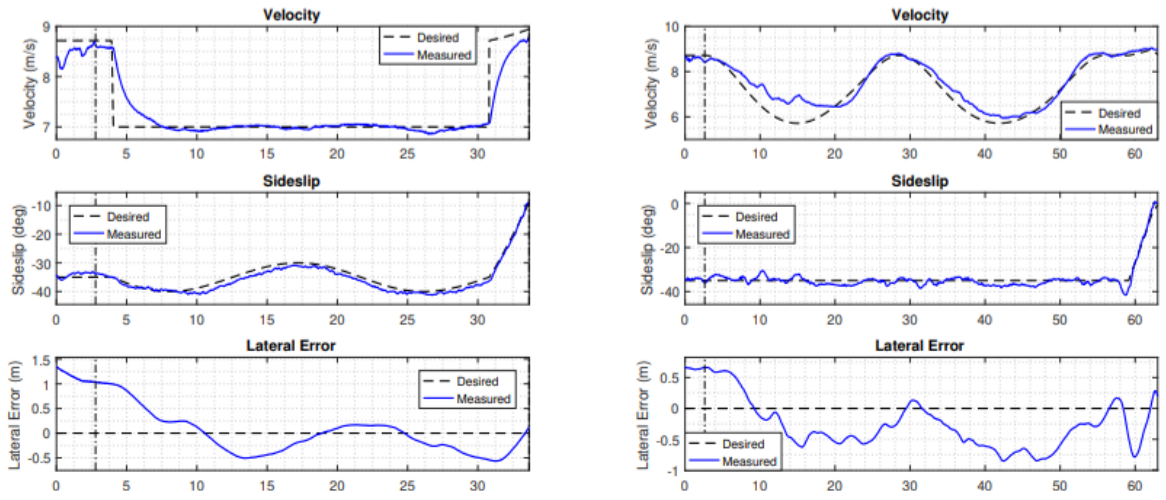


**Figure 2.4:** Experimental results of constant velocity test (left) and constant sideslip test (right). Vehicle velocity and sideslip were independently controlled, and yaw rate was used to maintain the desired path [7]

### 2.2.2. Driver-in-the-Loop Drift Control

In a study conducted by Vignati et al. [22], indirect control of the vehicle sideslip was achieved during driver-in-the-loop drifting. The required yaw moment $M_z$, which was calculated using equation (2.1), was generated through the use of torque vectoring. The resulting yaw moment helped to maintain a constant lateral velocity $v_y$, which prevented the vehicle from both spinning out and losing sideslip once the drift was initiated by the driver. It is worth noting that this approach did not rely on explicitly controlling the vehicle sideslip to a desired value but instead focused on making the vehicle easier to control for the driver by keeping it at a steady state.

$$M_z = k_Y \left( \frac{a_y}{v_x} - \dot{\psi} \right) \tag{2.1}$$

## 2.3. Interaction of Driver with Control System

This section presents a review examining the incorporation of the driver within vehicle control systems. The focus lies on understanding the various approaches and considerations taken to account for the driver's role and influence in the control process. The review commences by examining the integration of the driver within sideslip control systems, focusing on the approaches and considerations employed to incorporate the driver's inputs and intentions effectively. Subsequently, an exploration of shared control systems follows, where the coordination between the driver and the automation is meticulously managed to optimize comfort and performance. Lastly, an investigation is conducted into how drivers are accounted for in adaptive cruise control systems, encompassing the adaptation of longitudinal control parameters based on driver characteristics and preferences.

### 2.3.1. Sideslip Control Systems

For sideslip control systems focused on stability, steering input from the driver is used in calculating the reference values for the vehicle states - yaw rate and sideslip. In [26], a driver model is used to calculate the reference yaw rate, taking into account the lateral error, preview time and the driver's anticipation to vehicle response information. These references are passed to the high-level controllers, to be used to calculate the required control action.

Drift assist systems in literature, such as the one in Vignati et al. [22], don't account for driver inputs in calculating the control signal, only using steering for inferring driver intent to drift and activating the controller based on the following conditions (2.2):

$$\begin{aligned} sgn(\delta) &\neq sgn(\dot{\psi}) \\ \bar{\delta} \cdot sgn(\bar{\dot{\psi}}) &< 0 \end{aligned} \tag{2.2}$$

### 2.3.2. Shared Control Systems

Drift control systems, where the driver and the controller cooperate to maintain the vehicle at the drift equilibrium, can be considered shared control systems based on the following conditions proposed by Marcano et al. [13]:

1. The human and robot must act congruently, i.e., continuously and on the same specific task
2. The human and the robot must both be engaged in a perception-action cycle
3. The task must be individually feasible under ideal circumstances

The literature review conducted by Marcano et al. [13] presents two frameworks for shared control systems, namely coupled and uncoupled, which are distinguished by the interaction between the electronic actuator and the driver. In coupled systems, the automated system and the operator engage in force feedback, allowing for direct interaction and collaboration. On the other hand, uncoupled systems employ an intermediate controller that processes the driver's commands and complements them based on predefined automation goals. The review provides an in-depth analysis of shared steering control

systems, which have garnered significant attention in the literature. These systems prioritize not only path tracking performance but also the reduction of conflicts with the driver.

Additionally, incorporating driver models into model-based controllers has demonstrated notable advantages in the examined studies. In the study by Khosravani et al. [11], an active front steering system was developed, incorporating a driver model within the control loop. The driver's behavior was accounted for by employing an optimal path follower with a transient delay block. The design process considered only the current states of the vehicle and driver, modeling road preview information as an unknown bounded uncertainty. To ensure stability and accurate path tracking performance during lane change maneuvers, robust control methods were employed to handle the effects of delay and uncertainty. Khosravani et al. also implement a similar system using torque vectoring instead of active front steering in [12]. Sentouh et al. in [18] describe a cooperation strategy between the driver and steering assistance system, using a weighting function that depends on the lateral deviation error. This is used to determine the steering assist torque, providing assistance only in case of excessive lateral deviation from the desired path. In [6], Erlien et al. use a model predictive control to determine if the current driving command allows for a safe vehicle trajectory, and only intervenes when such a trajectory doesn't exist. This is achieved by including a term in the cost function penalizing the difference between front lateral forces intended by the driver and the controller along with terms ensuring vehicle stability. Ercan et al. [5] also use a model predictive control strategy, combining it with an online parameter identification scheme to account for the variations in the interaction dynamics between the driver and the vehicle.

While the utilization of similar shared control strategies has been observed in longitudinal control applications, such as car-following, traction control, and eco-driving, their occurrence remains relatively limited in the literature [13].

### 2.3.3. Adaptive Cruise Control Systems

Adaptive cruise control systems (ACC) form another class of controller where understanding the intent of the human driver plays as critical a role as controller performance. A review of implementation of human factors in ACC systems summarized the literature into two categories - the online control approach and the offline control approach [4]. The offline control approach does not vary during driving and is often collected from driving simulators or real world experiments. For example, in [15], the authors utilize real-world driving data to design their ACC algorithm which they show provides natural following performance similar to human manual driving in both high speed driving and low speed stop-and-go situations. The online control approach directly learns from the human driver to gain information that can be used in the controller using self-learning techniques such as data samplers, artificial neural networks and recursive least-squares algorithms. In [25], Wang et al. highlight the importance of considering individual driver behaviors and preferences to enhance the performance and acceptance of driving assistance systems. They use a self-learning algorithm to identify driver behavior when the vehicle is in manual mode, before feeding the identified driver model into the control algorithm when in automatic driving mode.

## 2.4. Summary

This chapter has provided an overview of the single-track model commonly used to describe planar vehicle dynamics, with a focus on understanding the dynamics through phase portrait analysis. Additionally, the state-of-the-art on drift control has been summarized, covering both autonomous drift control and driver-in-the-loop drift control systems. Autonomous drift control systems have primarily focused on stabilizing the vehicle to predetermined drifting equilibria. In contrast, driver-in-the-loop drift control systems aim to incorporate the driver's inputs and intentions into the control process, enabling the driver to actively participate in maintaining the vehicle at the desired drift states.

The interaction between the driver and control systems has been explored. Shared control systems have emerged as a promising approach, where the driver and the automation work together to optimize vehicle performance and driver experience. Incorporating driver models within the control loop has shown significant advantages in enhancing stability, path tracking, and driver-vehicle interaction.

Adaptive cruise control systems also highlight the importance of considering individual driver behaviors and preferences to improve system performance and acceptance.

In the subsequent chapters, these concepts and approaches will be applied to the problem of driver-in-the-loop drift control, aiming to design and evaluate a torque vectoring system that enables drivers to safely and effectively perform drifting maneuvers.

# 3

# Vehicle Dynamics Model

In order to develop an effective controller for the vehicle, it is crucial to have a model that accurately captures the system dynamics. This chapter presents a vehicle dynamics model that incorporates the necessary degrees of freedom to simulate drifting and wheel torque control. The model consists of a four-wheel planar representation of the vehicle, with seven degrees of freedom, including longitudinal, lateral, yaw rotation, and wheel rotations. By considering these degrees of freedom, the model can effectively represent drifting behavior and enable efficient simulation of the physical vehicle.

## 3.1. Seven Degree-of-Freedom Vehicle Model

The vehicle dynamics model utilized in this work is a four-wheel planar model, depicted in Figure 3.1. It incorporates seven degrees of freedom: longitudinal, lateral, yaw rotation, and wheel rotations.

### 3.1.1. Planar Vehicle Motion

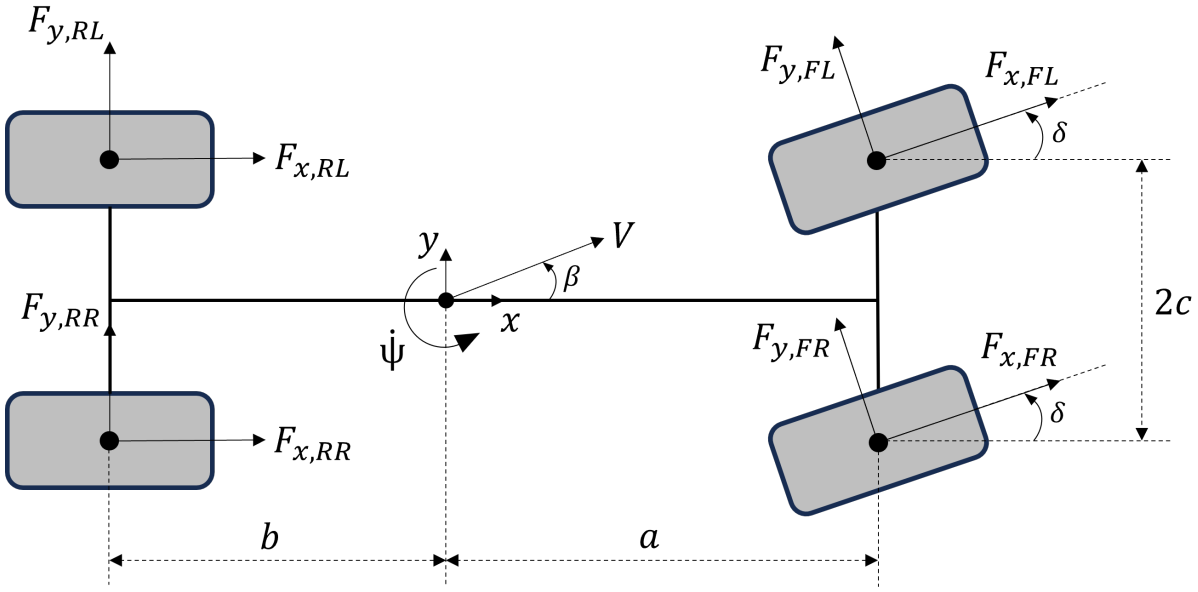


**Figure 3.1:** Figure illustrating the four wheel planar vehicle model

The dynamics of the planar vehicle can be described by the following equations:

$$
\begin{aligned}
ma_x &= (F_{x,FL} + F_{x,FR})\cos\delta - (F_{y,FL} + F_{y,FR})\sin\delta + (F_{x,RL} + F_{x,RR}) - F_{drag} \\
ma_y &= (F_{y,FL} + F_{y,FR})\cos\delta + (F_{x,FL} + F_{x,FR})\sin\delta + (F_{y,RL} + F_{y,RR}) \\
I_{zz}\ddot{\psi} &= a\,(F_{y,FL} + F_{y,FR})\cos\delta + a\,(F_{x,FL} + F_{x,FR})\sin\delta - b\,(F_{y,RL} + F_{y,RR}) \\
&\quad + ((F_{x,FR} - F_{x,FL})\cos\delta + F_{x,RR} - F_{x,RL})\,c
\end{aligned}
\tag{3.1}
$$

where, $F_{y,ij}$ is the lateral force produced by the tire, ($i = F, R$, $j = L, R$)
$F_{x,ij}$ is the longitudinal force produced by the tire, ($i = F, R$, $j = L, R$)
$m$ is the mass of the vehicle
$I_{zz}$ is the polar moment of inertia of the vehicle
$a$ and $b$ are the distances between vehicle CG and front and rear axles respectively
$c$ is half of the vehicle trackwidth
$\delta$ is the steering angle (road wheel angle)
$F_{drag}$ is the force due to aerodynamic drag
$a_x$ and $a_y$ are the accelerations in the longitudinal and lateral directions
$\dot{\psi}$ is the yaw rate and $\ddot{\psi}$ is the yaw acceleration

The lateral and longitudinal velocities were computed by integrating the following equations (3.2):

$$
\begin{aligned}
\dot{v}_x &= a_x + \dot{\psi} v_y \\
\dot{v}_y &= a_y - \dot{\psi} v_x
\end{aligned}
\tag{3.2}
$$

### 3.1.2. Wheel Dynamics

The wheel rotations are described by the following equations:

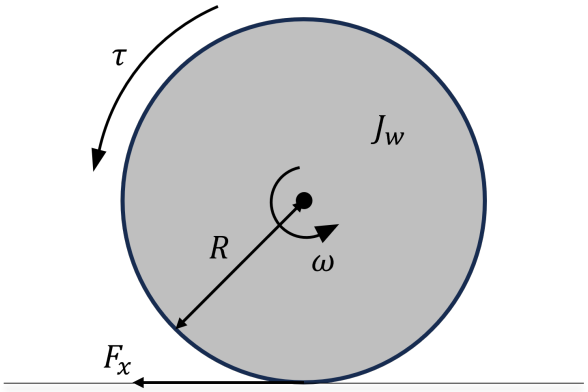


**Figure 3.2:** Figure illustrating wheel rotation dynamics

$$
\begin{aligned}
\dot{\omega}_{FL} &= \frac{\tau_{FL} - R_F F_{x,FL}}{J_{w,F}} \quad \dot{\omega}_{FR} = \frac{\tau_{FR} - R_F F_{x,FR}}{J_{w,F}} \\
\dot{\omega}_{RL} &= \frac{\tau_{RL} - R_R F_{x,RL}}{J_{w,R}} \quad \dot{\omega}_{RR} = \frac{\tau_{RR} - R_R F_{x,RR}}{J_{w,R}}
\end{aligned}
\tag{3.3}
$$

where, $R_i$ is the rolling radius of the tire ($i = F, R$)
$\omega_{ij}$ is the rotational velocity of the tire ($i = F, R$, $j = L, R$)
$\tau_{ij}$ is the torque acting on the wheel ($i = F, R$, $j = L, R$)
$J_{w,i}$ is the moment of inertia of the axle ($i = F, R$)

### 3.1.3. Tire Normal Load Calculation

The normal load on each tire was calculated using the following equations (3.4):

$$
\begin{aligned}
F_{z,FL} &= \frac{mgb}{2(a+b)} - \frac{ma_x h_{CG}}{2(a+b)} - \frac{ma_y h_{CG}}{4c} + \frac{F_{down,F}}{2} \\
F_{z,FR} &= \frac{mgb}{2(a+b)} - \frac{ma_x h_{CG}}{2(a+b)} + \frac{ma_y h_{CG}}{4c} + \frac{F_{down,F}}{2} \\
F_{z,RL} &= \frac{mgb}{2(a+b)} + \frac{ma_x h_{CG}}{2(a+b)} - \frac{ma_y h_{CG}}{4c} + \frac{F_{down,R}}{2} \\
F_{z,RR} &= \frac{mgb}{2(a+b)} + \frac{ma_x h_{CG}}{2(a+b)} + \frac{ma_y h_{CG}}{4c} + \frac{F_{down,R}}{2}
\end{aligned}
\tag{3.4}
$$

where, $F_{z,ij}$ is the normal load acting on the tire ($i = F, R$, $j = L, R$)
$h_{CG}$ is height of the vehicle CG from the ground
$F_{down,i}$ is the downforce acting on the axle ($i = F, R$)

### 3.1.4. Tire Slip Calculation

The following equations (3.5) were used to calculate the lateral and longitudinal slips required as inputs to the tire model:

$$
\begin{aligned}
\alpha_{FL} &= \delta - \tan^{-1}\left(\frac{v_y + \dot{\psi}a}{v_x - \dot{\psi}c}\right) & \alpha_{FR} &= \delta - \tan^{-1}\left(\frac{v_y + \dot{\psi}a}{v_x + \dot{\psi}c}\right) \\
\alpha_{RL} &= \tan^{-1}\left(\frac{-v_y + \dot{\psi}b}{v_x - \dot{\psi}c}\right) & \alpha_{RR} &= \tan^{-1}\left(\frac{-v_y + \dot{\psi}b}{v_x + \dot{\psi}c}\right) \\
\kappa_{FL} &= \frac{R_F\omega_{FL} - \left(v_x - \dot{\psi}c\right)}{\max\left(v_x - \dot{\psi}c, R_F\omega_{FL}\right)} & \kappa_{FR} &= \frac{R_F\omega_{FR} - \left(v_x + \dot{\psi}c\right)}{\max\left(v_x + \dot{\psi}c, R_F\omega_{FR}\right)} \\
\kappa_{RL} &= \frac{R_R\omega_{RL} - \left(v_x - \dot{\psi}c\right)}{\max\left(v_x - \dot{\psi}c, R_R\omega_{RL}\right)} & \kappa_{RR} &= \frac{R_R\omega_{RR} - \left(v_x + \dot{\psi}c\right)}{\max\left(v_x + \dot{\psi}c, R_R\omega_{RR}\right)}
\end{aligned}
\tag{3.5}
$$

where $\alpha_{ij}$ and $\kappa_{ij}$ are the lateral and longitudinal slips of the tire ($i = F, R$, $j = L, R$)

## 3.2. Pacejka Tire Model

In order to accurately model the behavior of the tires, the Pacejka tire model equations (3.6) and (3.7) from [16] were utilized to calculate the longitudinal and lateral tire forces, respectively. These equations take into account the slip angle ($\alpha$), slip ratio ($\kappa$), and normal load ($F_z$).

$$
\begin{aligned}
&F_x = G_{x\alpha}F_{x0} \\
&F_{x0} = D_x\left[F_z\right]\sin\left(C_x\tan^{-1}\left(B_x\left[F_z\right]\kappa_x - E_x\left[\kappa_x, F_z\right]\left(B_x\left[F_z\right]\kappa_x - \tan^{-1}\left(B_x\left[F_z\right]\kappa_x\right)\right)\right)\right) + S_{Vx}\left[F_z\right] \\
&\kappa_x = \kappa + S_{Hx}\left[F_z\right] \\
&G_{x\alpha} = \cos\left(C_{x\alpha}\tan^{-1}\left(B_{x\alpha}[\kappa]\alpha_S - E_{x\alpha}\left[F_z\right]\left(B_{x\alpha}[\kappa]\alpha_S - \tan^{-1}\left(B_{x\alpha}[\kappa]\alpha_S\right)\right)\right)\right)/G_{x\alpha 0} \\
&G_{x\alpha 0} = \cos\left(C_{x\alpha}\tan^{-1}\left(B_{x\alpha}[\kappa]S_{Hx\alpha} - E_{x\alpha}\left[F_z\right]\left(B_{x\alpha}[\kappa]S_{Hx\alpha} - \tan^{-1}\left(B_{x\alpha}[\kappa]S_{Hx\alpha}\right)\right)\right)\right) \\
&\alpha_S = \alpha + S_{Hx\alpha}
\end{aligned}
\tag{3.6}
$$

$$
\begin{aligned}
&F_y = G_{y\kappa} F_{y0} + S_{Vy\kappa}\left[\alpha, \kappa, F_z\right] \\
&F_{y0} = D_y\left[F_z\right] \sin\left(C_y \tan^{-1}\left(B_y\left[F_z\right]\alpha_y - E_y\left[\alpha_y, F_z\right]\left(B_y\left[F_z\right]\alpha_y - \tan^{-1}\left(B_y\left[F_z\right]\alpha_y\right)\right)\right)\right) + S_{Vy}\left[F_z\right] \\
&\alpha_y = \alpha + S_{Hy}\left[F_z\right] \\
&G_{y\kappa} = \cos\left(C_{y\kappa} \tan^{-1}\left(B_{y\kappa}[\alpha]\kappa_S - E_{y\kappa}\left[F_z\right]\left(B_{y\kappa}[\alpha]\kappa_S - \tan^{-1}\left(B_{y\kappa}[\alpha]\kappa_S\right)\right)\right)\right) / G_{y\kappa 0} \\
&G_{y\kappa 0} = \cos\left(C_{y\kappa} \tan^{-1}\left(B_{y\kappa}[\alpha] S_{Hy\kappa}\left[F_z\right] - E_{y\kappa}\left[F_z\right]\left(B_{y\kappa}[\alpha] S_{Hy\kappa}\left[F_z\right] - \tan^{-1}\left(B_{y\kappa}[\alpha] S_{Hy\kappa}\left[F_z\right]\right)\right)\right)\right) \\
&\kappa_S = \kappa + S_{Hy\kappa}\left[F_z\right]
\end{aligned}
\tag{3.7}
$$

The tire model parameters are obtained from the tire datasheet.

## 3.3. Parameter Fitting for Drift Data

To accurately model the tire behavior during drift, the Pacejka tire model parameters were optimized using logged data from the vehicle. The optimization process involved adjusting the parameters to match the lateral and longitudinal forces obtained from the logged data.

The lateral forces on each axle were calculated using the following equations. The logged data for lateral acceleration, yaw rate, and other vehicle parameters were utilized in these calculations:

$$F_{y,F} \cos\delta + F_{x,F} \sin\delta + F_{y,R} = m a_y \tag{3.8}$$

$$a F_{y,F} \cos\delta + a F_{y,F} \sin\delta - b F_{y,R} + M_{z,TV} = I_{zz} \ddot{\psi} \tag{3.9}$$

By multiplying Equation (3.8) by $b$, we obtain:

$$b F_{y,F} \cos\delta + b F_{x,F} \sin\delta + b F_{y,R} = b m a_y \tag{3.10}$$

Adding Equation (3.9) to Equation (3.10), we get:

$$(a+b) F_{y,F} \cos\delta + (a+b) F_{x,F} \sin\delta + M_{z,TV} = b m a_y + I_{zz} \ddot{\psi} \tag{3.11}$$

Using Equation (3.11), we can calculate the lateral force on the front axle, $F_{y,F}$:

$$F_{y,F} \cos\delta = \frac{b m a_y + I_{zz} \ddot{\psi} - M_{z,TV}}{a+b} - F_{x,F} \sin\delta \tag{3.12}$$

Finally, the rear lateral force, $F_{y,R}$, can be calculated using:

$$F_{y,R} = m a_y - F_{y,F} \cos\delta \tag{3.13}$$

### 3.3.1. Manual optimization results

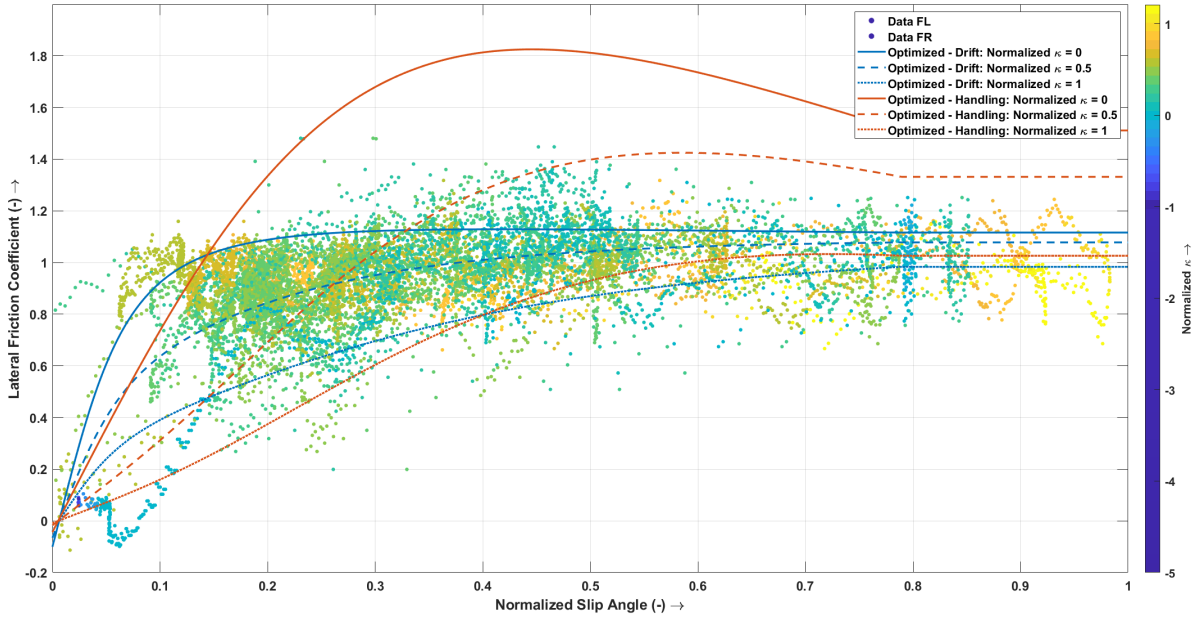


**Figure 3.3:** Front Tire Model comparison with logged data

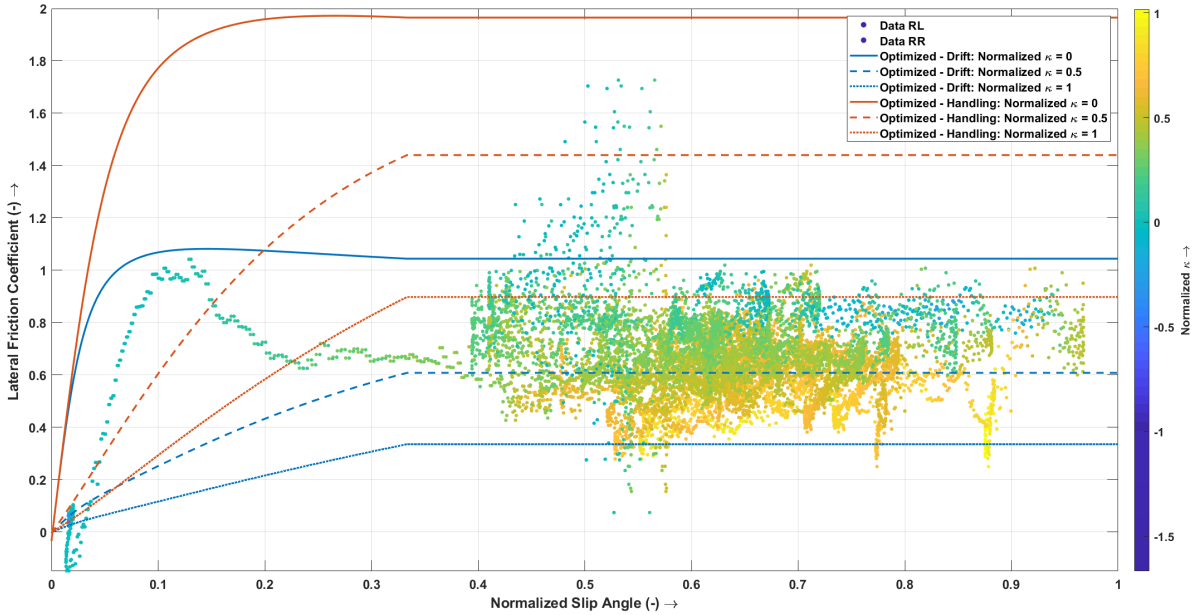


**Figure 3.4:** Rear Tire Model comparison with logged data

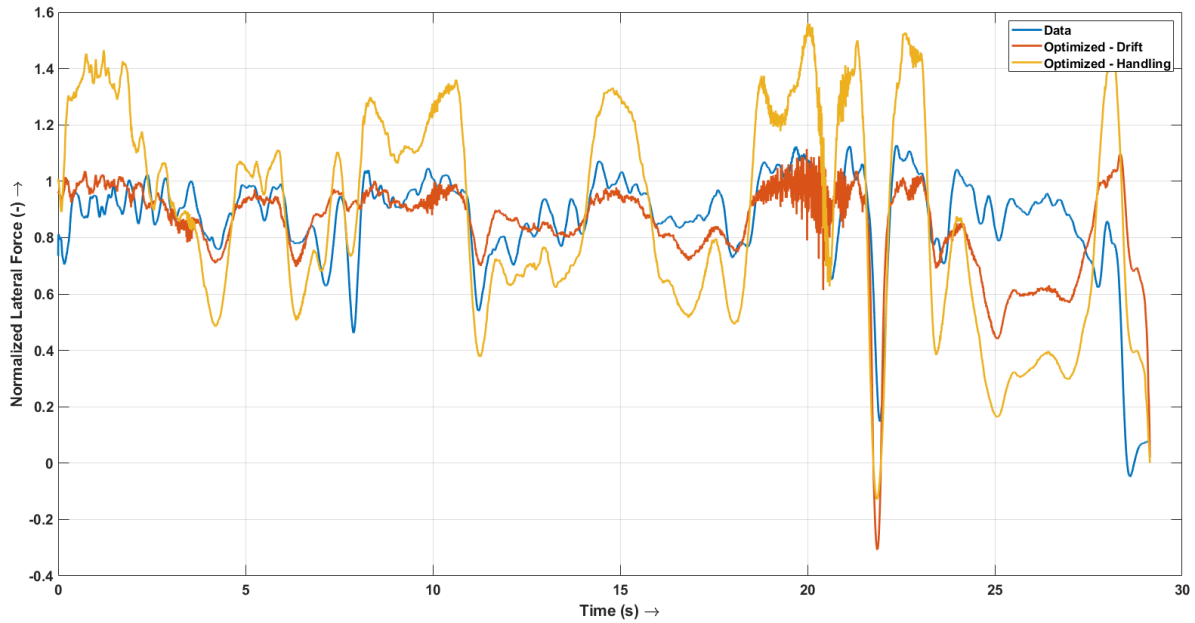


**Figure 3.5:** Comparison of front axle lateral force from logged data, optimized tire model and initial tire model

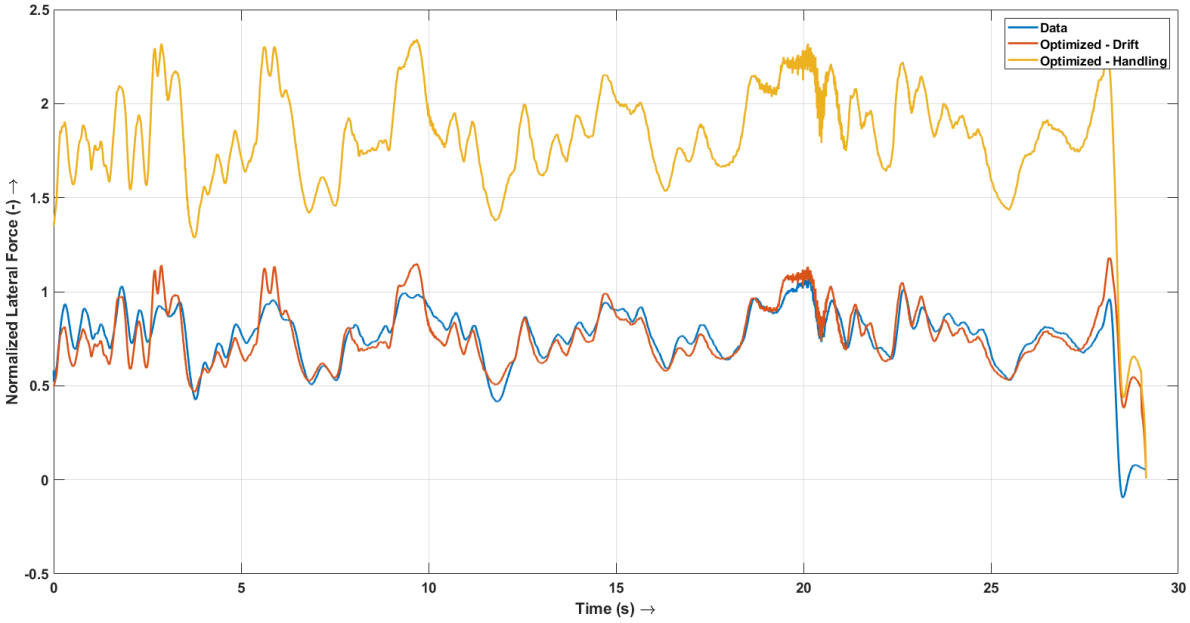


**Figure 3.6:** Comparison of rear axle lateral force from logged data, optimized tire model and initial tire model

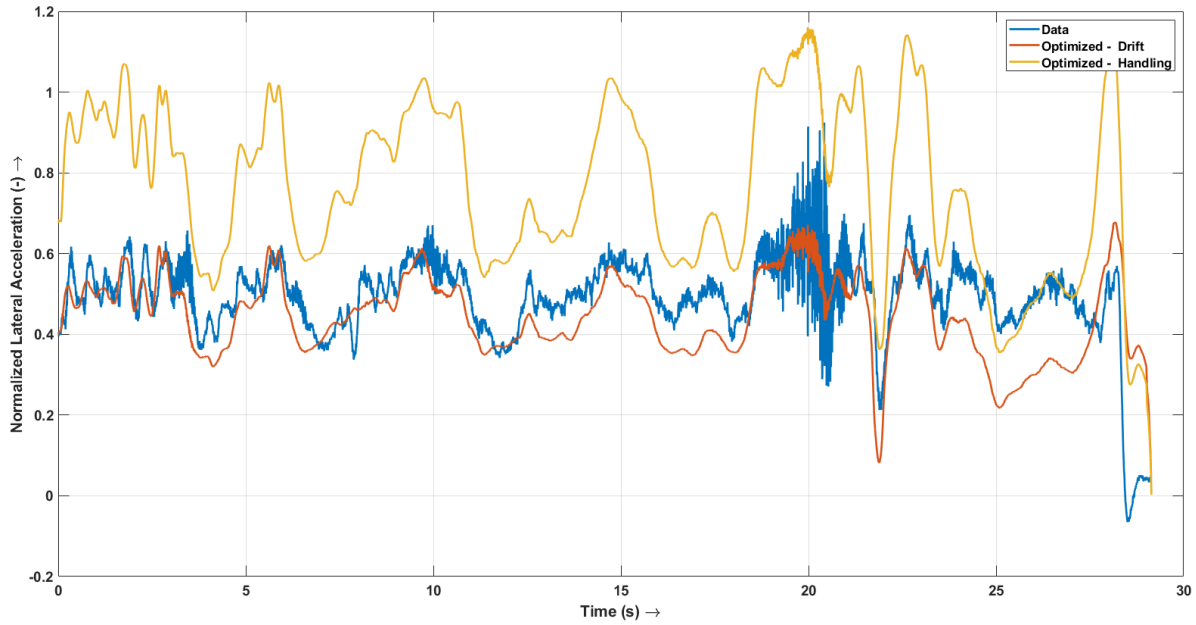


**Figure 3.7:** Comparison of lateral acceleration from logged data, optimized tire model and initial tire model

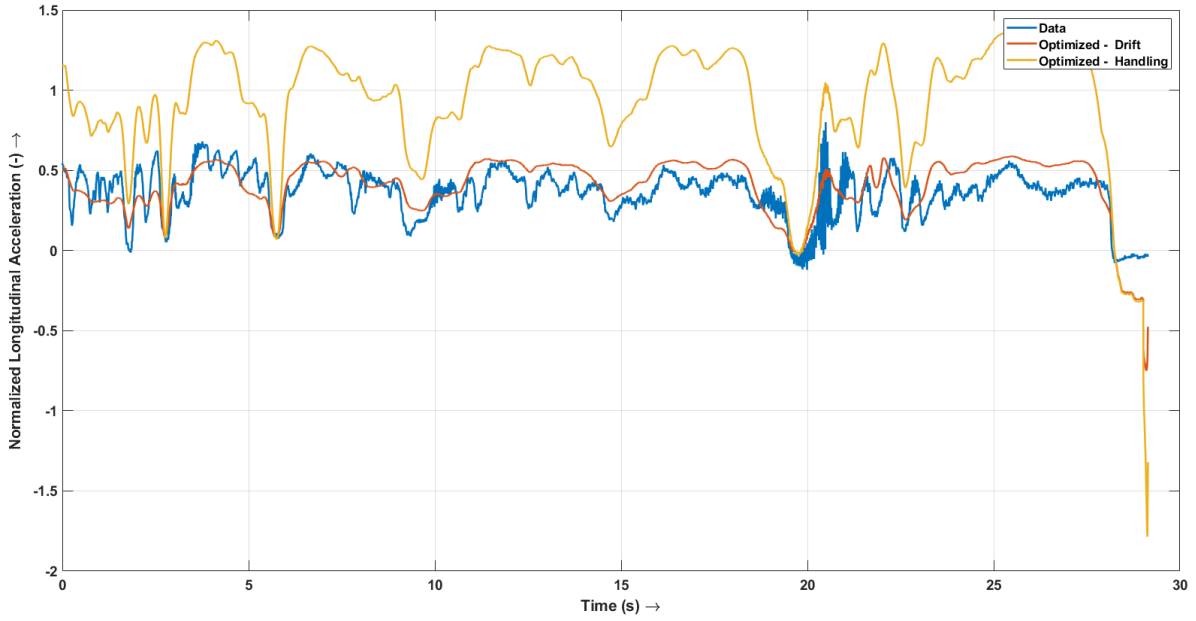


**Figure 3.8:** Comparison of longitudinal acceleration from logged data, optimized tire model and initial tire model

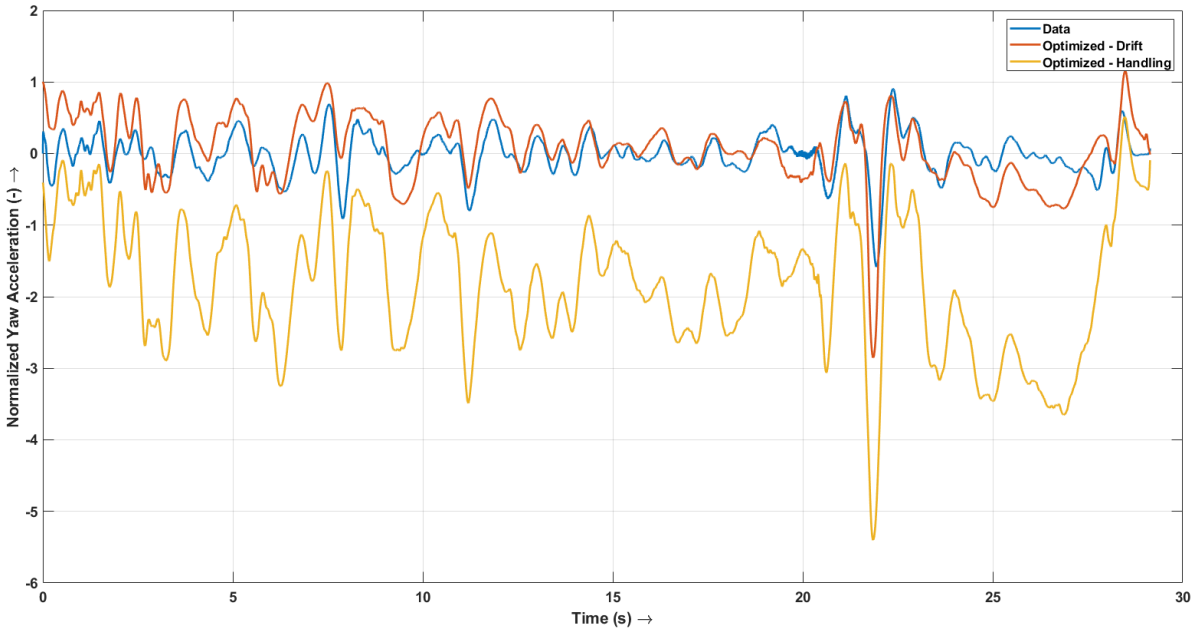


**Figure 3.9:** Comparison of yaw acceleration from logged data, optimized tire model and initial tire model

The front and rear tire models were manually optimized to better capture the behavior of the tires during drifting. The optimized front tire model significantly improved the accuracy of lateral force prediction, both in terms of magnitude and variation with slip ratio, compared to the original tire model fitted for ”Handling” maneuvers. Similarly, the optimized rear tire model better captured the variation of lateral force with slip ratio compared to the original tire model.

The comparison of front axle lateral force (Figure 3.5) revealed that the tire model for ”Handling” had much lower cornering stiffness compared to the new drift tire model. The optimized drift tire model showed that the front lateral force did not vary significantly for slip angles above 2°.

The comparison of rear axle lateral force (Figure 3.6) indicated that the tire model optimized for drift achieved the correct value of friction coefficient ($\mu$) and better represented the variation of rear lateral force with slip ratio ($\kappa$).

The comparison of accelerations in the lateral, longitudinal, and yaw directions (Figures 3.7 and 3.9) demonstrated that the tire model optimized for drift outperformed the model optimized for ”Handling” maneuvers.

### 3.3.2. Tire Data Analysis on New Drift Dataset

The new tire model was evaluated using another dataset where the vehicle was drifting. The data from this drift maneuver (Figure 3.10) exhibited a near steady-state drift between $t = 6.5$ s and $t = 19.5$ s.

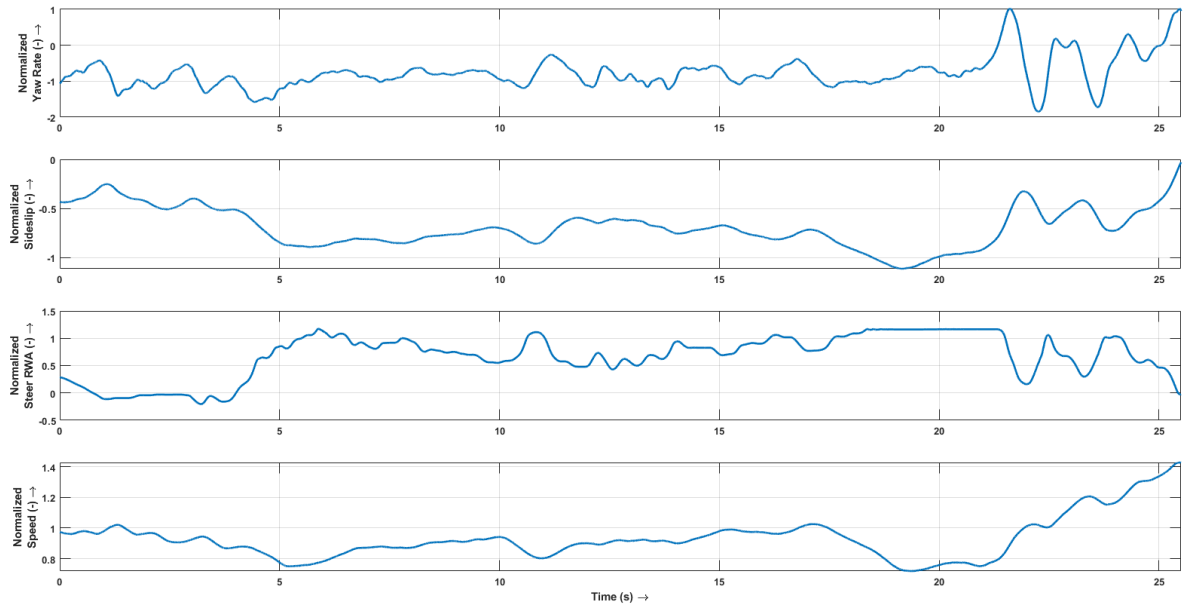


**Figure 3.10:** Data from the drift maneuver

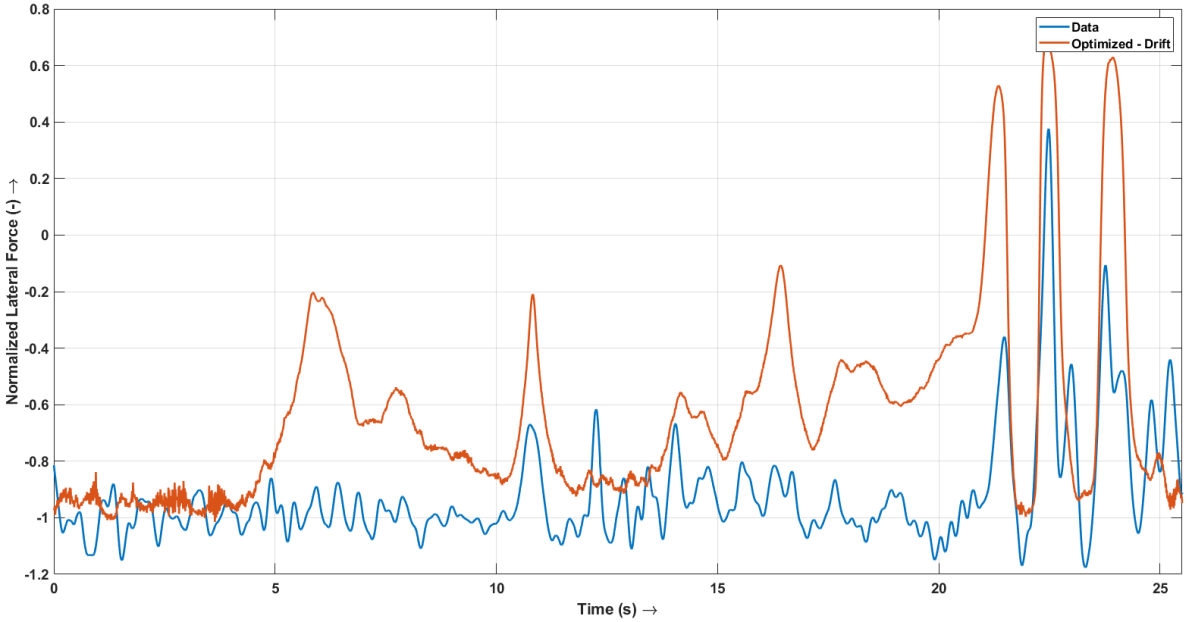


**Figure 3.11:** Comparison of front axle lateral force from logged data and optimized tire model

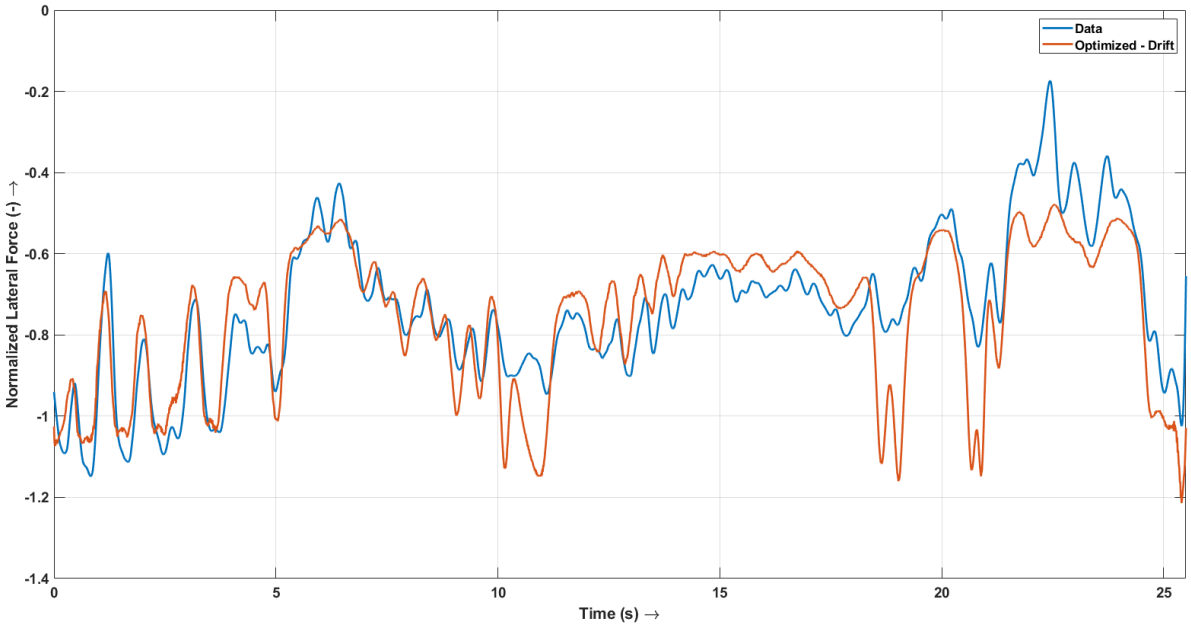


**Figure 3.12:** Comparison of rear axle lateral force from logged data and optimized tire model

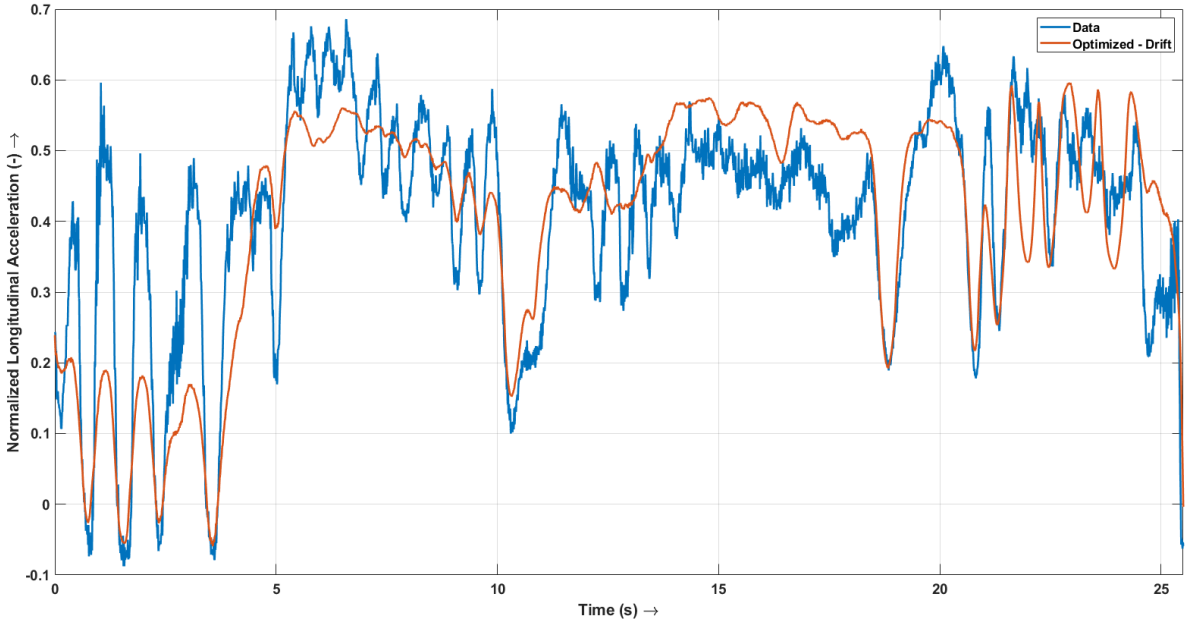


**Figure 3.13:** Comparison of longitudinal acceleration from logged data and optimized tire model

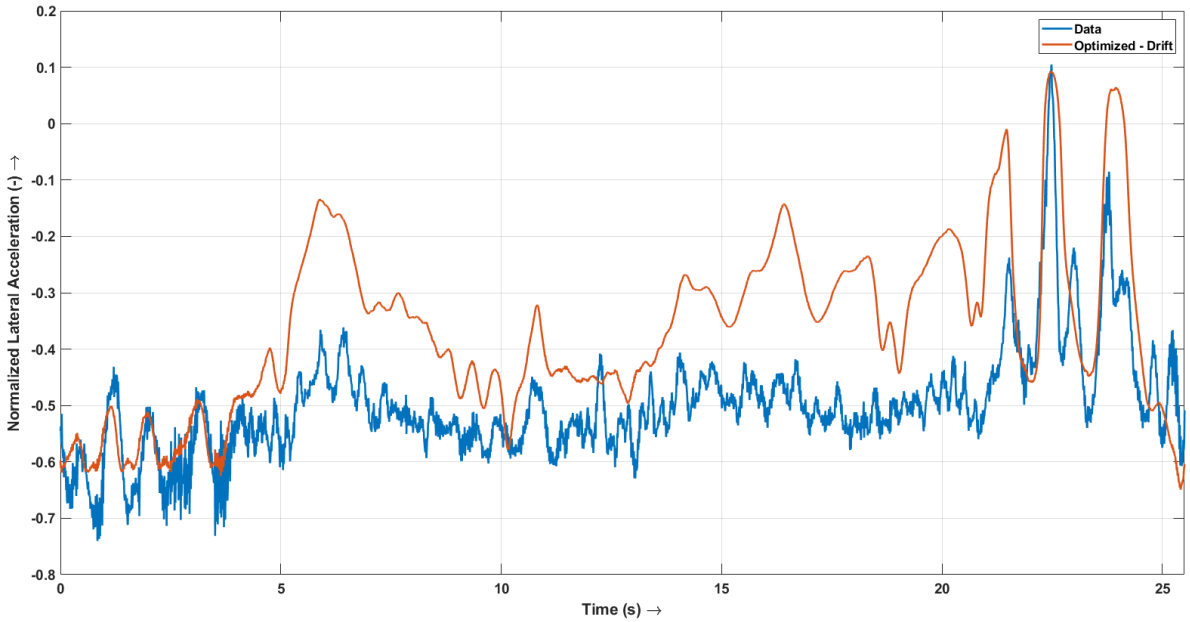


**Figure 3.14:** Comparison of lateral acceleration from logged data and optimized tire model

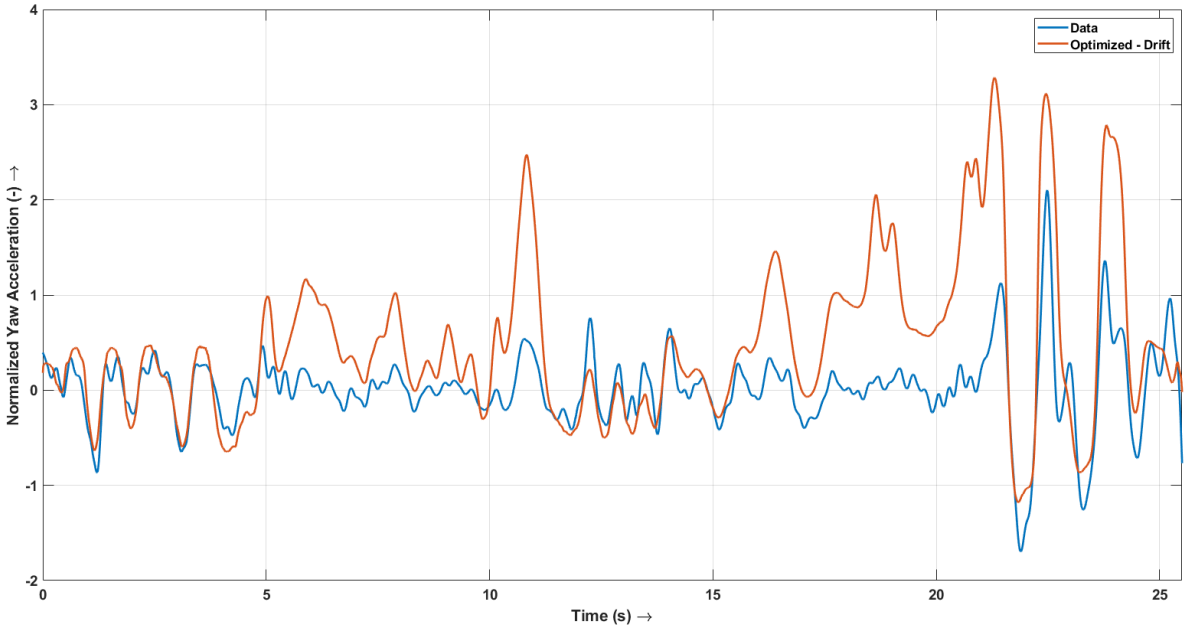


**Figure 3.15:** Comparison of yaw acceleration from logged data and optimized tire model

The comparison of front axle lateral force (Figure 3.11) revealed mismatches during rapid changes in steering angle, which can be attributed to the lack of transient tire dynamics in the vehicle model.

Similarly, the mismatches in rear axle lateral force (Figure 3.12) occurred when the rear slip ratio dropped suddenly, causing the tire to enter the low slip ratio and high slip angle regime.

The tire model accurately captured the dynamics of longitudinal acceleration ($a_x$) but exhibited mismatches in lateral acceleration ($a_y$) and yaw acceleration ($\dot{r}$) when the front lateral force ($F_y$) was underestimated (Figures 3.13, 3.14, and 3.15).

## 3.4. Summary

This chapter presented the modeling of the physical vehicle in simulation using a seven degree-of-freedom model that accounted for planar vehicle and wheel rotation dynamics. The Pacejka tire model, which incorporates tire dynamics considering various factors such as normal load, lateral slip, and longitudinal slip, was employed to capture the behavior of the tires.

To accurately simulate drift behavior, a new tire model was developed because the manufacturer-provided model was inadequate for capturing the vehicle's behavior during drift. The reason for this inadequacy is that the parameters of the manufacturer-provided tire model were obtained from standard tests that do not cover extreme maneuvers such as drift. Standard tire tests are typically designed to evaluate tire performance under normal driving conditions and maneuvers such as braking, cornering, and acceleration. These tests aim to provide information about tire characteristics that are relevant for everyday driving scenarios. However, they often do not encompass the extreme and specialized dynamics involved in drifting. During drift maneuvers, the vehicle experiences highly nonlinear and complex tire behaviors, including significant slip angles, high slip ratios, and sustained lateral forces. These conditions are not adequately represented in the parameters obtained from standard tests, as those tests focus on more typical driving scenarios where the tires operate within a different range of slip angles and slip ratios.

Therefore, a new tire model had to be developed by optimizing the parameters specifically for this driving behavior. This involved manually adjusting the tire model parameters using logged data from drifting maneuvers to ensure that the tire model accurately represented the lateral and longitudinal forces observed during drift. By developing and optimizing a new tire model specifically for drift, it was possible to achieve significant improvements in accurately simulating the vehicle's behavior during these extreme maneuvers. The new tire model exhibited higher cornering stiffness and better captured the variation of lateral force with slip angle and slip ratio, enabling more realistic and precise drift simulations.

However, the new rear tire model still had limitations in capturing the lateral force variation in the low slip ratio and high slip angle regime. Additionally, the model did not account for transient tire dynamics, leading to deviations from the data during quick steering maneuvers.

The developed vehicle and tire models will be utilized to test the control system in simulation. The subsequent chapter will focus on evaluating the dynamics of the vehicle and new tire model during drift using phase portraits, allowing for an understanding of the effects of different driver inputs and vehicle states.

# 4

# Phase Plane Analysis and Reference Generation

## 4.1. Phase Plane Analysis

Phase plane analysis was employed to investigate the dynamics of a drifting vehicle and to assess the impact of different vehicle states on the drift equilibrium.

### 4.1.1. Vehicle and Tire Model

A two-degree-of-freedom single-track model was utilized to examine the drifting dynamics on the phase plane with the yaw rate ($\dot{\psi}$) and sideslip angle ($\beta$) as the vehicle states. The inputs to the model included steering angle ($\delta$), longitudinal velocity ($v_x$), and slip ratios ($\kappa_F$ and $\kappa_R$). The lateral forces generated by the tires were calculated using the Pacejka Model, with the optimized parameters from Chapter 3.

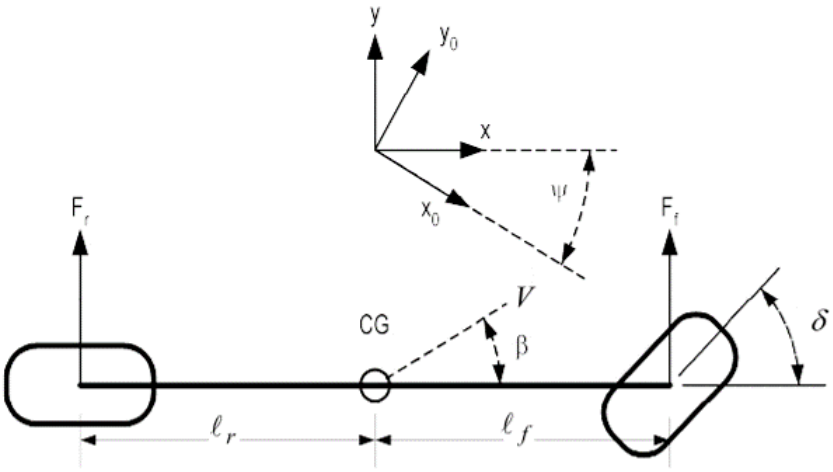


**Figure 4.1:** Single-track model for vehicle lateral dynamics [17]

$$\begin{aligned} \dot{v}_y &= \frac{1}{m}\left(F_{y,F}\cos\delta + F_{y,R}\right) - \dot{\psi}v_x \\ I_{zz}\ddot{\psi} &= l_f F_{y,F}\cos\delta - l_r F_{y,R} \end{aligned} \tag{4.1}$$

$$\begin{aligned} \beta &= \tan^{-1}\left(\frac{v_y}{v_x}\right) & \dot{\beta} &= \frac{1}{1+\left(\frac{v_y}{v_x}\right)^2}\frac{\dot{v_y}}{v_x} \\ \alpha_F &= \delta - \tan^{-1}\left(\frac{v_y + \dot{\psi} l_f}{v_x}\right) & \alpha_R &= \tan^{-1}\left(\frac{-v_y + \dot{\psi} l_r}{v_x}\right) \end{aligned} \tag{4.2}$$

where, $F_{y,F}$ is the lateral force produced by front tires
$F_{y,R}$ is the lateral force produced by rear tires
$m$ is the mass of the vehicle
$I_{zz}$ is the polar moment of inertia of the vehicle
$l_f$ is the distance between vehicle CG and front axle
$l_r$ is the distance between vehicle CG and rear axle

### 4.1.2. Phase Portraits for Drift Tire

A phase portrait depicting the vehicle's behavior is presented below. The analysis is conducted with a longitudinal velocity of 15 m/s and a steering angle of 20°. The slip ratios for the front and rear tires are set to 10% and 40% respectively.

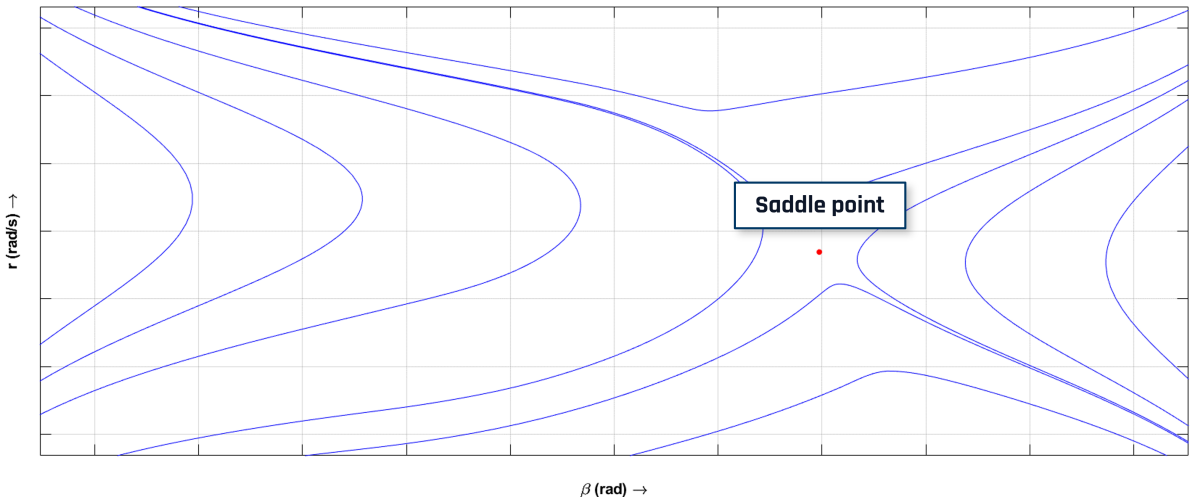


**Figure 4.2:** Phase portrait of vehicle at 15 m/s and 20° steering. Front and rear slip ratios are set to 10% and 40% respectively

As illustrated in 4.2, the phase portrait reveals the presence of only one unstable drift equilibrium under these specific conditions. This finding suggests an oversteer characteristic of the vehicle. The direction of equilibrium yaw rate is opposite to that of the steering, indicating the driver would need to counter-steer to maintain the drift and prevent a spin-out.

### Effect of Velocity ($v_x$) on Drift Equilibria (constant $\kappa_F$ and $\kappa_R$, $v_{x1} < v_{x2}$)

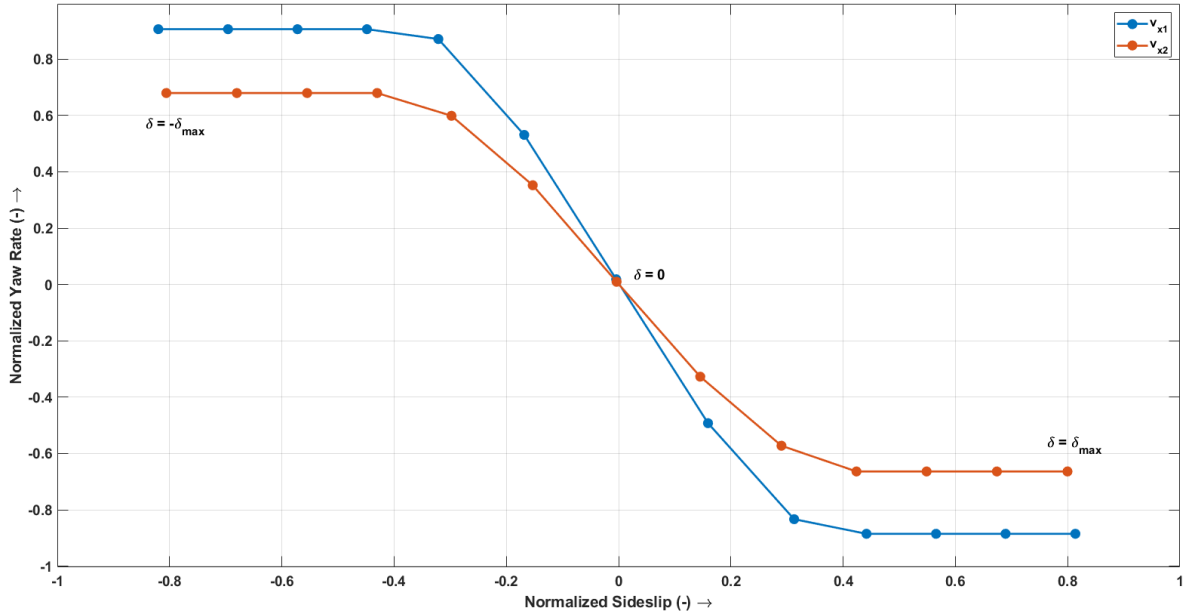


**Figure 4.3:** Effect of velocity on drift equilibrium

### Effect of Rear Slip Ratio ($\kappa_R$) on Drift Equilibria (constant $v_x$ and $\kappa_F$, $\kappa_{R2} < \kappa_{R1}$)

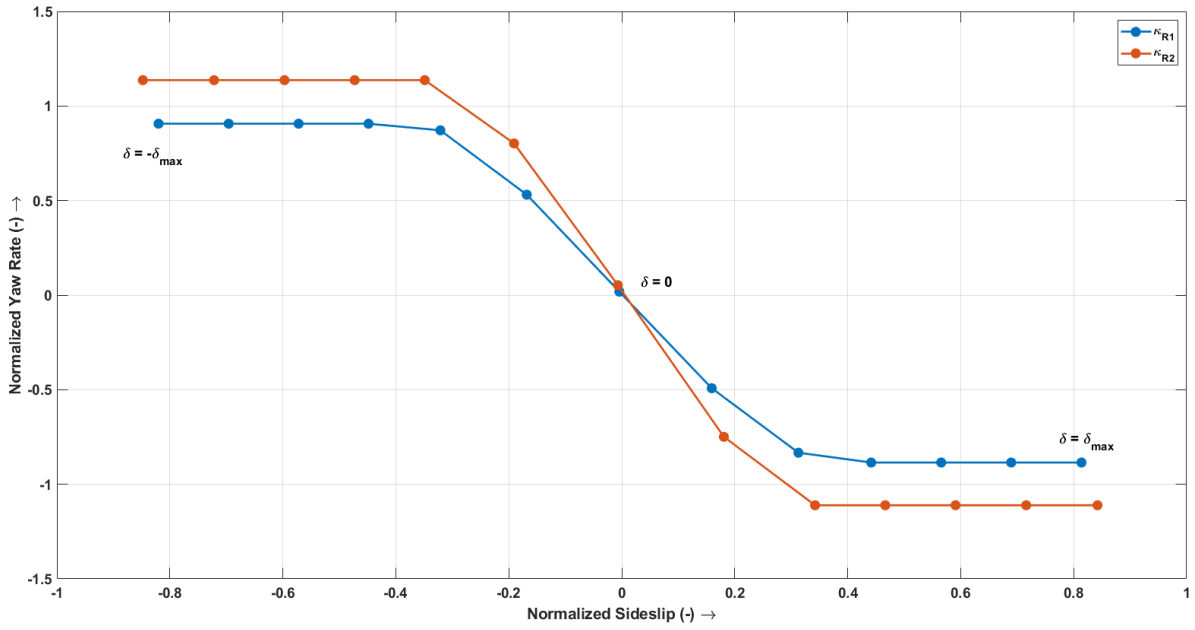


**Figure 4.4:** Effect of rear slip ratio on drift equilibrium

Effect of Front Slip Ratio ($\kappa_F$) on Drift Equilibria (constant $v_x$ and $\kappa_R$, $\kappa_{F1} < \kappa_{F2} < \kappa_{F3}$)

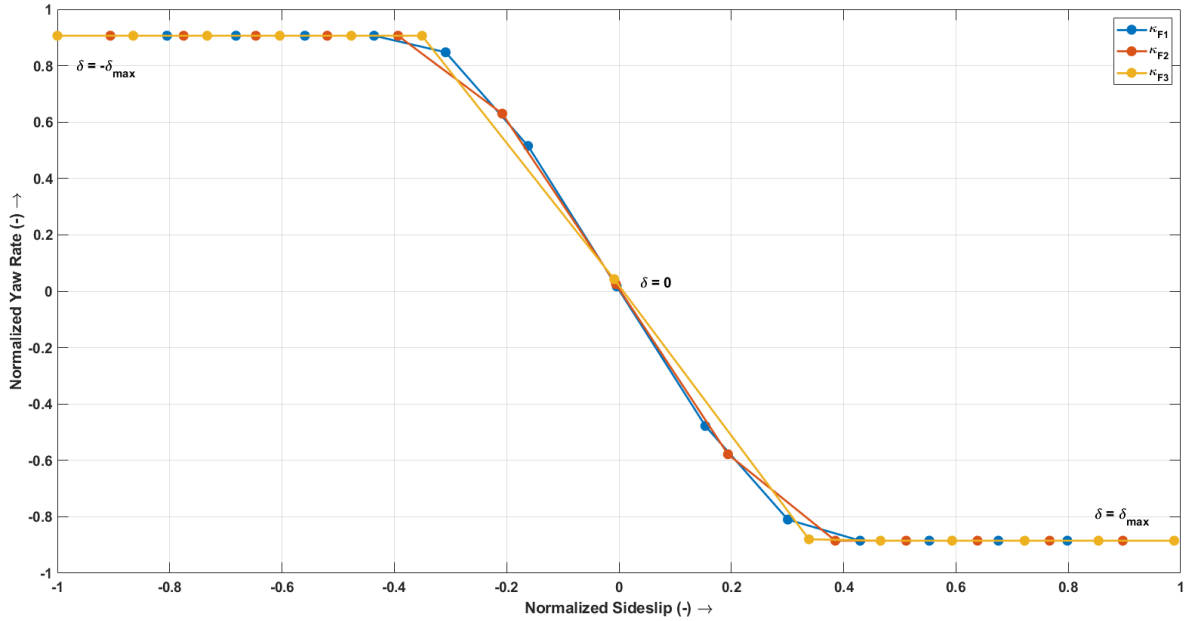


**Figure 4.5:** Effect of front slip ratio on drift equilibrium

### Inferences

From the phase plane analysis, it is observed that only counter-steer drift equilibria exist for rear slip ratios $\geq$ 10%. This is an indication of oversteer behavior. From studying the effects of various inputs on the drift equilibria, the following can be summarized:

As velocity ($v_x$) increases (figure 4.3), the equilibrium value of yaw rate decreases. This is because the maximum possible yaw rate, limited by tire-road friction, decreases with speed as

$$\dot{\psi}_{max} = \frac{\mu g}{v_x} \tag{4.3}$$

This behavior can be derived from the condition:

$$a_{y,SS} = v_x \dot{\psi} \leq \mu g \tag{4.4}$$

On decreasing rear slip ratio ($\kappa_R$, see figure 4.4), the equilibrium value of yaw rate increases due to the increase in lateral force from the rear tire. The equilibrium value of sideslip for the same counter-steer angle also increases since the increased lateral force on the rear axle must be counteracted by a similar increase on the front axle, requiring less counter-steer to achieve the moment balance.

Increasing the longitudinal slip of the front tires ($\kappa_F$, see figure 4.5) leads to increased equilibrium sideslip angle for the same steering angle. This is because the higher slip reduces the lateral grip at the front axle, necessitating less counter-steer to achieve the desired yaw moment balance with the rear axle. The equilibrium yaw rate remains largely unaffected, as it's still limited by the lateral grip of the rear tires. However, the dominant factor influencing the equilibrium sideslip angle remains the counter-steer angle.

## 4.2. Reference Generation

The reference generation process consists of two main components: enabling and disabling the controller based on the driver's intention to drift, and translating driver inputs through throttle and steering into state targets for the controller.

### 4.2.1. Enable/Disable

The detection of driver intent to drift is achieved by analyzing various parameters, including lateral acceleration, steering wheel angle, and pedal position. Once the driver engages drift control, it is automatically disabled if the driver releases the throttle or applies the brakes, or if the vehicle's speed drops below a certain threshold (e.g., 15 km/h). Additionally, the driver has the option to exit the drift maneuver by applying high throttle for a set duration of time.

To verify the performance of this module in detecting driver intention to drift, it is compared with on-track data from a drift lap. The subsystem takes vehicle data and driver inputs as inputs and produces an output that determines whether the drift assist should be enabled or disabled. This output is then compared with the inferred occurrence of vehicle drifting in the real-world scenario, based on the analysis of vehicle sideslip data. By correlating the subsystem's output with the observed sideslip behavior during drifting, the validation process ensures the accuracy and reliability of the subsystem in accurately identifying and responding to the driver's intention to initiate a drift maneuver.

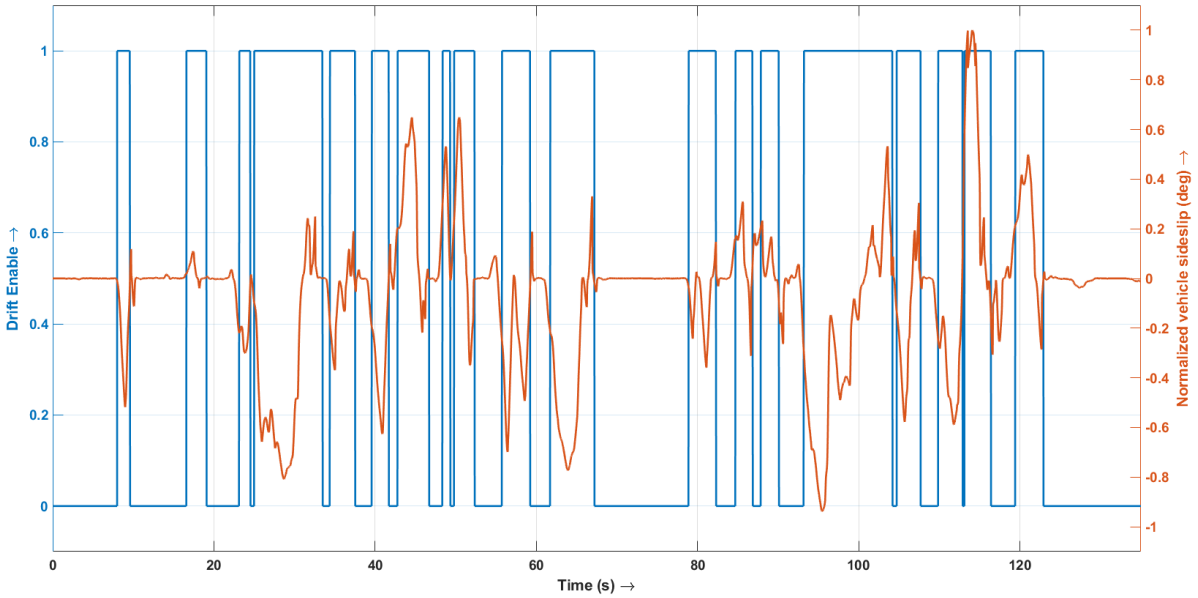


**Figure 4.6:** Comparison of Drift Enable/Disable with on-track data

As shown in 4.6, the enable/disable module is capable of detecting the driver's intent to drift. The module accurately detects driver intent and hypothetically enables drift control each time the driver intents for the vehicle to develop high sideslip.

### 4.2.2. State Target Generation

Using the insights gained from the phase plane analysis and logged data from actual drift maneuvers, the state targets for the controller are generated. The driver's inputs, namely steering and throttle, are translated into targets for longitudinal velocity, sideslip angle, and yaw rate for the vehicle.

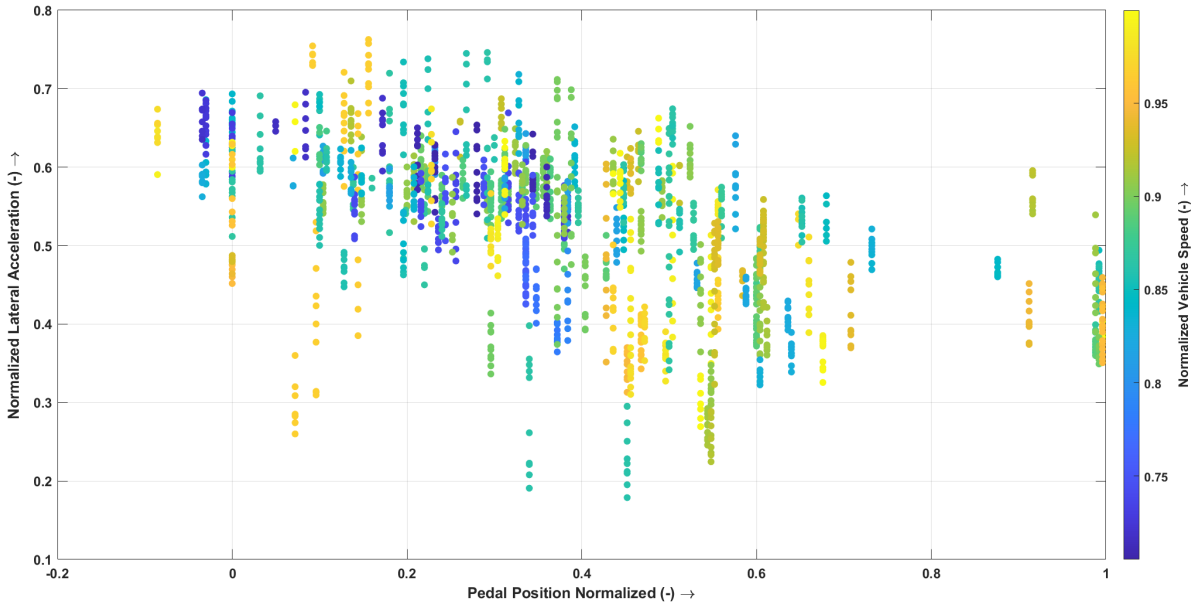


**Figure 4.7:** Vehicle data showing correlation between pedal position and lateral acceleration while drifting

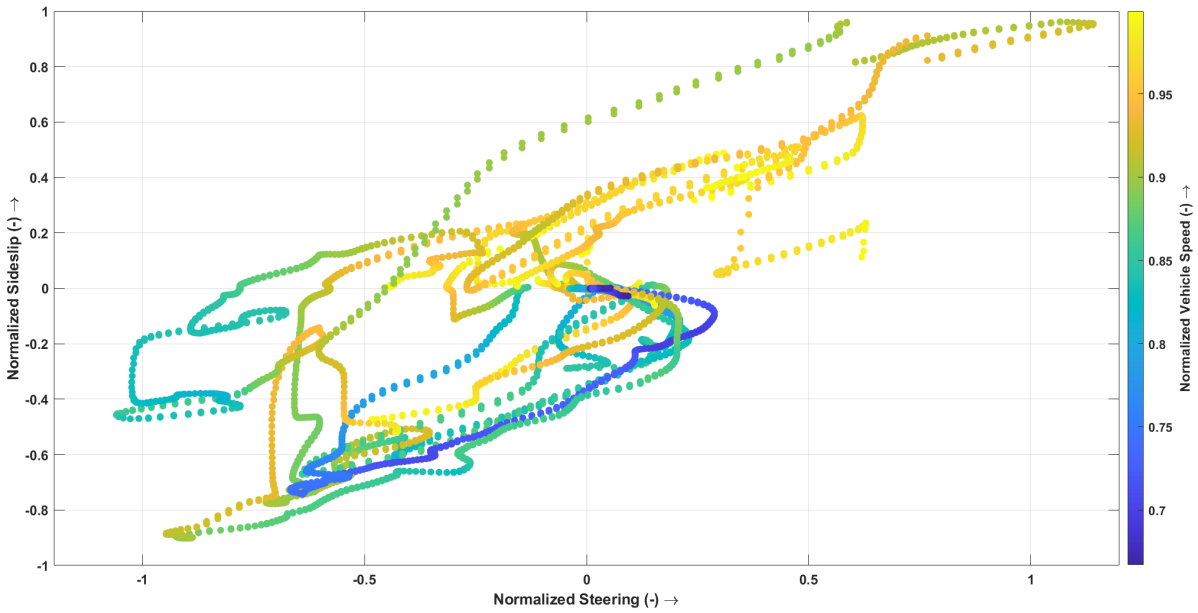


**Figure 4.8:** Vehicle data showing correlation between countersteer angle and vehicle sideslip while drifting

High throttle pedal input from the driver indicates a desire for higher longitudinal acceleration from the vehicle, while compromising on lateral acceleration (see figure 4.7). Consequently, the target longitudinal velocity increases, while the target yaw rate decreases with higher throttle pedal input. The sideslip target is obtained from the steering input, with an increase in countersteer from the driver resulting in a higher sideslip target for the controller similar to the behavior seen in figure 4.8. Countersteer is detected when the direction of the steering input is opposite to the direction of the vehicle's lateral motion, as observed through lateral acceleration. The vehicle's sideslip target is increased to the higher values observed during drifting only in the presence of countersteer, with a slightly lower setpoint to initiate drift without the risk of spinning out and losing control.

## 4.3. Summary

This chapter delves into the intricate dynamics of drifting and leverages the phase portrait as a powerful tool for visualizing and analyzing the behavior of the drifting vehicle. By investigating the effects of various inputs and states on the vehicle's dynamics, valuable insights are gained to inform the reference generation aspect of the control system.

The reference generation process comprises two key components: enabling and disabling the controller based on the driver's intention to drift, and translating driver inputs through throttle and steering into meaningful state targets for the controller. Through a comprehensive analysis of parameters such as lateral acceleration, steering wheel angle, and pedal position, the driver's intent to drift is accurately detected.

The enable/disable module is validated by comparing its outputs with on-track data from drift laps. This validation process ensures that the module effectively responds to the driver's intention to initiate a drift maneuver, thereby enabling precise control system activation.

Furthermore, the generation of state targets for the controller is based on inferences drawn from the phase plane analysis and logged data from real drift maneuvers. By translating driver inputs, such as steering and throttle, into longitudinal velocity, sideslip angle, and yaw rate targets, the reference generator enables the control system to accurately respond to the driver's desired drift behavior.

The integration of simulation data and empirical evidence from drift laps allows for the design and evaluation of a comprehensive reference generation methodology. This methodology not only enables the controller to maintain vehicle stability during drifts but also facilitates intuitive and responsive control based on the driver's inputs.

In conclusion, this chapter provides crucial insights into drift dynamics through phase plane analysis and presents a robust reference generation approach that enables precise control system activation based on the driver's intentions. The next chapter will focus on the design of the controller which will leverage the capabilities of all-wheel torque vectoring to ensure precise control over the drifting vehicle. Subsequently, the following chapter will delve into the testing of the entire control system within a simulated environment. This comprehensive testing phase will assess the effectiveness and reliability of the control system in maintaining vehicle stability during drifting.

# 5

# Controller Design

## 5.1. Drift Control using Steering & Wheel Torques

To thoroughly evaluate the efficacy of the newly optimized tire model, a comprehensive drift control system was developed, integrating both steering and motor torques. The vehicle was initially programmed to move straight at the desired velocity, followed by a deliberate transition towards an equilibrium state approximated using data from prior logged experiments.

The control strategy involves the utilization of rear motor torques ($\tau_{RL}$ and $\tau_{RR}$) to achieve and maintain a target slip ratio ($\kappa_R$), while front motor torques ($\tau_{FL}$ and $\tau_{FR}$) are employed to maintain the desired longitudinal velocity ($v_x$) (5.1). The steering angle ($\delta$) is employed to control both lateral velocity ($v_y$) and yaw rate ($\dot{\psi}$), ensuring that they are maintained at their respective equilibrium values (5.2), following a control strategy akin to the one proposed in [24].

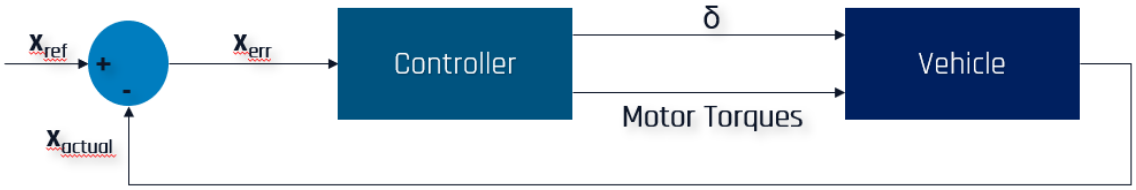


**Figure 5.1:** Block diagram of vehicle model and controller. "x" is a state vector consisting of yaw rate, sideslip and longitudinal velocity

$$\begin{aligned} \tau_{FL} &= \tau_{FR} = PI\left(v_{x,target} - v_x\right) \\ \tau_{RL} &= PI\left(\kappa_{target,RL} - \kappa_{RL}\right) \end{aligned} \tag{5.1}$$

$$\delta = \delta_{eq} + G_{\delta,vy}\left(v_{y,target} - v_y\right) + G_{\delta,\dot{\psi}}\left(\dot{\psi}_{target} - \dot{\psi}\right) \tag{5.2}$$

### 5.1.1. Simulation Results

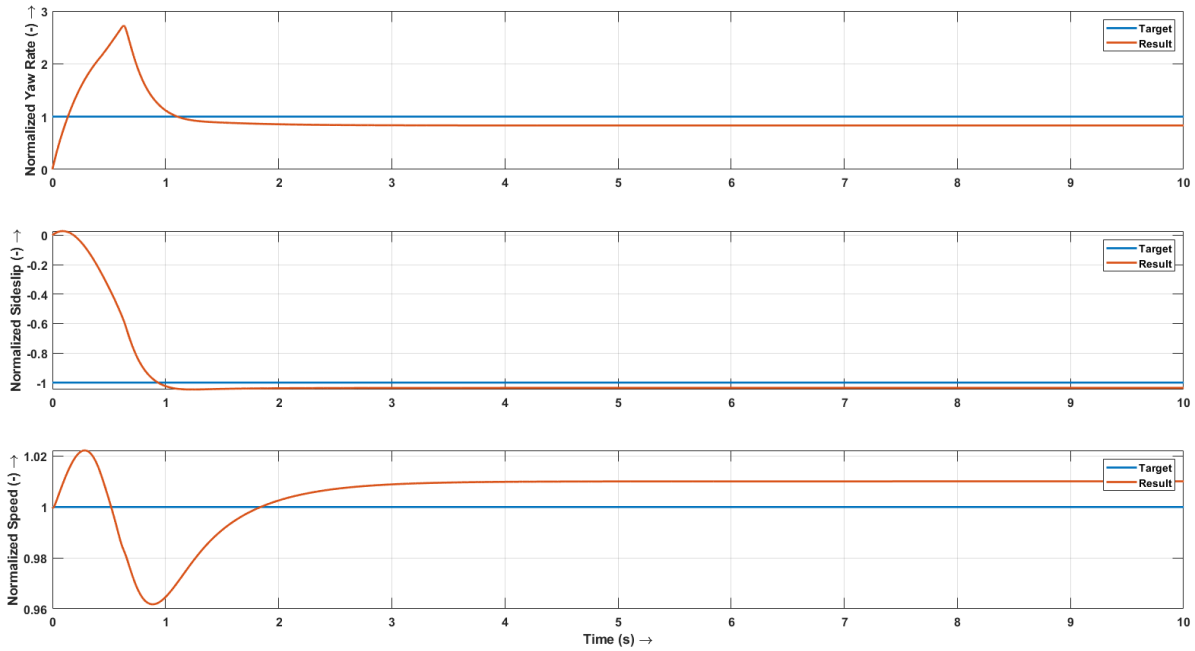


**Figure 5.2:** Result of simulation - vehicle states

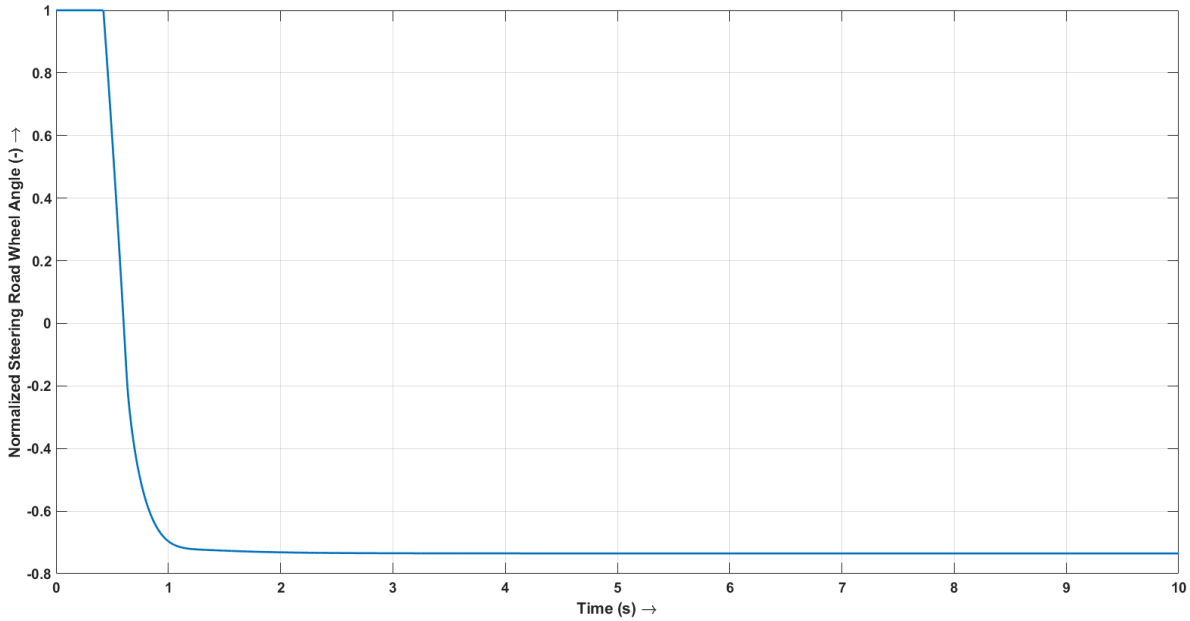


**Figure 5.3:** Result of simulation - steering (road wheel angle)

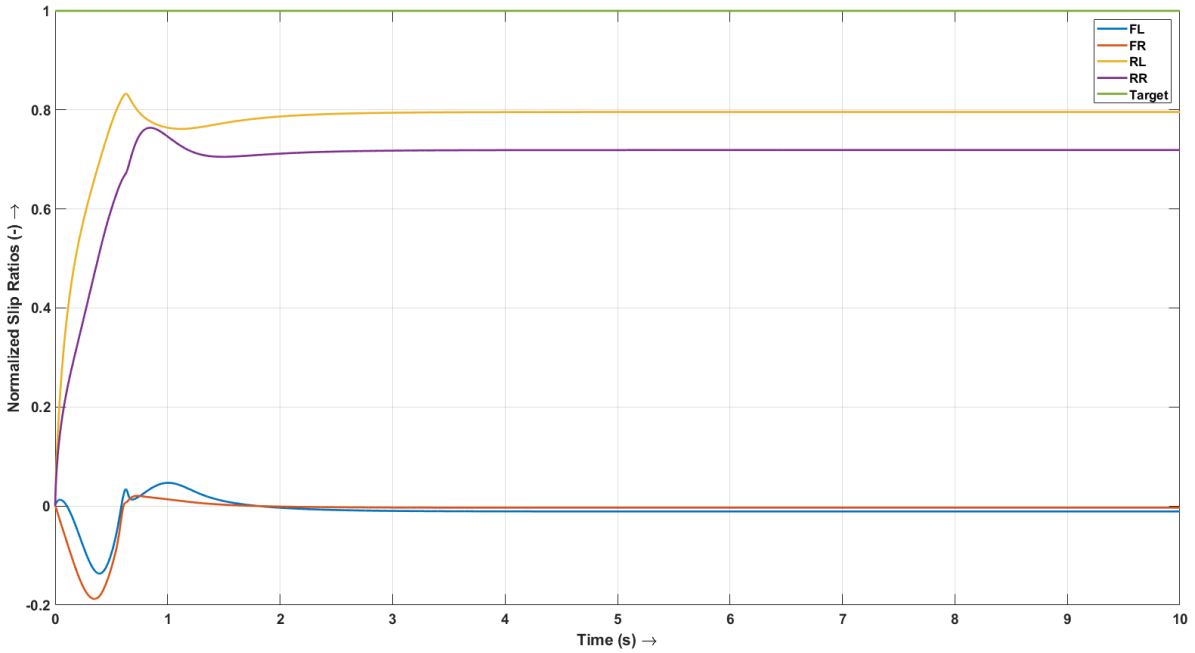


**Figure 5.4:** Result of simulation - slip ratios

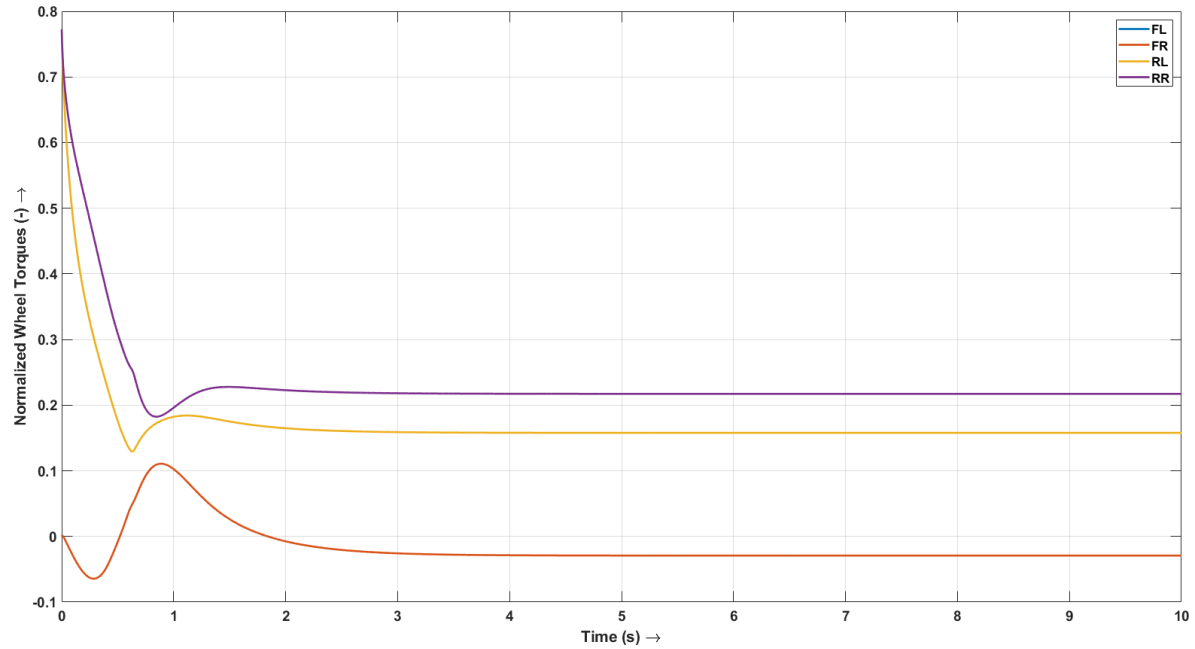


**Figure 5.5:** Result of simulation - wheel torques

The implemented controller demonstrates the capability to successfully initiate and sustain the vehicle in the desired drift state with the new tire model optimized for drift manoeuvres. However, it is observed that the target yaw rate is not fully attained, potentially due to the high target rear slip ratios. Nevertheless, the controller effectively maintains the longitudinal velocity at the desired value, with only minor deviations in steering from the equilibrium position. The steering profile reveals that the controller initially steers into the turn to generate the necessary yaw rate for initiating the drift, and subsequently counter-steers to prevent the vehicle from spinning out during the maneuver.

## 5.2. Drift Control using only Wheel Torques

Subsequently, the steer controller was disengaged from the previous control system and set to its equilibrium value ($\delta_{eq}$). The vehicle's initial conditions were chosen to be in close proximity to the computed drift equilibrium, allowing for a smooth transition as the car was propelled towards the equilibrium state, relying solely on wheel torques for control.

In this modified approach, the rear motor torques ($\tau_{RL}$ and $\tau_{RR}$) were exclusively utilized to achieve a target slip ratio ($\kappa_R$). Meanwhile, the front motor torques ($\tau_{FL}$ and $\tau_{FR}$) took on the responsibility of maintaining the desired longitudinal velocity ($v_x$) and generating the essential yaw moment ($M_z$) to ensure the vehicle adhered to the target lateral velocity ($v_y$) and yaw rate ($\dot{\psi}$). These control actions are effectively illustrated in the flowchart depicted in Figure 5.7, and the overall structure of the controller is visually represented in the block diagram showcased in Figure 5.6.

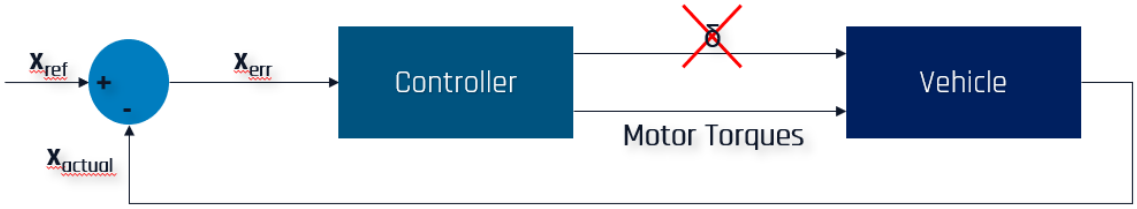


**Figure 5.6:** Block diagram of vehicle model and controller. "x" is a state vector consisting of yaw rate, sideslip and longitudinal velocity

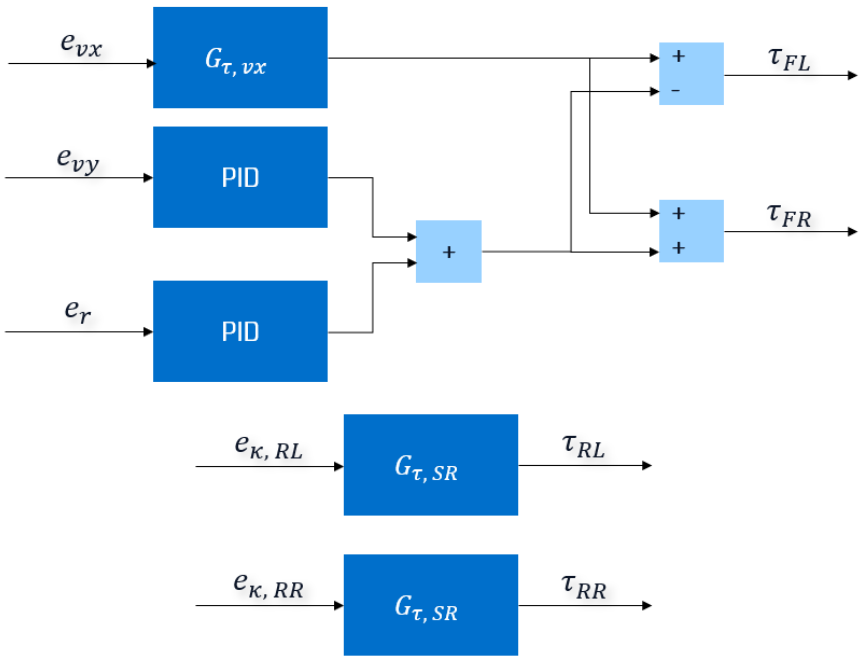


**Figure 5.7:** Flowchart showing the drift controller using only wheel torques

### 5.2.1. Simulation Results and Inferences

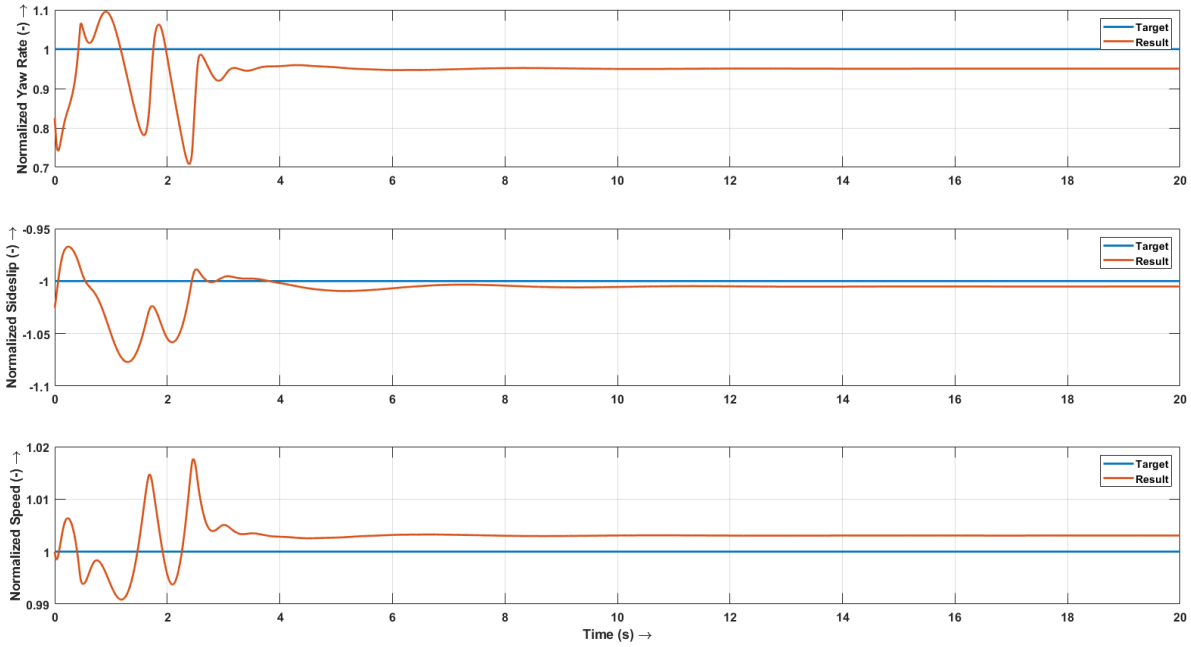


**Figure 5.8:** Result of simulation - vehicle states

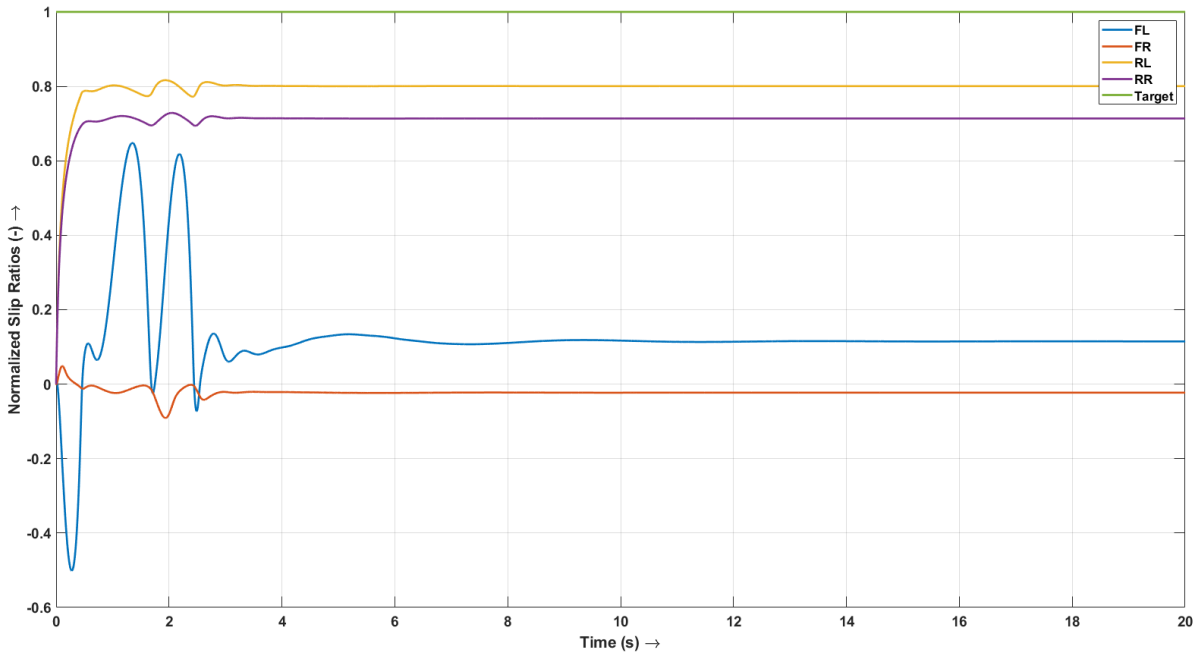


**Figure 5.9:** Result of simulation - slip ratios

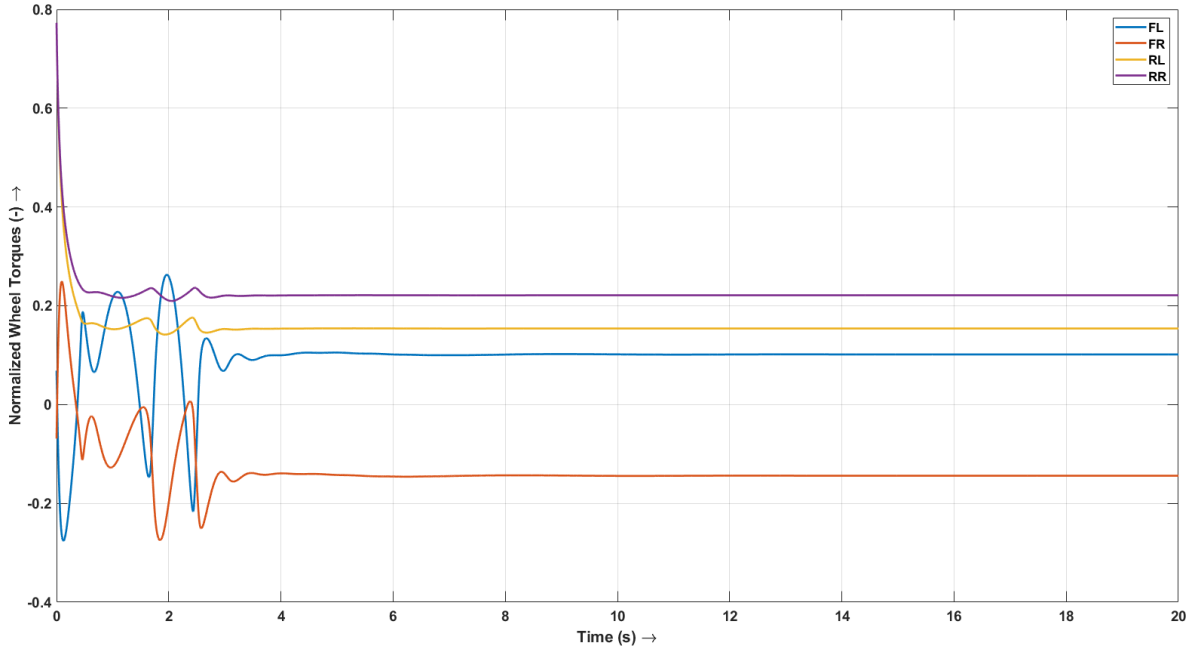


**Figure 5.10:** Result of simulation - wheel torques

The controller successfully achieves and maintains the vehicle in the desired drift state, as evidenced by its ability to closely match the steady-state values of longitudinal velocity, sideslip, and yaw rate with the target values.

Furthermore, to assess the controller's ability to handle different scenarios, a second simulation was conducted, intentionally inducing slightly higher vehicle sideslip. The objective was to evaluate whether the controller could effectively stabilize the vehicle and sustain the drift under such conditions.

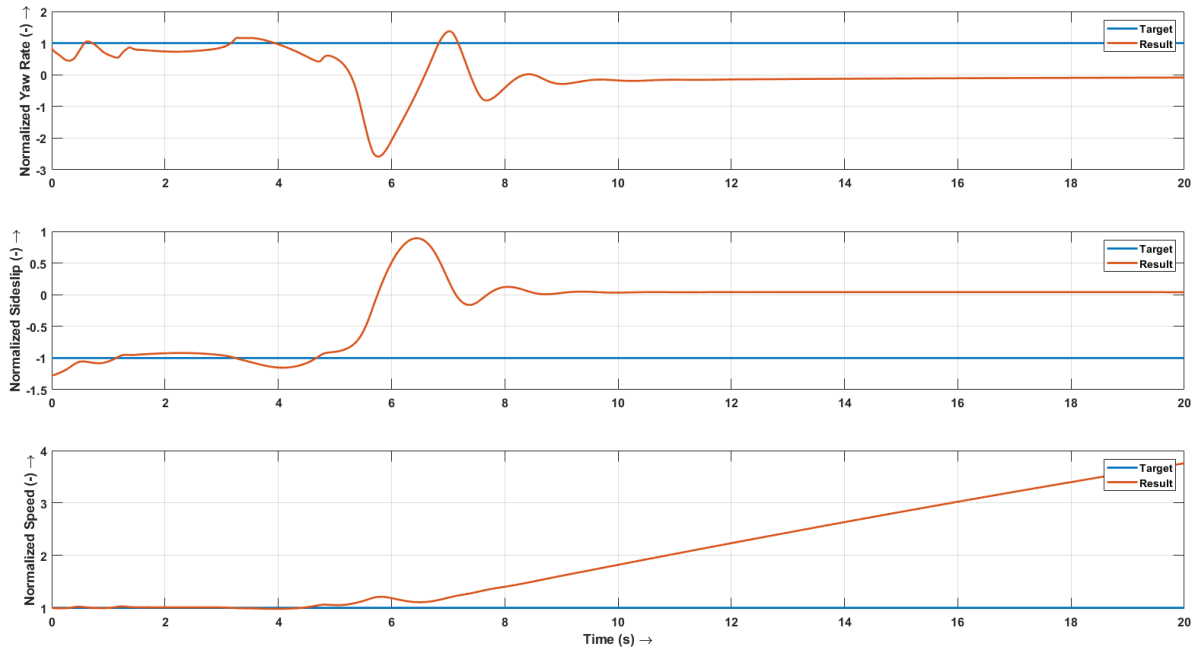


**Figure 5.11:** Result of simulation - vehicle states

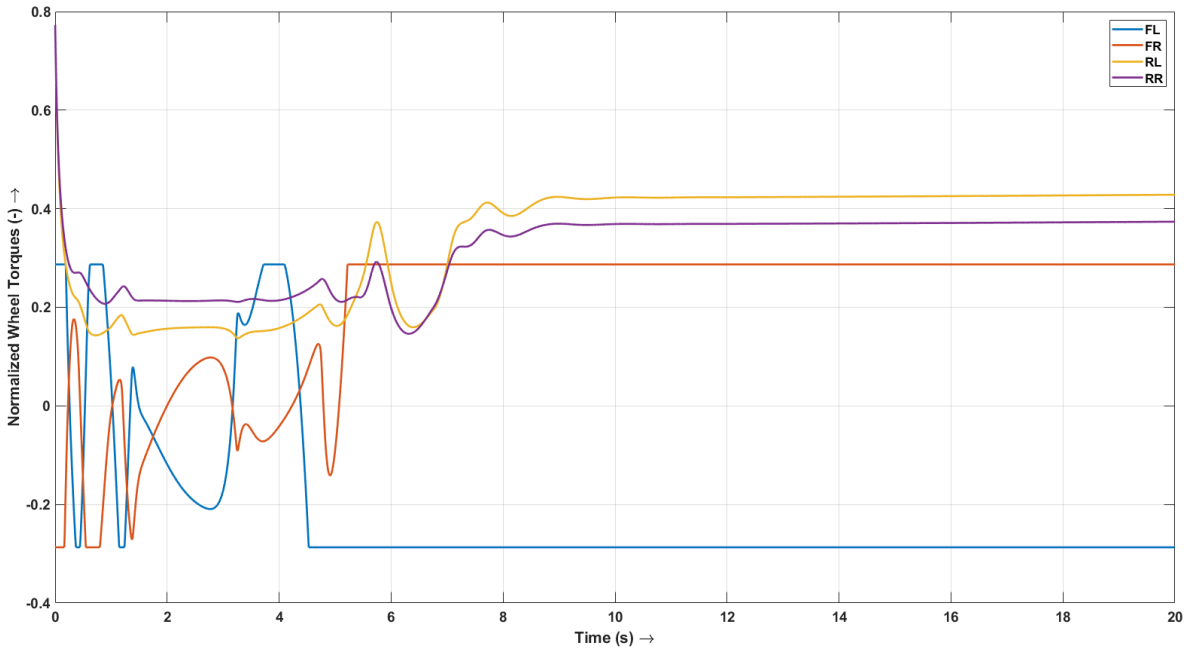


**Figure 5.12:** Result of simulation - wheel torques

Unfortunately, the controller fails to maintain the vehicle in the drift state under the given conditions. As a consequence, the vehicle experiences a loss of sideslip and begins to align with the direction of steering. The initial efforts to stabilize the vehicle inadvertently result in a reduction of the yaw rate. Moreover, the limitations on front motor torques prevent the generation of sufficient yaw moment to increase the yaw rate to the target value. This outcome brings to light a significant flaw in the approach that relies on the front axle alone to control longitudinal velocity, sideslip, and yaw rate.

## 5.3. Optimization Method

To address the limitations of the previous approach and create a more comprehensive and effective controller, an optimization method was devised. This novel optimization scheme aims to optimize the allocation of wheel torques, ultimately achieving the target values for longitudinal force ($F_{x,target}$), lateral force ($F_{y,target}$), and yaw moment ($M_{z,target}$) at the vehicle level. The incorporation of this optimization method allows the controller to take a more holistic approach to drift control, overcoming the difficulties faced due to actuator limits.

Formulation:

$$\begin{gathered}\min_{\tau} w_1 \left(F_x(\tau) - F_{x,target}\right)^2 + w_2 \left(F_y(\tau) - F_{y,target}\right)^2 + w_3 \left(M_z(\tau) - M_{z,target}\right)^2 \\ \text{subject to: (3.1), (3.3), (3.4), (3.5) and (3.2)} \\ \tau_{\text{min}} \leq \tau \leq \tau_{\text{max}}\end{gathered} \tag{5.3}$$

The optimization process was carried out using the `fmincon` function within MATLAB, employing the `sqp` algorithm. The primary focus of the optimization was to achieve state derivative targets through forces and moments at the vehicle level, rather than directly optimizing the vehicle states. This approach ensures that the controller can effectively stabilize the vehicle, even if the state targets do not precisely align with the drift equilibrium.

To guide the optimization process, specific weights were assigned to different objectives. The weights $w_1$, $w_2$, and $w_3$ were set to 1, 2, and 6, respectively, reflecting the priority given to yaw rate tracking. This prioritization plays a crucial role in ensuring that the vehicle remains at the drift state, preventing any deviations that could compromise the stability of the drift maneuver [7].

During the simulations, the steering angle ($\delta$) was set to its equilibrium value ($\delta_{eq}$), not relying on corrections from the driver to keep the vehicle from spinning out or losing sideslip.

$$\begin{aligned} F_{x,target} &= m\left(\dot{v}_{x,reqd} - v_{y,target}\,\dot{\psi}_{target}\right) & \dot{v}_{x,reqd} &= k_{P,vx}\left(v_{x,target} - v_x\right) \\ F_{y,target} &= m\left(\dot{v}_{y,reqd} + v_{x,target}\,\dot{\psi}_{target}\right) & \dot{v}_{y,reqd} &= k_{P,vy}\left(v_{y,target} - v_y\right) \\ M_{z,target} &= I_{zz}\ddot{\psi}_{reqd} & \ddot{\psi}_{reqd} &= PID\left(\dot{\psi}_{target} - \dot{\psi}\right) \end{aligned} \tag{5.4}$$

### 5.3.1. Simulation Results and Inferences

The evaluation of the optimization method commenced by subjecting it to the same two simulation cases used to assess the simpler wheel torque controller.

Case 1

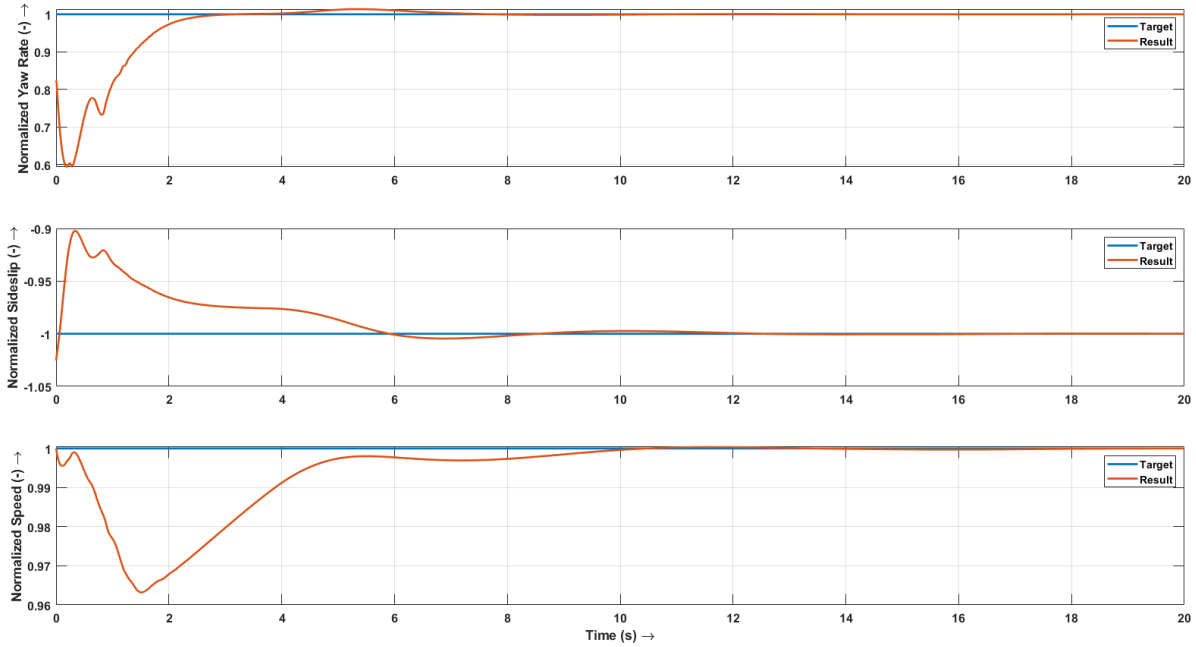


**Figure 5.13:** Result of simulation - vehicle states

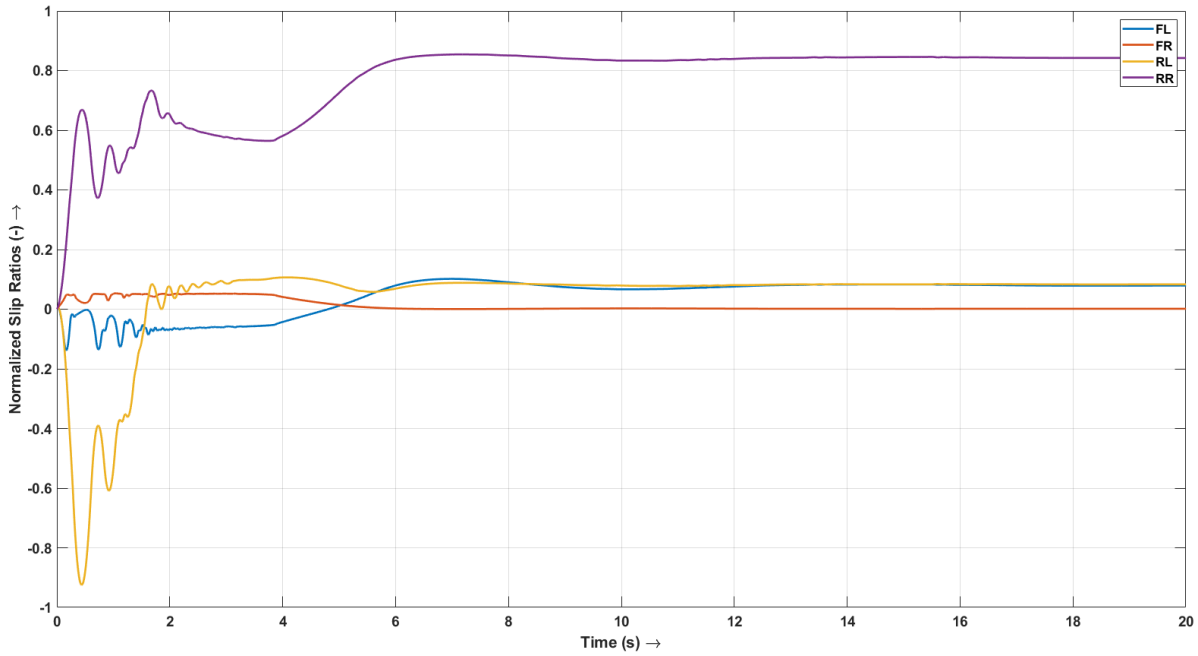


**Figure 5.14:** Result of simulation - slip ratios

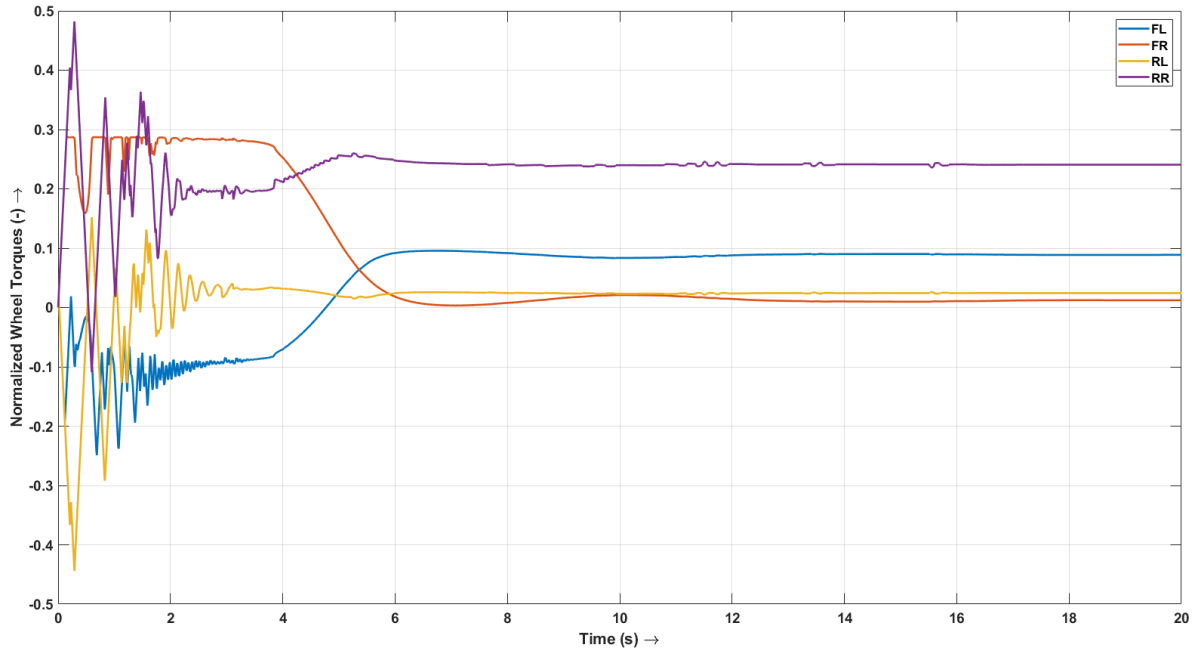


**Figure 5.15:** Result of simulation - wheel torques

The optimization method exhibited excellent performance, successfully maintaining the vehicle at the desired drift state. The steady-state values for longitudinal velocity, sideslip, and yaw rate closely matched the target values, indicative of the controller's ability to achieve precise control over these critical parameters.

During the initial phase of the simulation, where the rear tires experience zero slip, the vehicle encountered understeer and deviated from the drift state at $t = 0.5$ seconds. However, the optimizer promptly responded to this situation, strategically applying rear wheel torques. This action effectively reduced the lateral force on the axle while generating a yaw moment through the longitudinal forces.

This demonstrates the optimizer's capability to control the longitudinal slip, thus influencing both the lateral force on the axle and the torque vectoring yaw moment.

Case 2

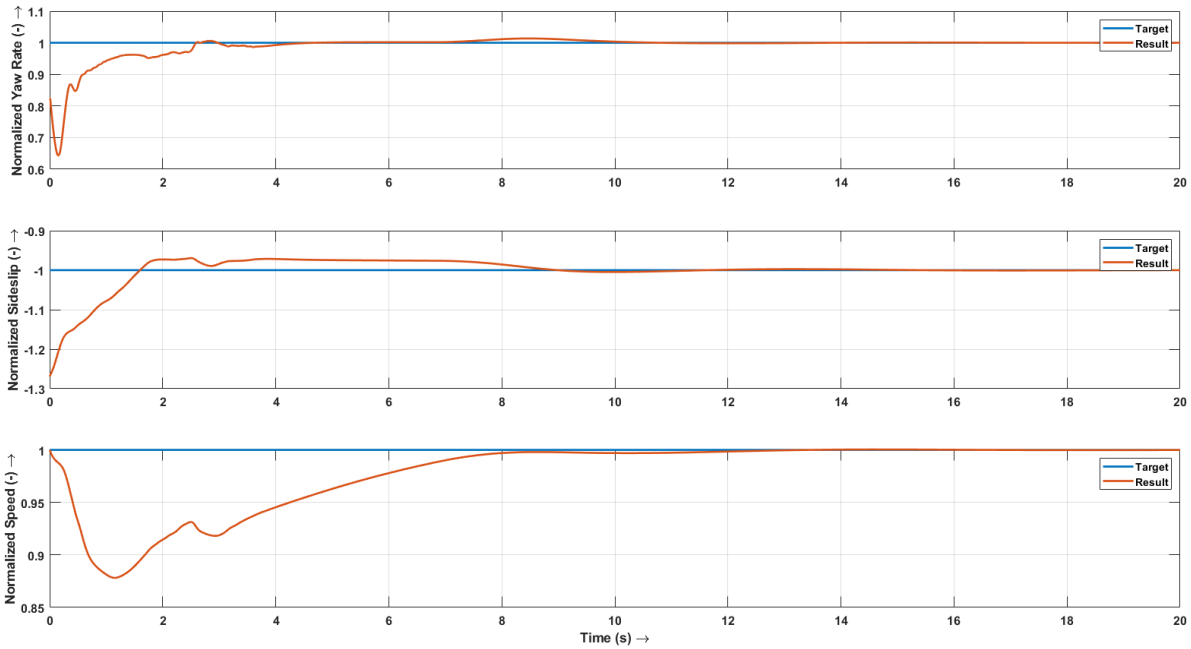


**Figure 5.16:** Result of simulation - vehicle states

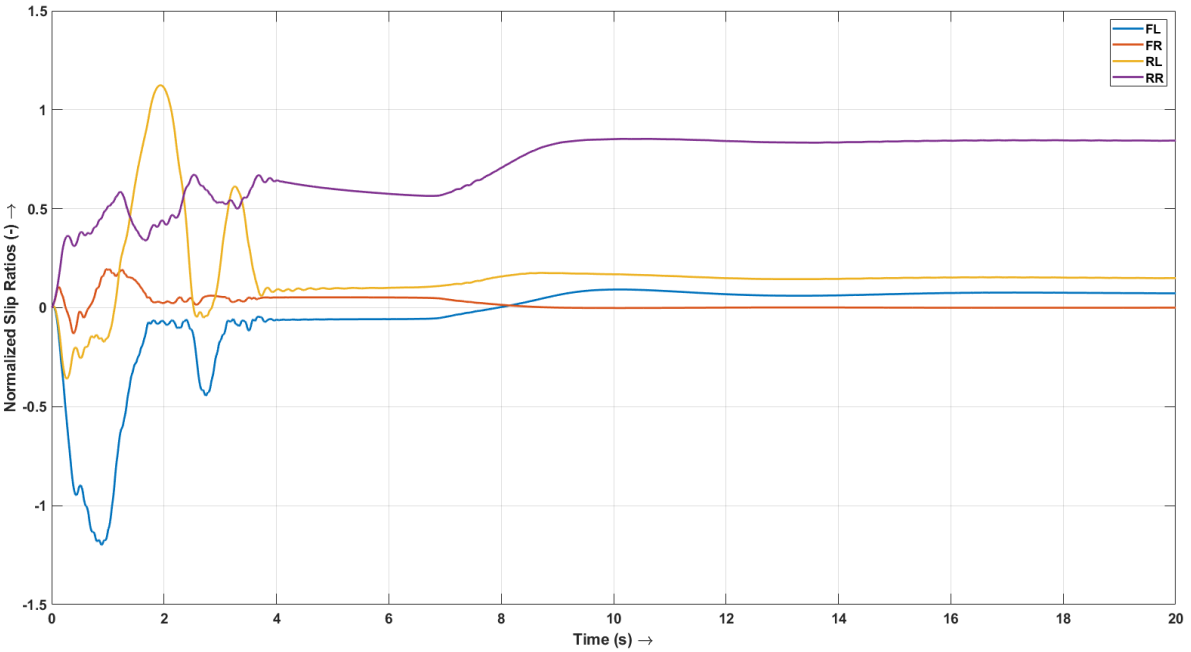


**Figure 5.17:** Result of simulation - slip ratios

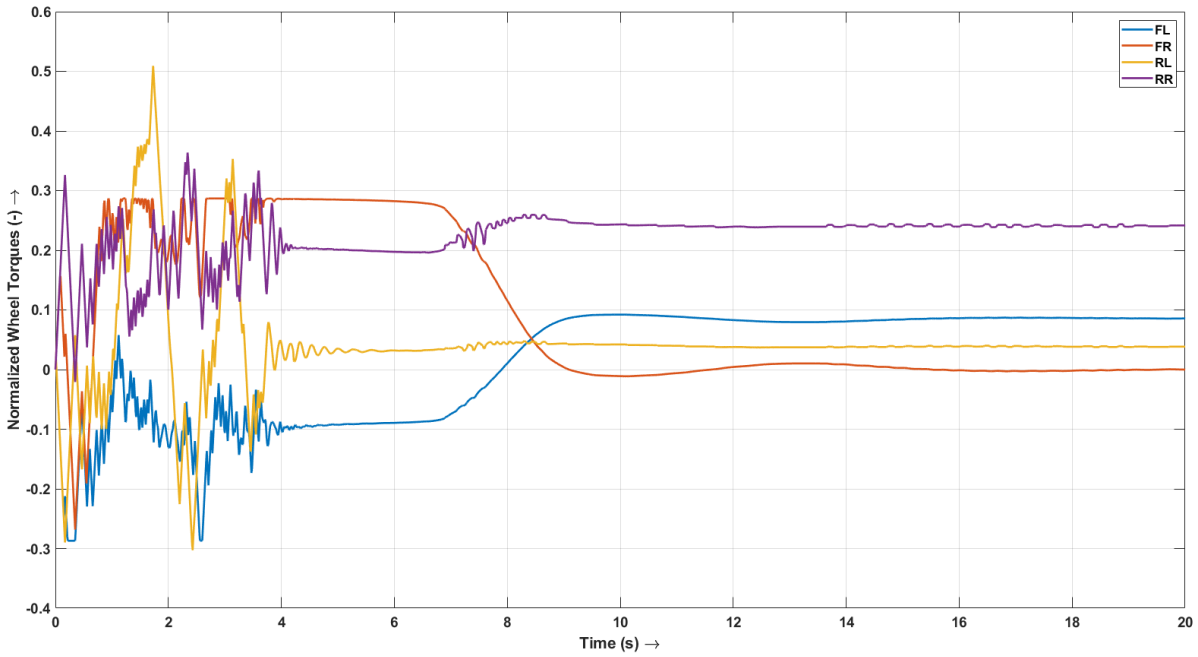


**Figure 5.18:** Result of simulation - wheel torques

The controller effectively sustains the vehicle in the desired drift state, achieving steady-state values for longitudinal velocity, sideslip, and yaw rate that precisely align with the target values. The control strategy follows a well-coordinated sequence: initially, the controller prioritizes reaching the target yaw rate, ensuring that it is attained within the first second ($t < 2$s) of the simulation. Subsequently, the controller shifts its focus towards reaching the target longitudinal velocity, utilizing the rear wheel torques to achieve this objective. During this period, the front wheel torques play a vital role in controlling the yaw rate, ensuring it remains stable and in line with the desired value.

## 5.4. Simulation Results

In this section, the simulation results demonstrate the controller's advanced capabilities in handling various complex driving scenarios. The objective was to showcase its ability to not only stabilize the vehicle and maintain it in a drift state but also to effectively interact with a human driver, follow a designated trajectory, and maintain high sideslip angles.

To achieve this, simulations were conducted where the controller was tasked with initiating a drift, sustaining it for a considerable duration, changing directions, and subsequently initiating and maintaining another drift in the opposite direction. The steering profile was thoughtfully designed to first align with the initial turn direction and then counter-steer as the vehicle began to destabilize and develop sideslip. During the change in direction, the motor torque was momentarily cut, allowing the target states of the controller to be altered. It was during this phase, at $t = 21$ seconds, that the counter-steer for the opposite direction was initiated.

Additionally, the system was subjected to delays in both the input and output sides. This was essential to create a more realistic environment, emulating the real-world challenges and feedback delays often encountered during implementation.

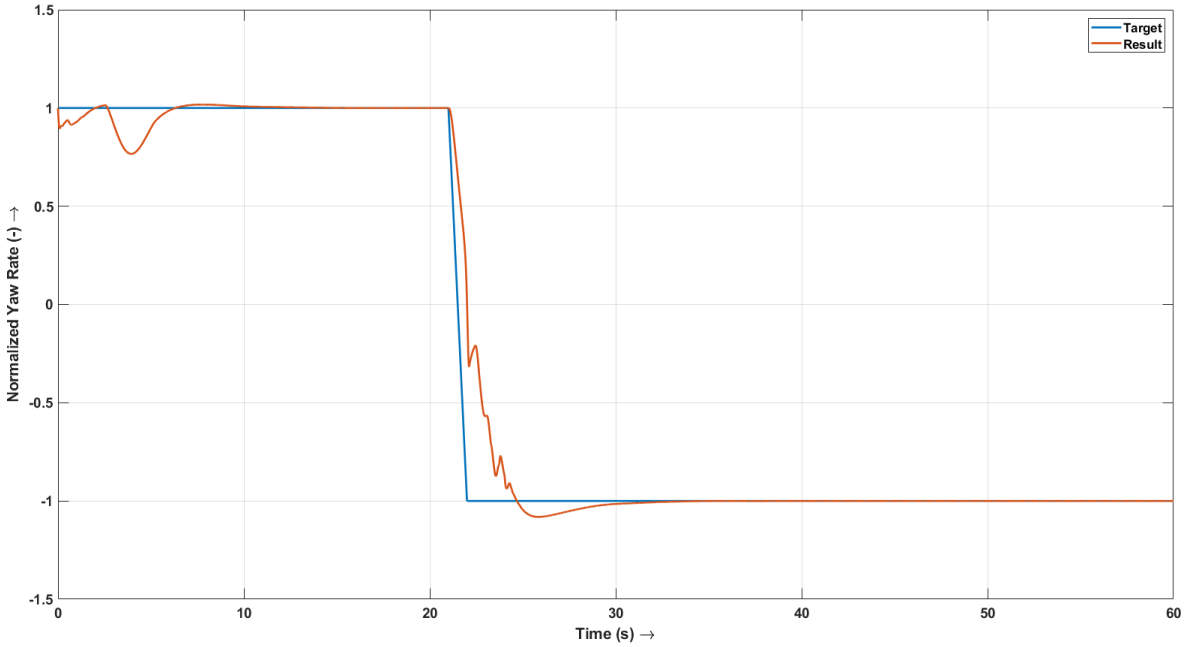


**Figure 5.19:** Result of simulation - yaw rate

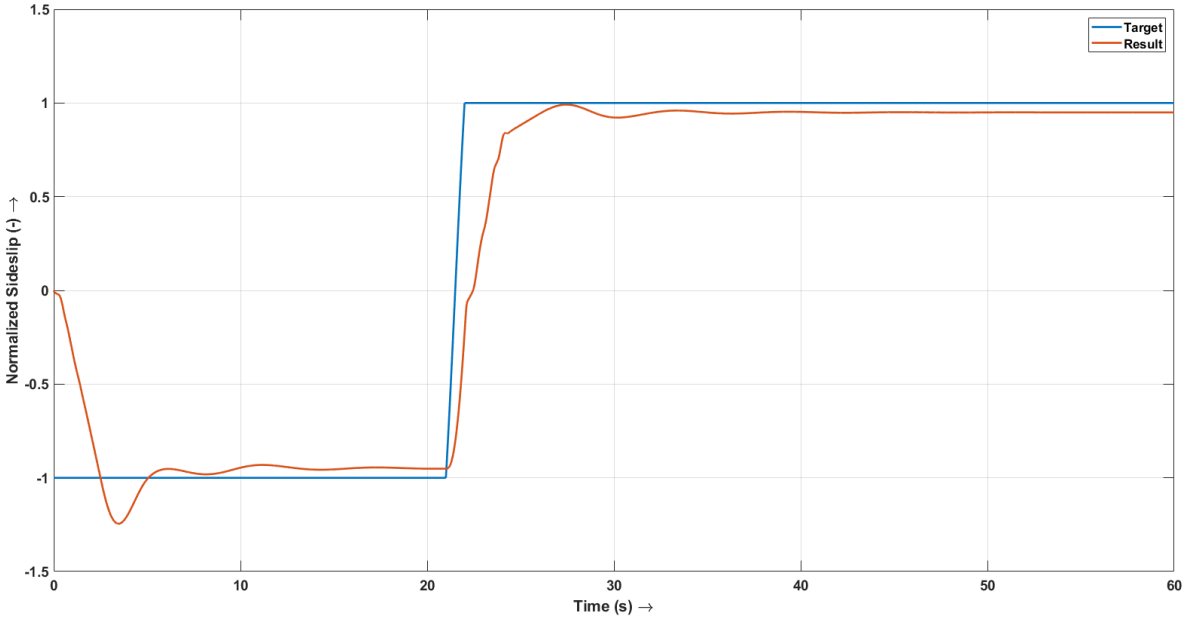


**Figure 5.20:** Result of simulation - sideslip

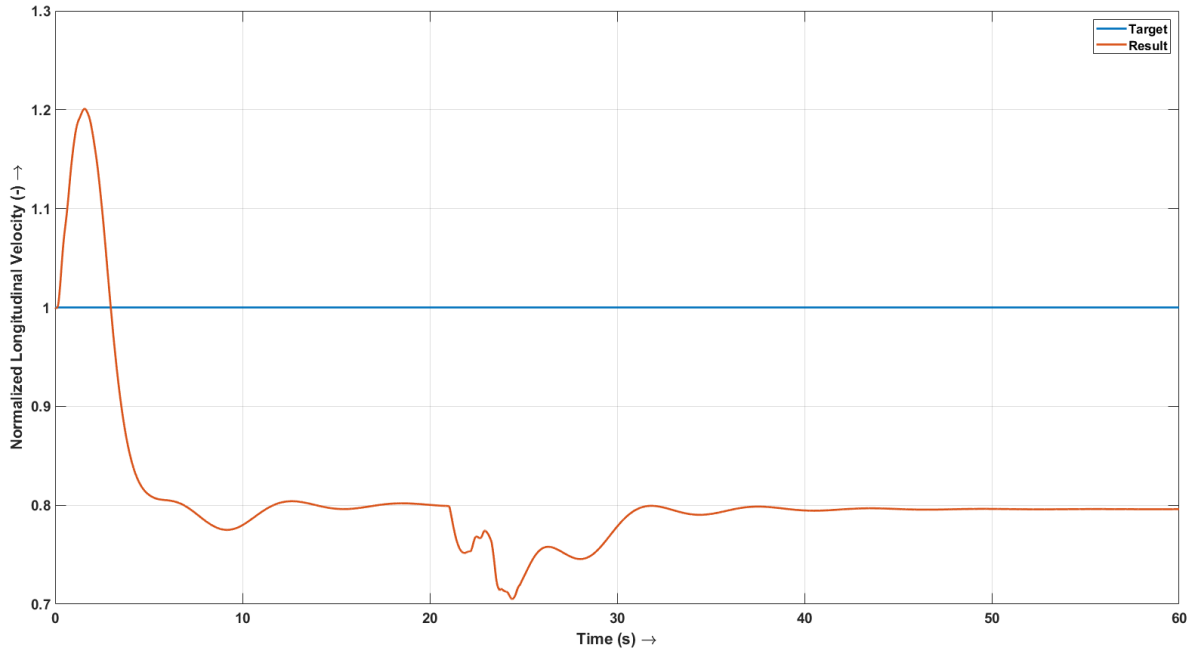


**Figure 5.21:** Result of simulation - longitudinal velocity

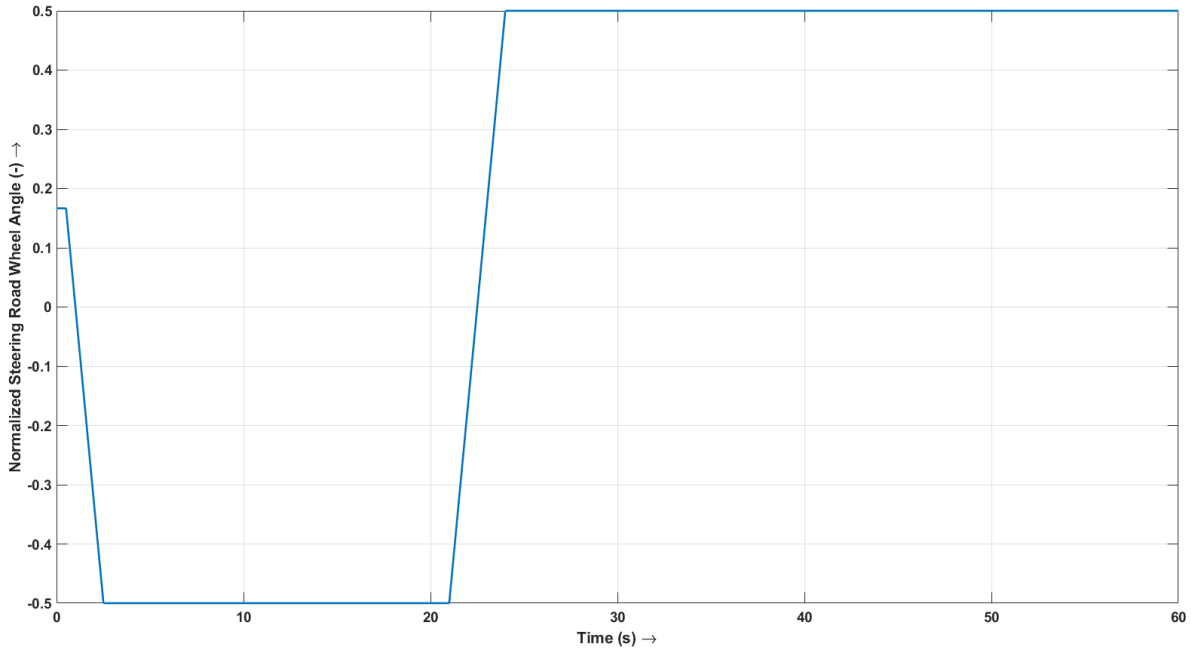


**Figure 5.22:** Result of simulation - steering (road wheel angle)

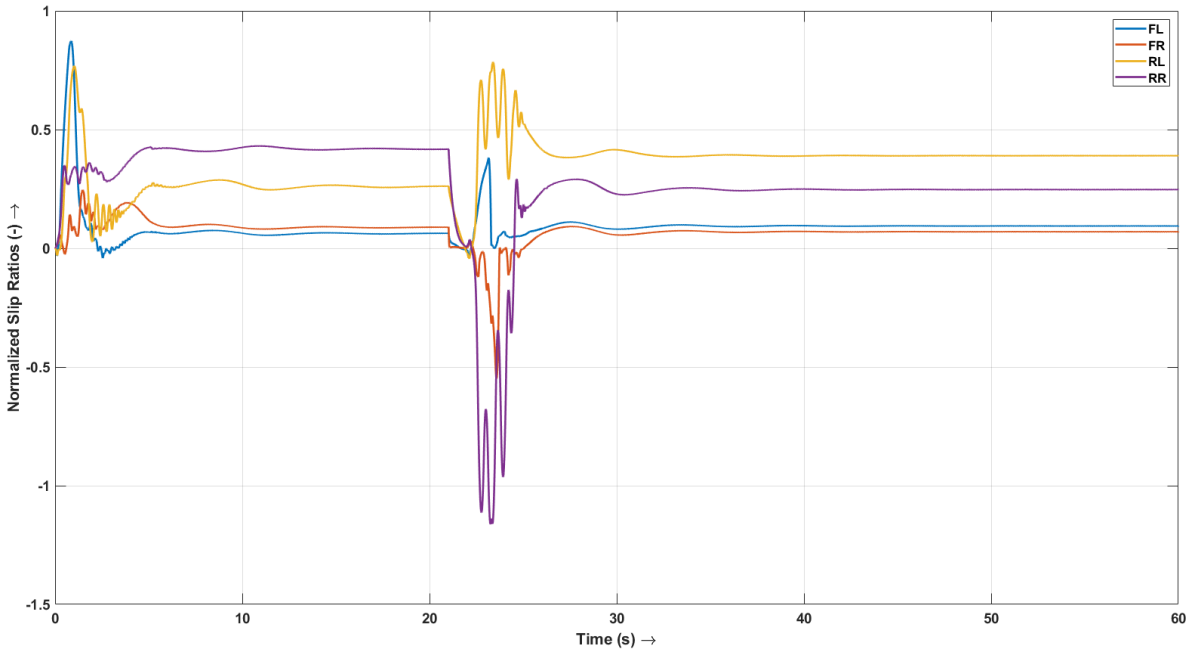


**Figure 5.23:** Result of simulation - slip ratio

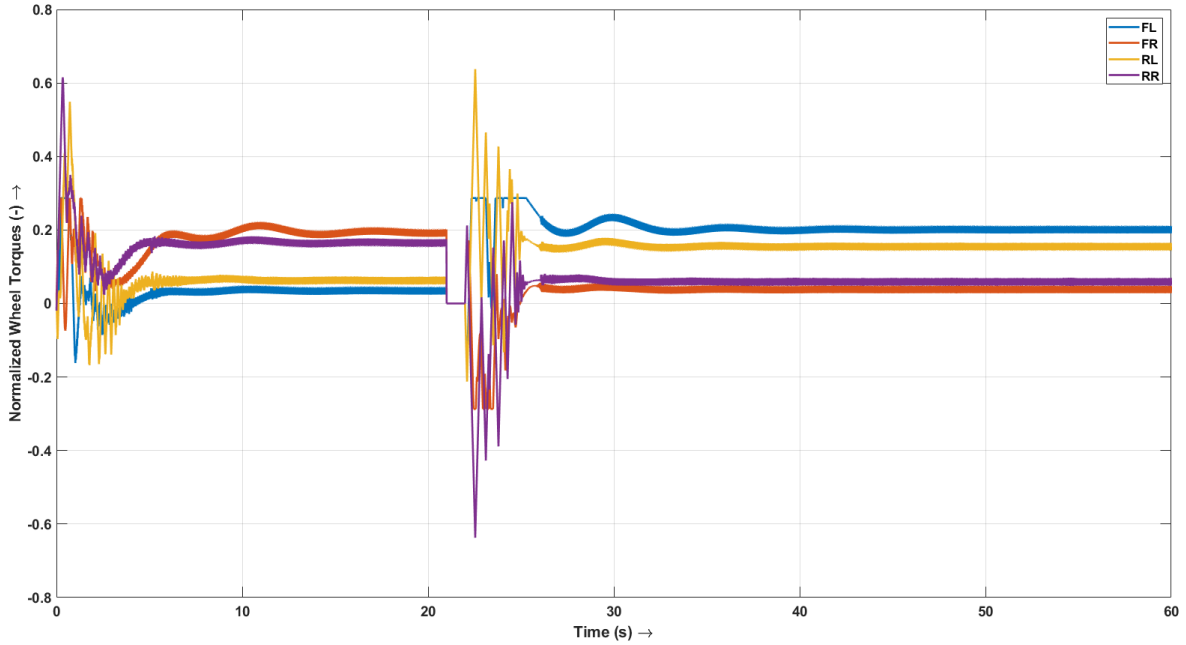


**Figure 5.24:** Result of simulation - wheel torques

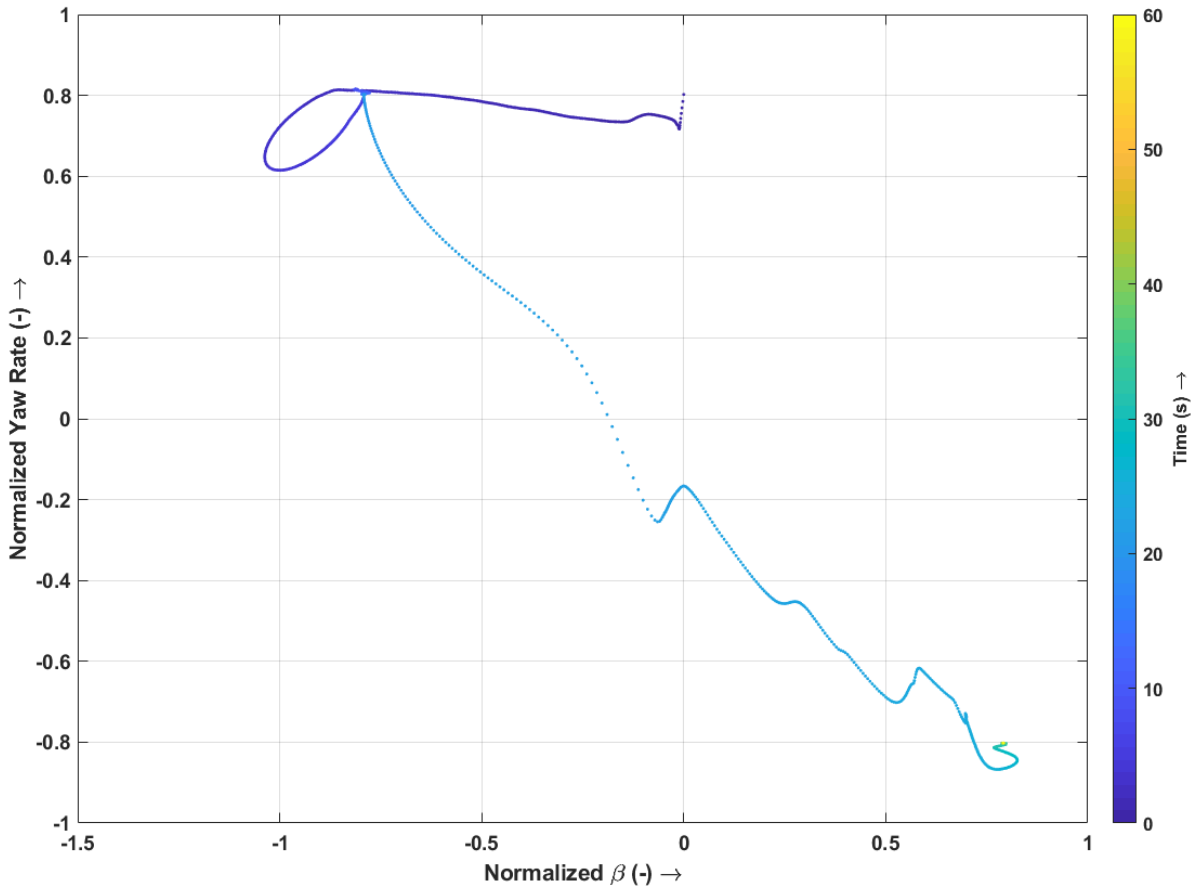


**Figure 5.25:** Result of simulation - phase plane

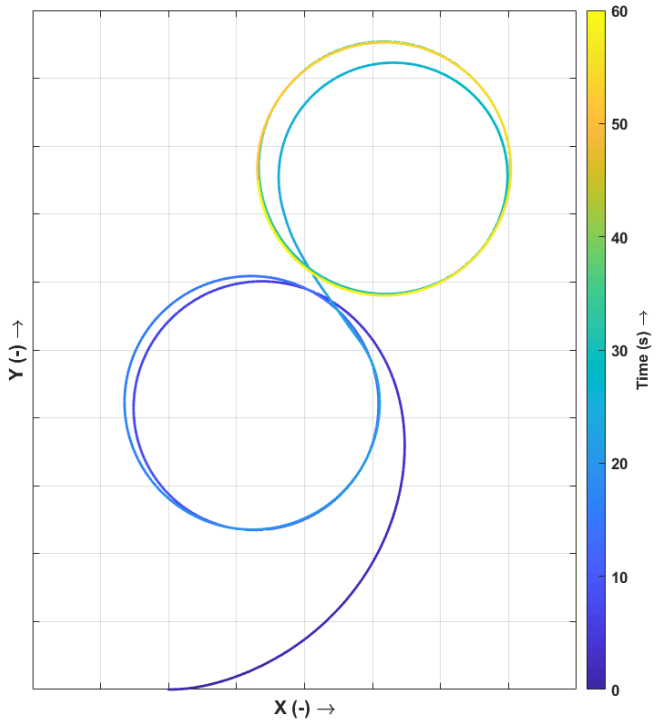


**Figure 5.26:** Result of simulation - vehicle path

The controller's performance is evident as it successfully initiates and maintains drift in both directions. Notably, it achieves identical steady-state magnitudes for equilibrium yaw rate, sideslip, and longitudinal velocity in both cases. However, it is worth noting that the achieved equilibrium value of longitudinal velocity falls below the target due to the limitations imposed by tire-road friction. The lateral forces required to achieve the desired target longitudinal velocity and yaw rate at equilibrium exceed the maximum capabilities of the tires. Consequently, the controller faces a trade-off between achieving the desired yaw rate and maintaining the longitudinal velocity target, and prioritizes yaw rate over longitudinal velocity due to its higher weight in the cost function. Also, the path followed by the vehicle closely aligns with the steady-state trajectory during the first complete circle in both directions, signifying the controller's precision and ability to consistently maintain the desired drift behavior.

After the critical torque cut period from $t = 21$ seconds to $t = 22$ seconds, the controller expertly handles the maneuver. The yaw rate experiences a temporary drop and changes direction, seamlessly following the steering inputs. Subsequently, the controller deftly utilizes the wheel torques to generate the necessary vehicle sideslip in the opposite direction, facilitating a smooth and controlled transition from one drift direction to the other.

## 5.5. Theoretical Basis for Optimization Method

The theoretical basis for the optimization method relies on demonstrating two crucial aspects of the controller's capabilities. Firstly, it is essential to show that the target forces and moments calculated based on state errors for longitudinal velocity, lateral velocity, and yaw rate effectively lead the system to achieve its desired target states. Secondly, it is vital to establish that the optimizer can indeed allocate individual wheel torques to achieve these target forces and moments.

To establish the first part, the Lyapunov method is employed to demonstrate the asymptotic stability of the closed-loop system. For each state variable, a Lyapunov function is chosen, represented by the equation (5.5). The function involves the target state and the difference between the target and actual states. By analyzing the time derivative of this function, the system's stability characteristics can be discerned. In particular, equations (5.6) and (5.7) illustrate the stability conditions for longitudinal velocity ($v_x$), lateral velocity ($v_y$), and yaw rate ($r$) with appropriate proportional and PID controllers.

$$\begin{aligned} V(x) &= \frac{1}{2}(x_{target} - x)^2 \\ \dot{V}(x) &= -(x_{target} - x)\dot{x} \end{aligned} \tag{5.5}$$

For the first 2 states, $v_x$ and $v_y$,

$$\dot{V}(x) = -k_P\,(x_{target} - x)^2 \tag{5.6}$$

since $\dot{x} = k_P\,(x_{target} - x)$ from (5.4), where $k_P > 0$.

For yaw rate, $\dot{\psi}$, which uses a PID controller instead of just a proportional gain, the gains are chosen and the integral contribution is limited such that $\ddot{\psi}\,(\dot{\psi}_{target} - \dot{\psi}) > 0$ if $x \neq x_{target}$. This would ensure

$$\dot{V}(\dot{\psi}) < 0 \quad \text{when} \quad \dot{\psi} \neq \dot{\psi}_{target} \tag{5.7}$$

From the above equations (5.5), (5.6) and (5.7), it is clear that the Lyapunov conditions for asymptotic stability at the target state are met, namely:

1. $V(x) = 0$ if and only if $x = x_{target}$
2. $V(x) > 0$ if and only if $x \neq x_{target}$
3. $\dot{V}(x) < 0$ for all values of $x \neq x_{target}$

The second part involves a controllability analysis, which explores the possible state derivatives achievable by manipulating individual wheel torques. The figure 5.27 showcases the tangent space for the vehicle in a drifting equilibrium condition, with longitudinal velocity $v_x = 15$ m/s, steering angle $\delta = 20°$,

yaw rate $\dot{\psi} = -30.21°$/s, sideslip $\beta = 29.24°$ and longitudinal slip of $4\%$, $12\%$, $18\%$ and $20\%$ across the four tires. The plot highlights the ability of the all-wheel torque vectoring system to independently control all three state derivatives. The plot reveals a lack of bidirectionality in controlling sideslip and speed, with the controller capable of only increasing the magnitude of sideslip and reducing the vehicle's speed. The limitation in achieving higher speeds is attributed to the fact that the equilibrium slips, have already reached or surpassed the threshold at which the tires generate the maximum longitudinal force. Likewise, increasing the magnitude of the vehicle sideslip proves to be difficult since the lateral forces have already reached their maximum potential at the selected equilibrium point. Consequently, pushing the sideslip further becomes impracticable as the system has already reached its peak lateral force capacity.

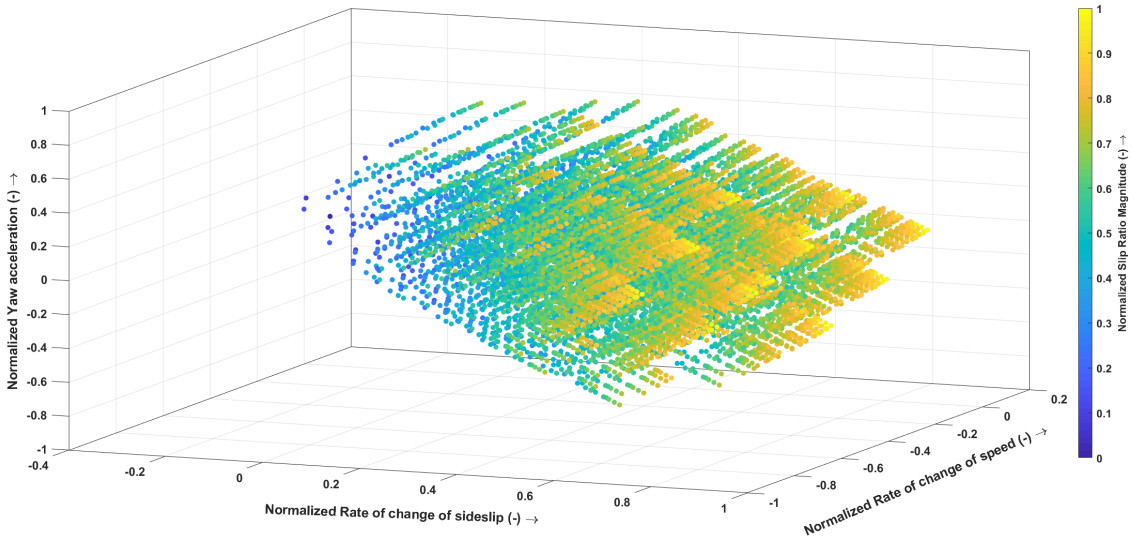


**Figure 5.27:** Tangent space with all-wheel torque vectoring

Furthermore, to verify the controller's effectiveness in driving the vehicle to its target state from various initial conditions, simulations were conducted. The phase portraits resulting from these simulations provide valuable insights into the controller's ability to guide the vehicle to its desired state, showcasing its robustness and adaptability in handling different scenarios.

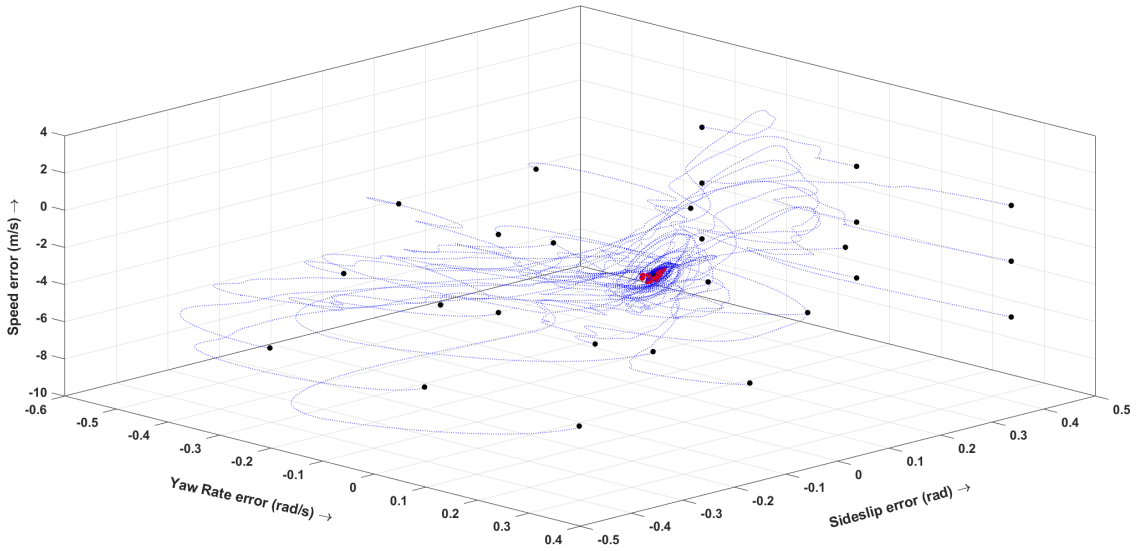


**Figure 5.28:** Phase portraits demonstrating controller capability from different initial conditions. The controller is able to drive the vehicle to the equilibrium (shown in red) from all the initial conditions

Overall, the theoretical underpinnings of the optimization method, coupled with the controllability analysis and simulation results, provide strong evidence of the controller's capability in achieving precise control and stability during drift maneuvers.

## 5.6. Controller Sensitivity to Model Parameters

The controller's sensitivity to mismatches between the vehicle model used in simulations and its internal model was thoroughly examined. This analysis encompassed several key vehicle and tire parameters, all evaluated under the same equilibrium steer position from the driver. The parameters taken into consideration were as follows:

1. Vehicle mass
2. Weight distribution
3. Yaw moment of inertia of vehicle
4. Rotational inertia of wheel and drivetrain
5. Tire friction coefficient - front and rear

To comprehensively assess the controller's robustness, deviations of $\pm 20\%$ were considered for vehicle mass, vehicle inertia, and tire properties, while $\pm 10\%$ deviations were applied to the remaining parameters.

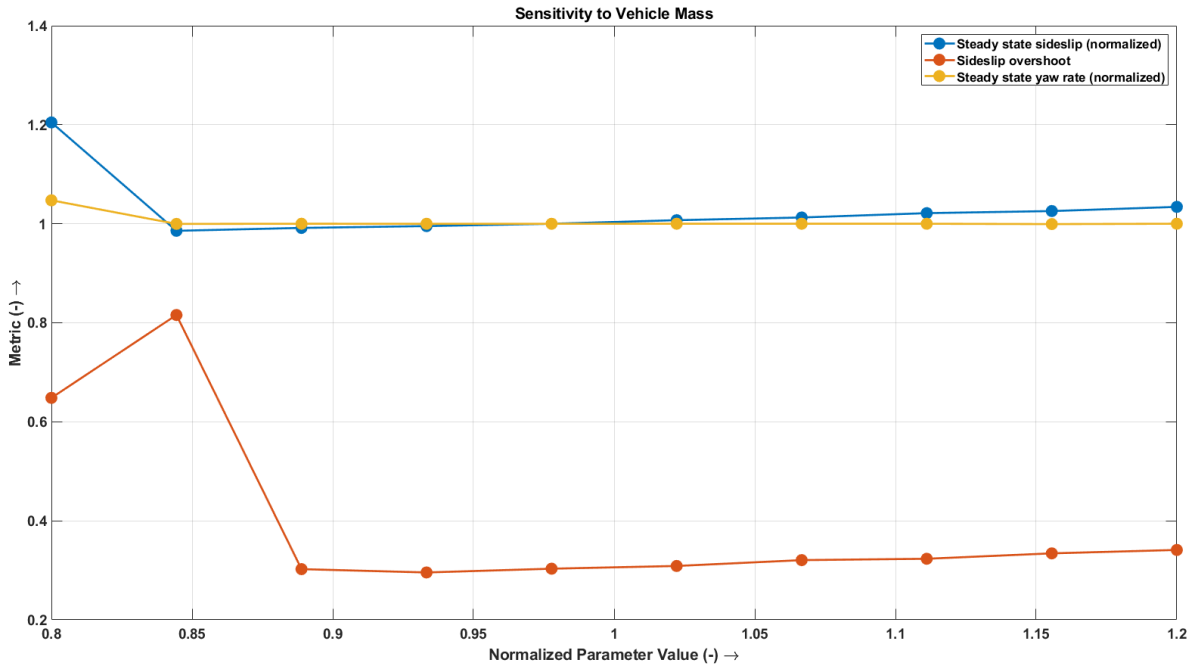


**Figure 5.29:** Sensitivity of controller performance to vehicle mass

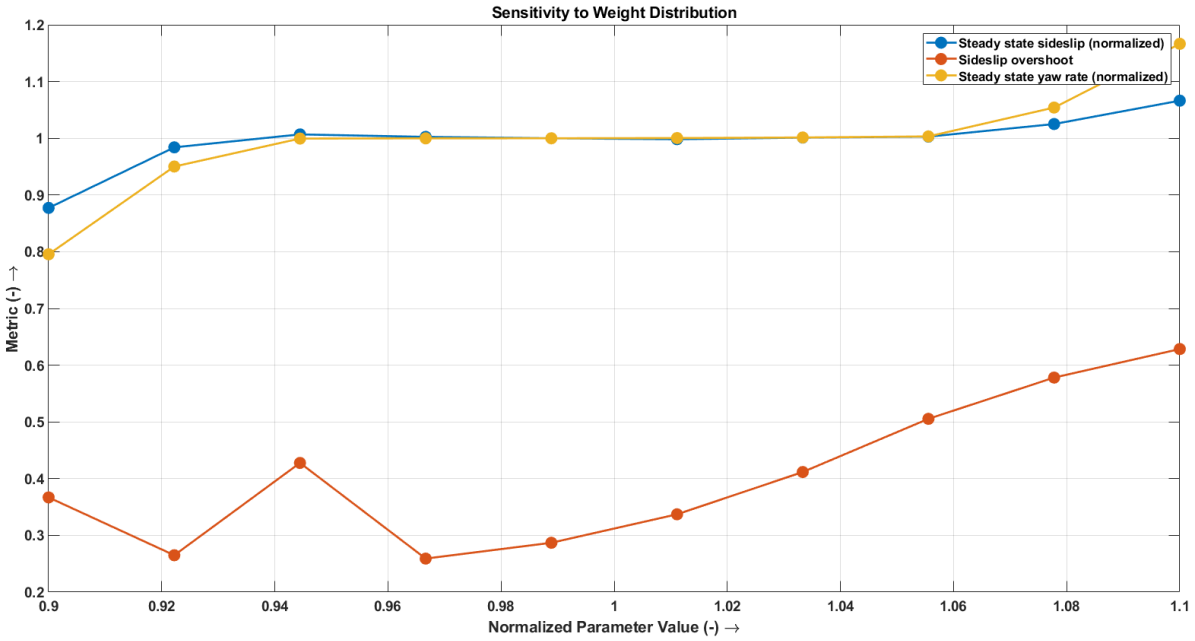


**Figure 5.30:** Sensitivity of controller performance to weight distribution

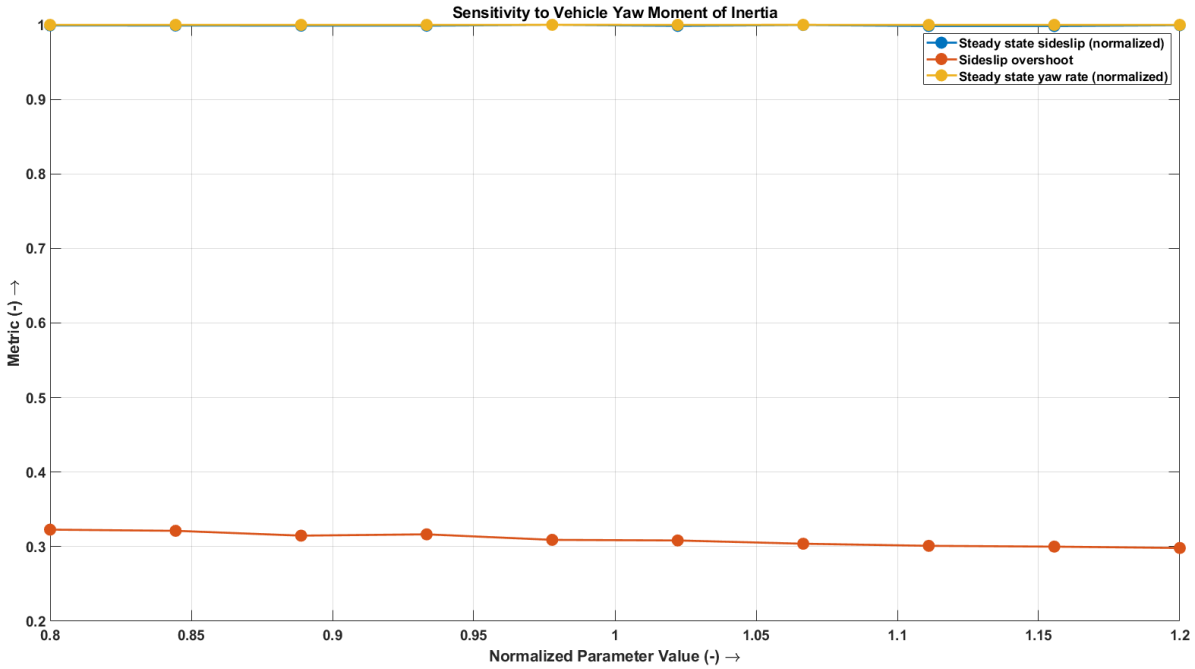


**Figure 5.31:** Sensitivity of controller performance to vehicle yaw moment of inertia

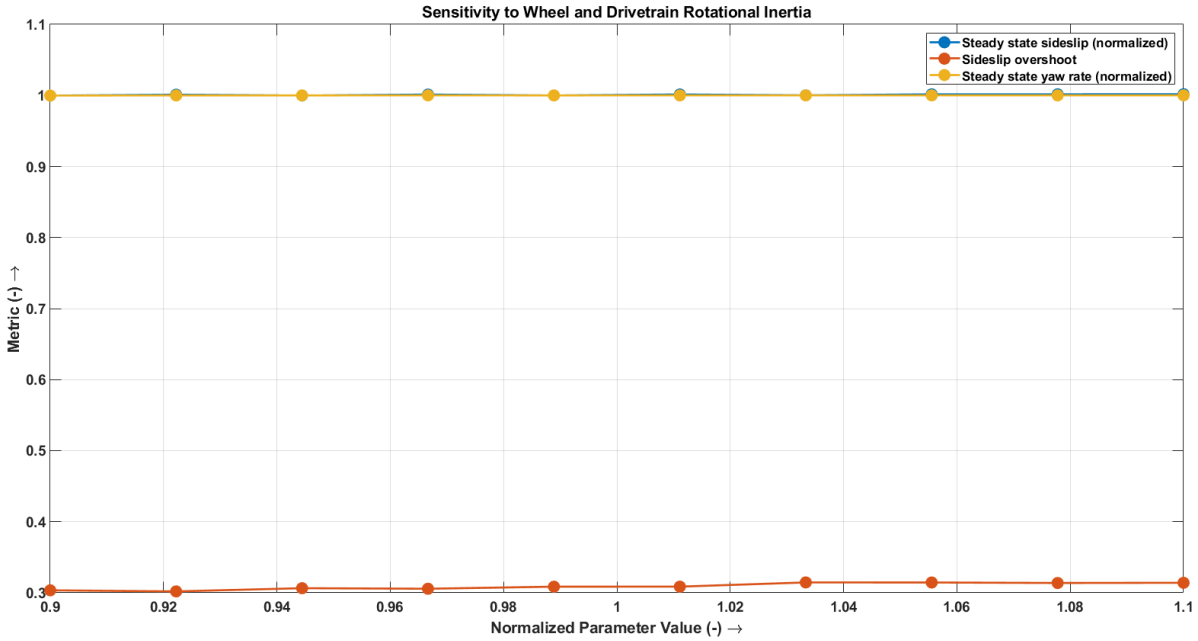


**Figure 5.32:** Sensitivity of controller performance to wheel and drivetrain rotational inertia

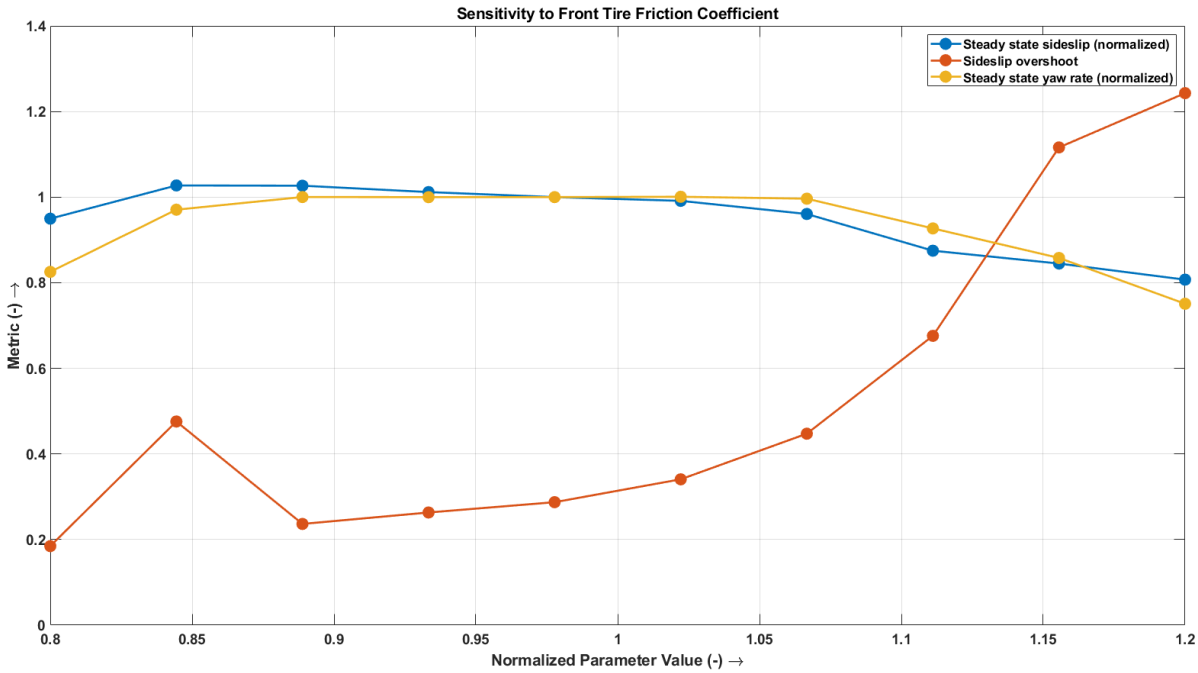


**Figure 5.33:** Sensitivity of controller performance to front tire friction coefficient

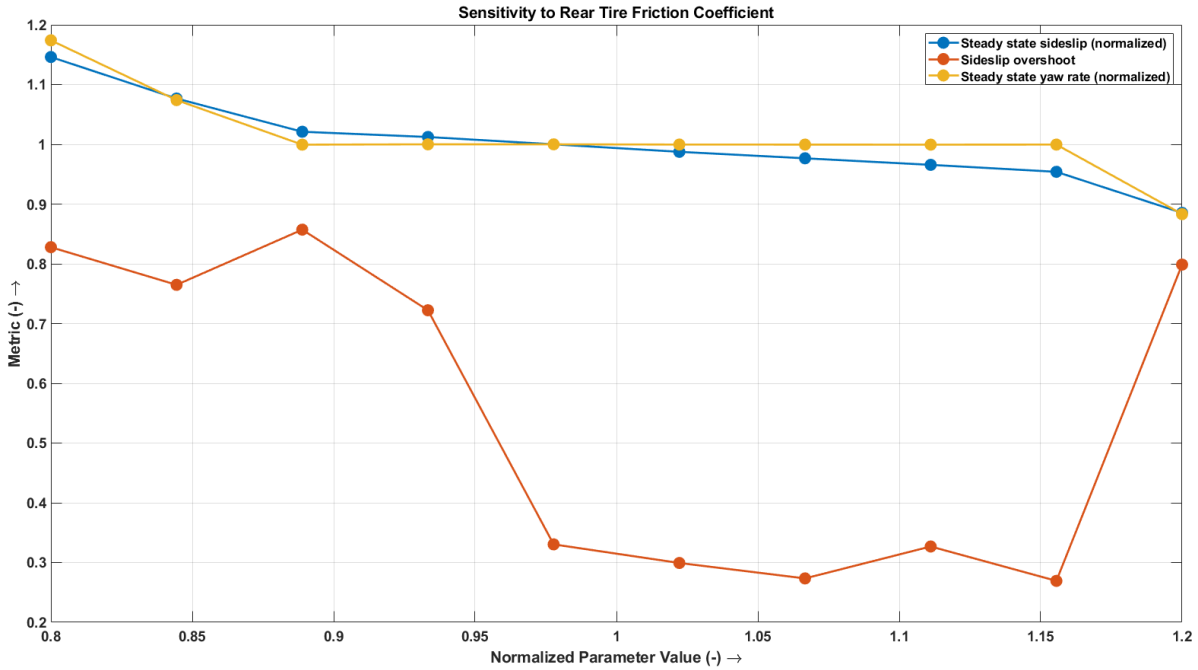


**Figure 5.34:** Sensitivity of controller performance to rear tire friction coefficient

The figures presented above clearly demonstrate the remarkable robustness of the controller when faced with parameter uncertainty in the vehicle model. Across the majority of parameters, with the exception of tire friction coefficients, the variation in steady-state yaw rate and sideslip remains within a commendable 20% even when subjected to extreme parameter mismatches. Moreover, the controller exhibits minimal sideslip overshoot, except under extreme tire friction coefficient mismatches.

Notably, even when facing the challenging scenario of extreme tire friction coefficient mismatches, the controller impressively maintains the vehicle's stability and prevents it from spinning out, all without requiring any evasive action from the driver. This exemplifies the controller's capacity to handle adverse conditions and adapt to parameter variations, making it a reliable and effective tool for maintaining precise control and stability during drift maneuvers.

## 5.7. Controller Sensitivity to Noise

The effect of noise on state inputs to the controller was analyzed in simulation and the results are plotted below. Band-limited white noise was added to the inputs of the controller to simulate state measurement noise. The robustness of the controller is evident and the vehicle is stablized to an equilibrium state close to the one in the absence of noise (figures 5.19, 5.21 and 5.20).

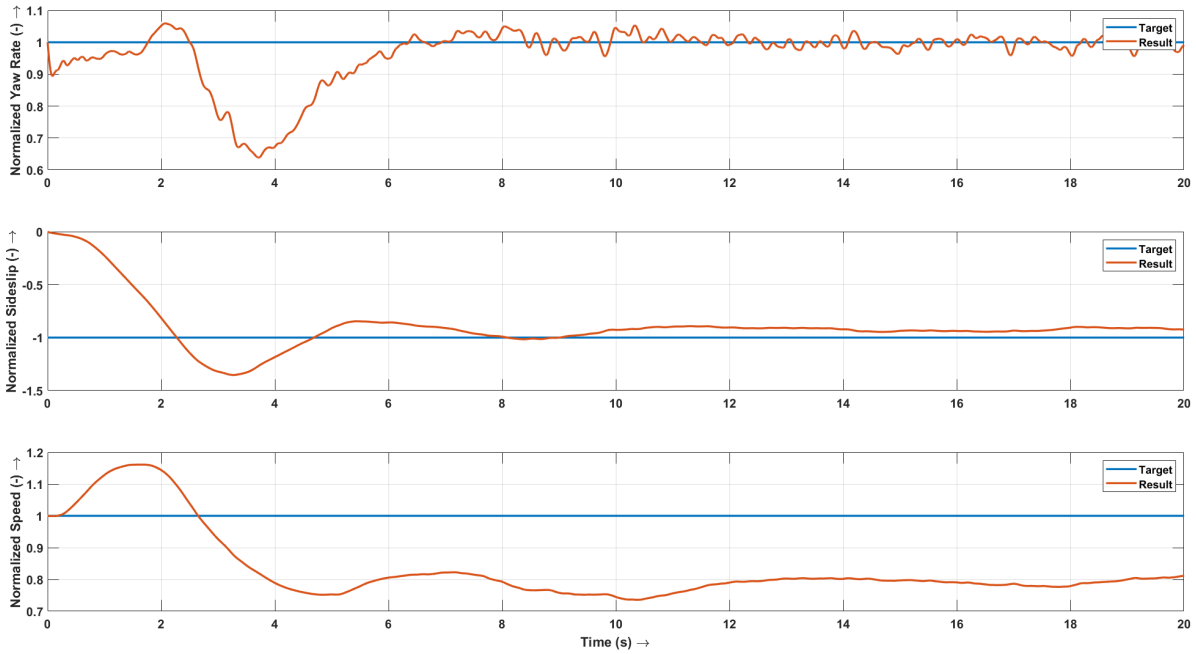


**Figure 5.35:** Simulation results - vehicle states

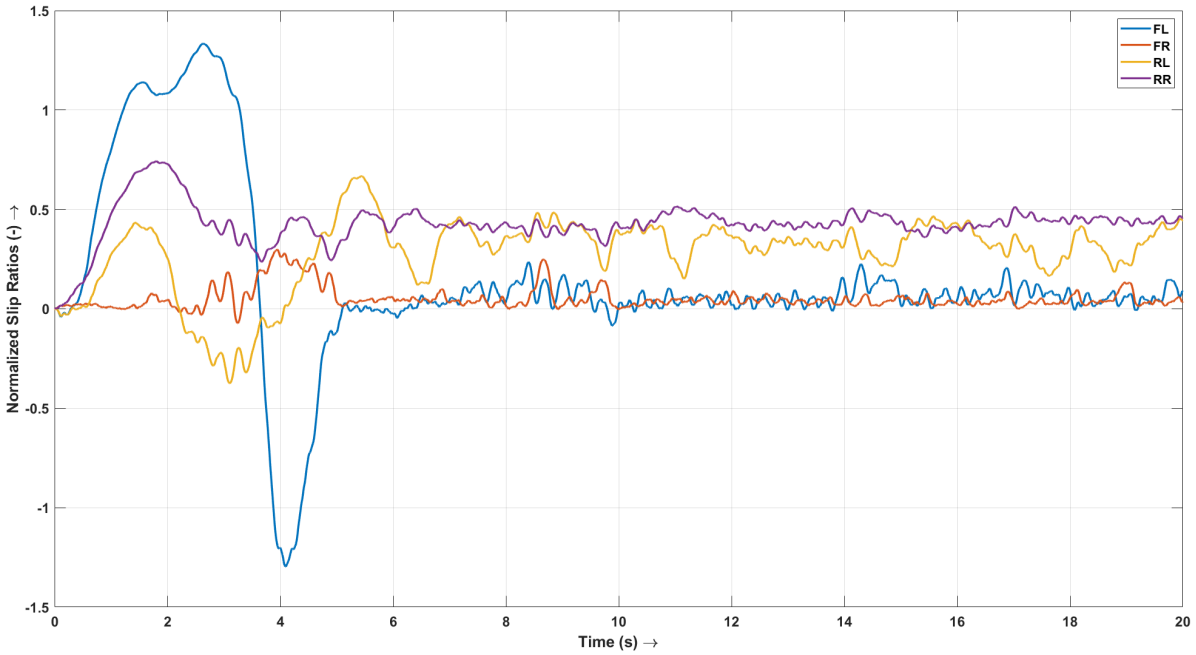


**Figure 5.36:** Simulation results - slip ratios

## 5.8. Summary

In this chapter, the design and evaluation of a controller for drift control are discussed. The controller aims to maintain the vehicle in a drift state while controlling the vehicle states - longitudinal velocity, lateral velocity, and yaw rate. The performance of the controller is evaluated through simulation results and sensitivity analysis to model parameters.

An initial simulation was developed controlling steering along with wheel torques to verify that the newly obtained tire parameters (from Chapter 3) can capture drift dynamics in simulation. Thereafter, the

steering position was fixed to the equilibrium position and the vehicle was made to initiate and stabilize drift using only the four wheel torques. The initial attempt of decoupling control over lateral dynamics - the sideslip and yaw rate and the longitudinal dynamics - longitudinal velocity, did not work due to actuator limits, and a more holistic optimization-based method was chosen.

The method optimizes the wheel torques to achieve target longitudinal force, lateral force, and yaw moment on the vehicle. The optimization is performed using the MATLAB `fmincon` function with the `sqp` algorithm. Simulation results demonstrate the effectiveness of the optimization method in maintaining the vehicle in a drift state while achieving the desired target values for longitudinal velocity, sideslip, and yaw rate.

Furthermore, the controller's capability to initiate and maintain drifts in both directions and follow a trajectory is evaluated through simulations. The controller successfully initiates and maintains drifts in both directions, with the vehicle reaching steady-state values for equilibrium yaw rate, sideslip, and longitudinal velocity. The path followed closely aligns with the steady-state path within the first complete circle in both directions.

The chapter also presents the theoretical basis for the optimization method, employing the Lyapunov method to demonstrate asymptotic stability of the closed-loop system. Additionally, a controllability analysis illustrates the ability of the controller to access and control individual wheel torques to achieve desired state derivatives. Simulations further validate the controller's capability to drive the vehicle to its target state from various initial conditions.

Lastly, the controller's sensitivity to model parameters and noise is assessed. The robustness of the controller to parameter uncertainties in the vehicle model is demonstrated, showing minimal variation in steady-state yaw rate and sideslip, except for extreme mismatches in tire friction coefficients. Even under such extreme cases, the controller can effectively prevent the vehicle from spinning out without requiring driver intervention. Additionally, the controller's performance in the presence of input noise is demonstrated, further affirming its ability to maintain stable and precise drift behavior under challenging conditions.

In the subsequent chapter, the developed controller will be utilized in conjunction with the reference generator outlined in Chapter 4. The combined system aims to detect the driver's intention to initiate a drift, effectively trigger the drift, stabilize the vehicle in the desired drift state, and enable the vehicle to follow the trajectory indicated by the driver.

# 6

# Verification and Validation

## 6.1. IPG CarMaker Simulations

The study utilized the powerful and high-fidelity vehicle dynamic simulation software, IPG CarMaker, as a pivotal tool to validate the performance of the proposed controller. A comprehensive vehicle model of the Rimac Nevera, a high performance electric car with four independent wheel motors, was created within the CarMaker environment, incorporating intricate details of the car's physical characteristics, including its electric powertrain, suspension system, aerodynamics, and tire properties. By accurately replicating the vehicle's dynamics, the CarMaker-based model provided a realistic representation of the Rimac Nevera's behavior in virtual simulations. This integration allowed extensive controller experiments to be conducted, assessing the effectiveness and performance of the proposed control algorithm across various driving scenarios. The CarMaker-based Rimac Nevera model served as a robust and reliable platform for rigorously evaluating the controller's performance, leading to the validation and refinement of the control system.

### 6.1.1. Maneuvers and Results

The following maneuvers were employed to evaluate the control system:

1. Drifting along a constant radius of 30 m
2. Drifting through a section of a track

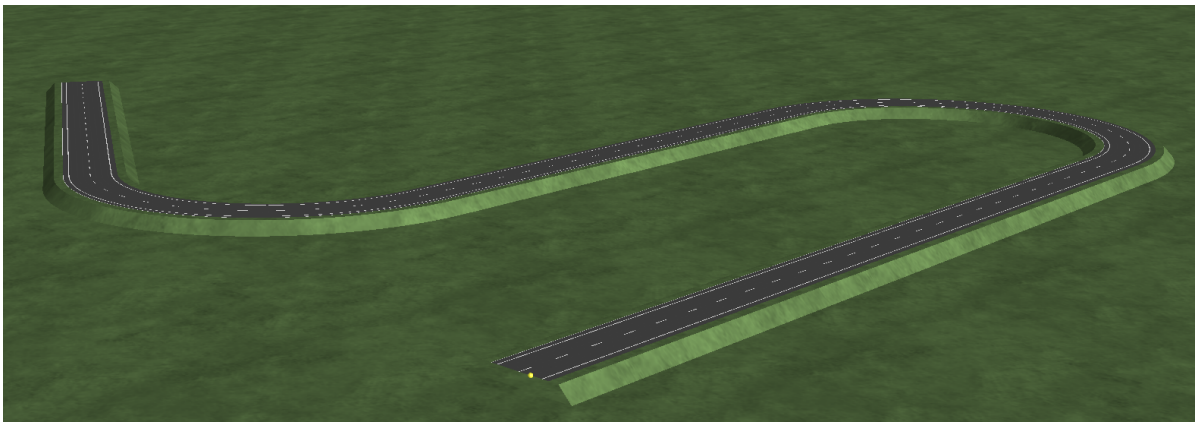

**Figure 6.1:** Track layout for simulation

To emulate human driving behavior and achieve the desired target speed, the IPGDriver feature inside IPG CarMaker was utilized to control steering, throttle, and brakes. The optimization problem

formulation from the Simulink model (5.3) was employed, with additional tuning for the proportional-integral-derivative (PID) controllers that calculate force and moment targets from the state targets.

### Constant Radius Simulation

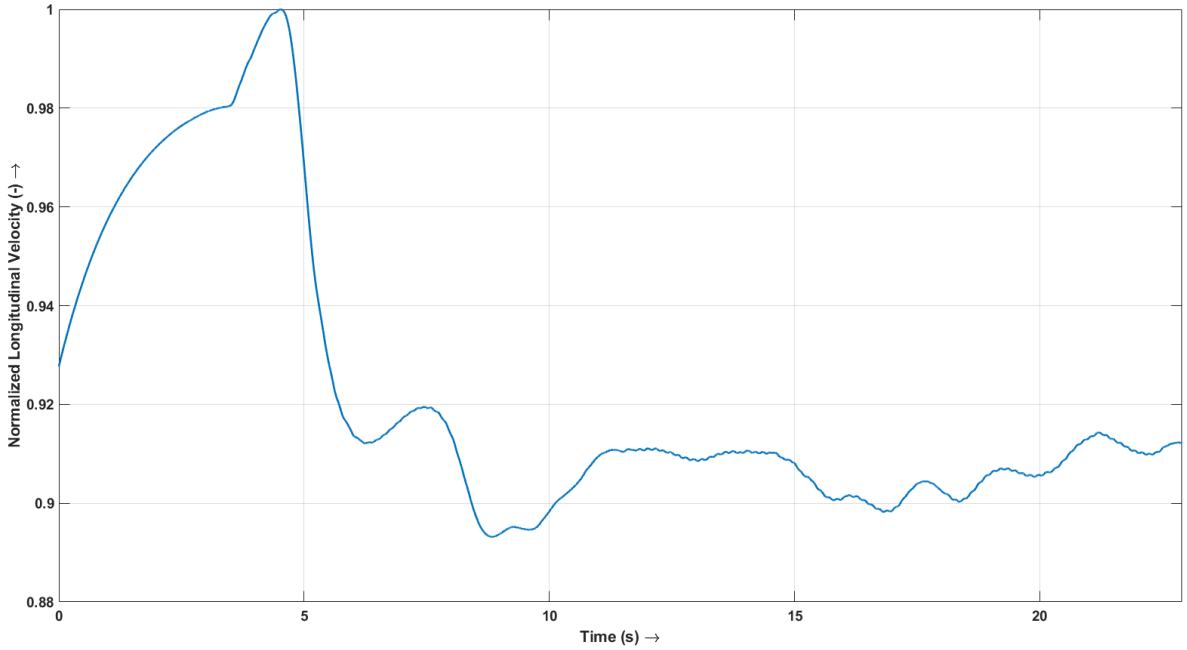


**Figure 6.2:** Result of simulation - longitudinal velocity

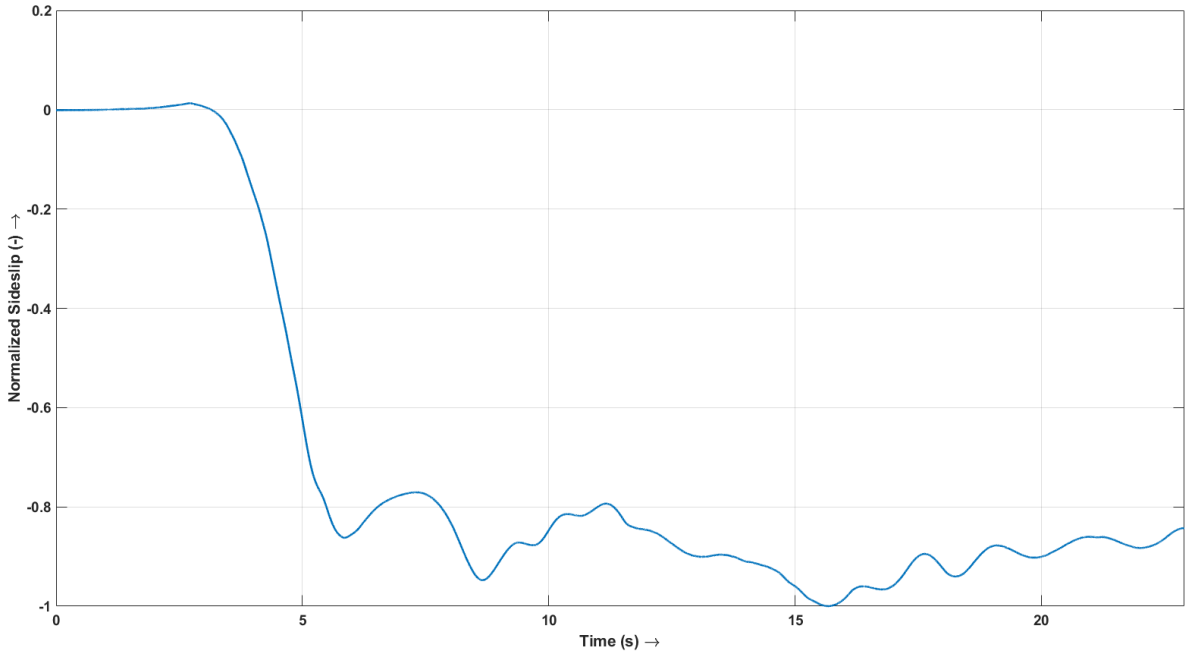


**Figure 6.3:** Result of simulation - sideslip

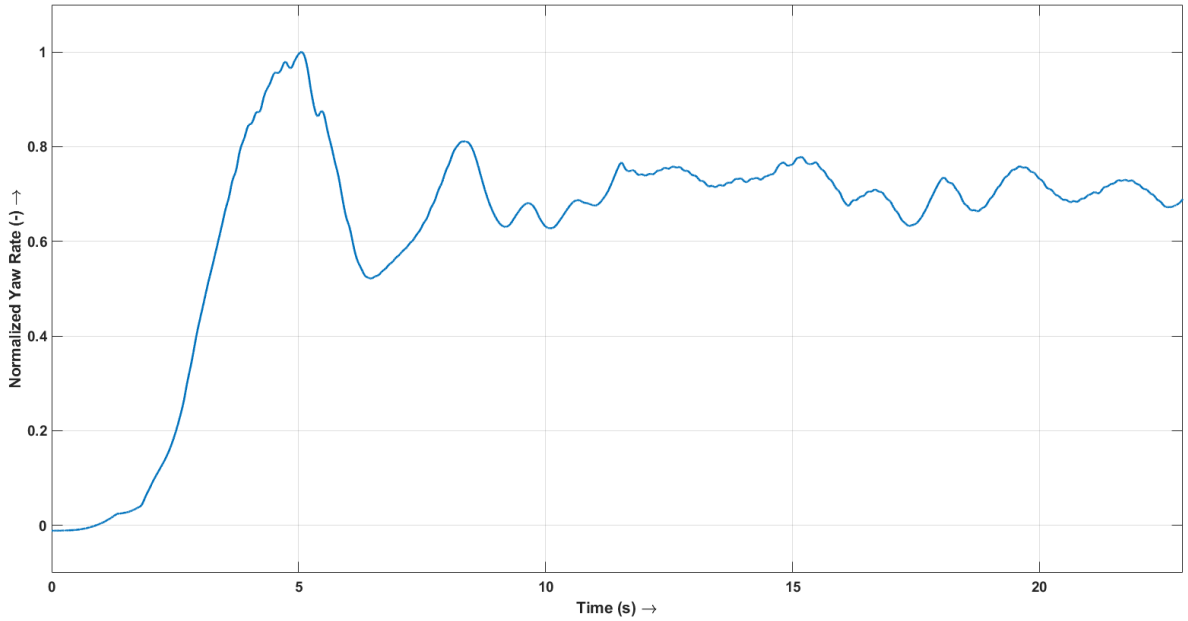


**Figure 6.4:** Result of simulation - yaw rate

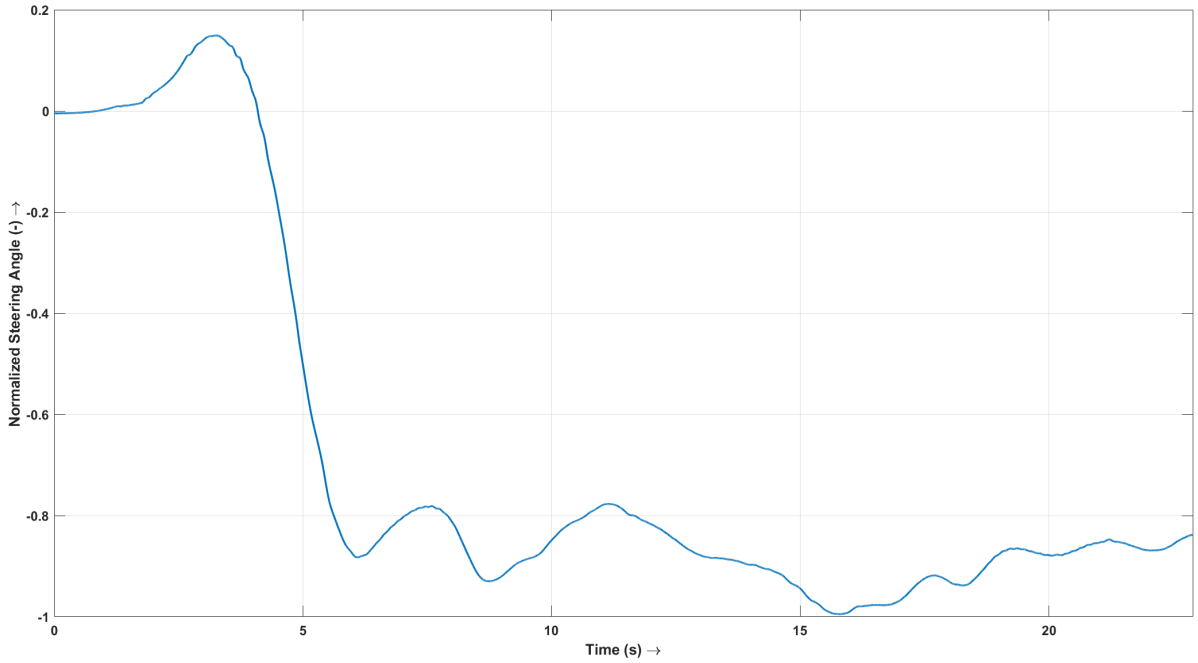


**Figure 6.5:** Result of simulation - steering angle

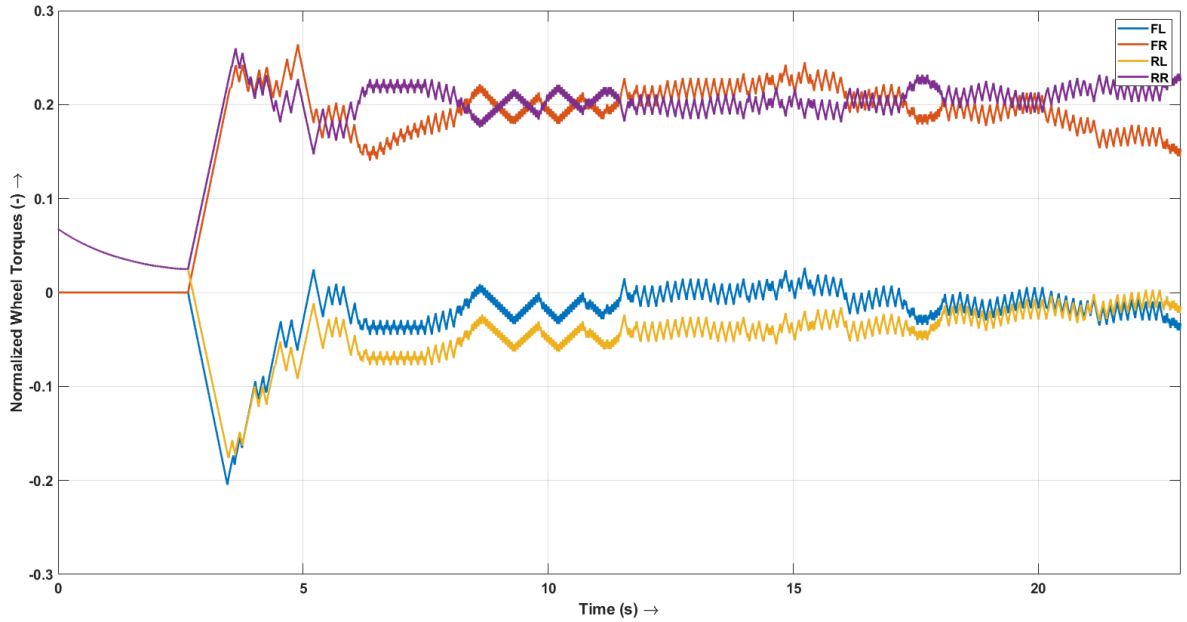


**Figure 6.6:** Result of simulation - wheel torques

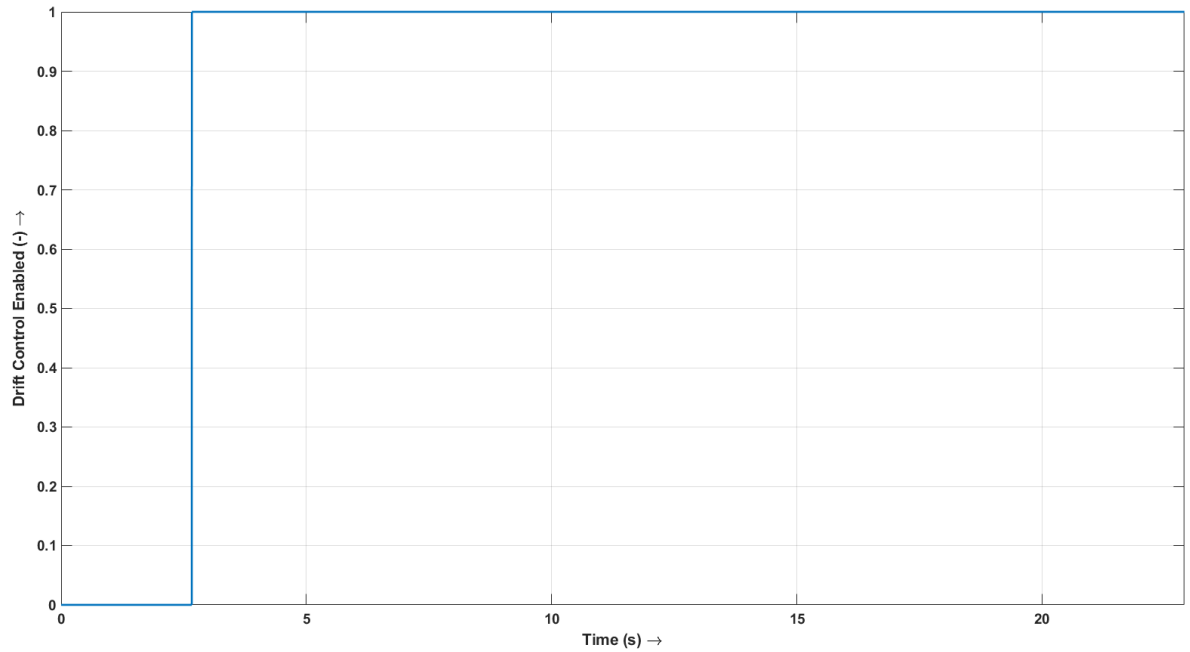


**Figure 6.7:** Result of simulation - drift enable

### Track Drift

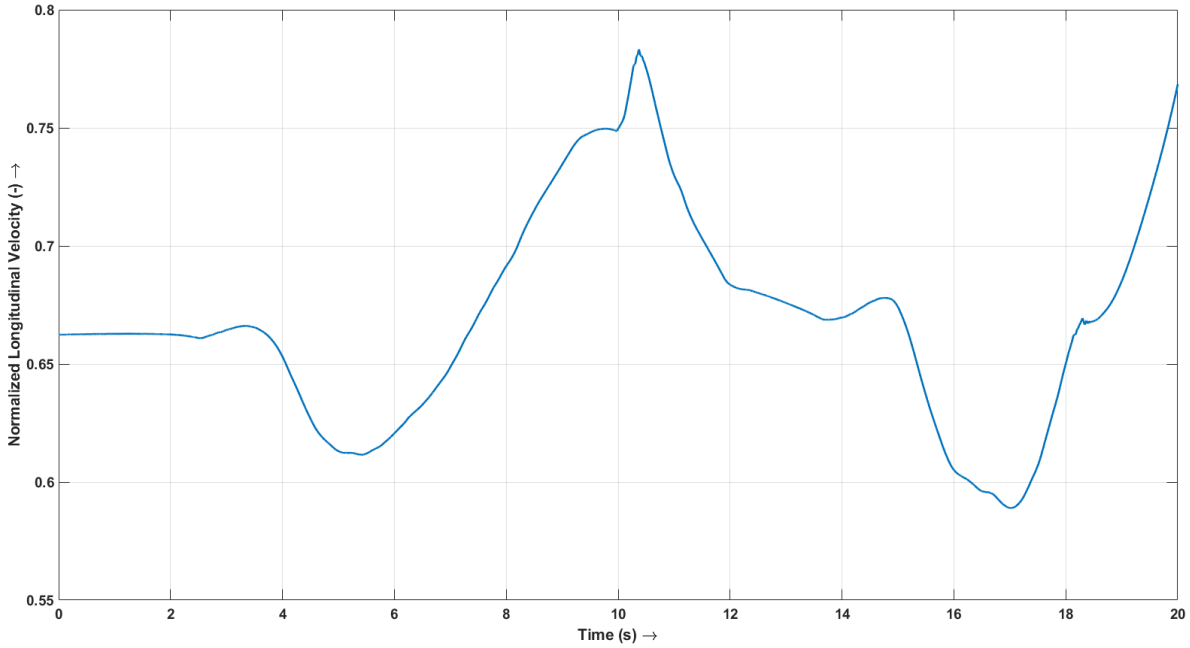


**Figure 6.8:** Result of simulation - longitudinal velocity

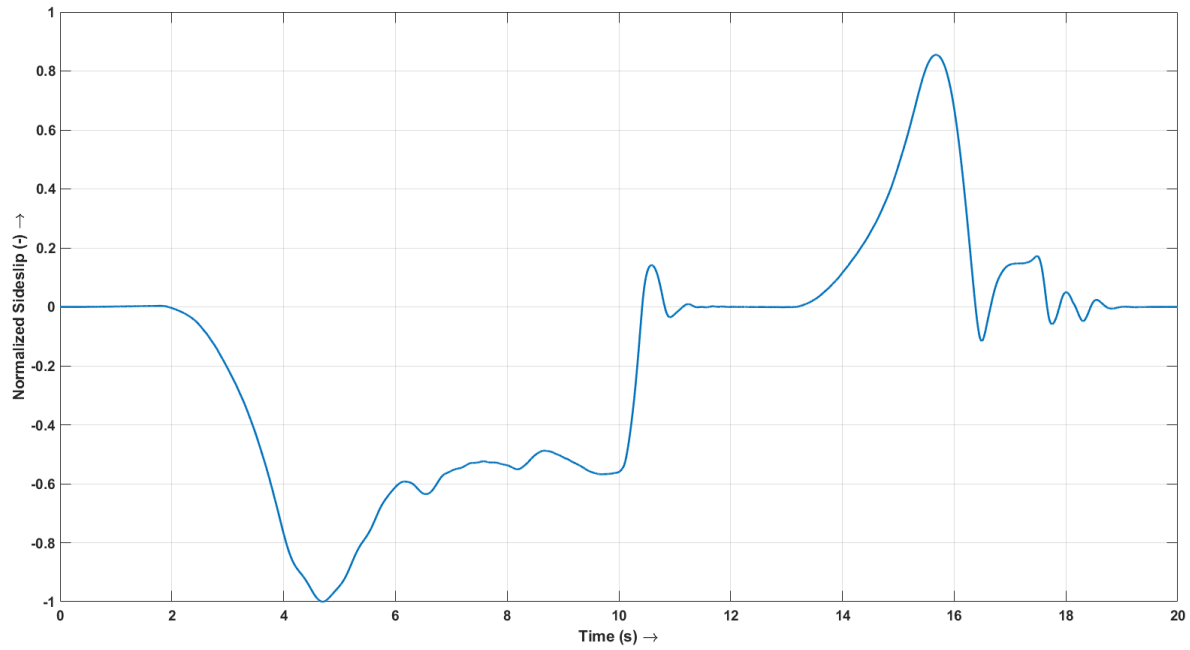


**Figure 6.9:** Result of simulation - sideslip

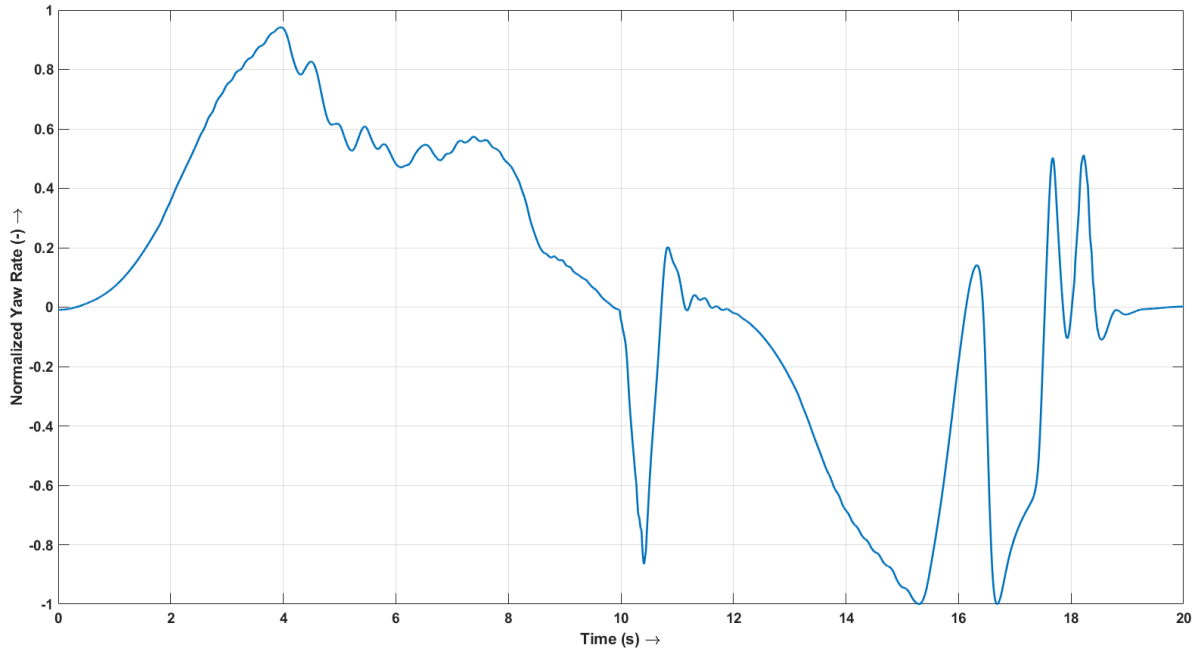


**Figure 6.10:** Result of simulation - yaw rate

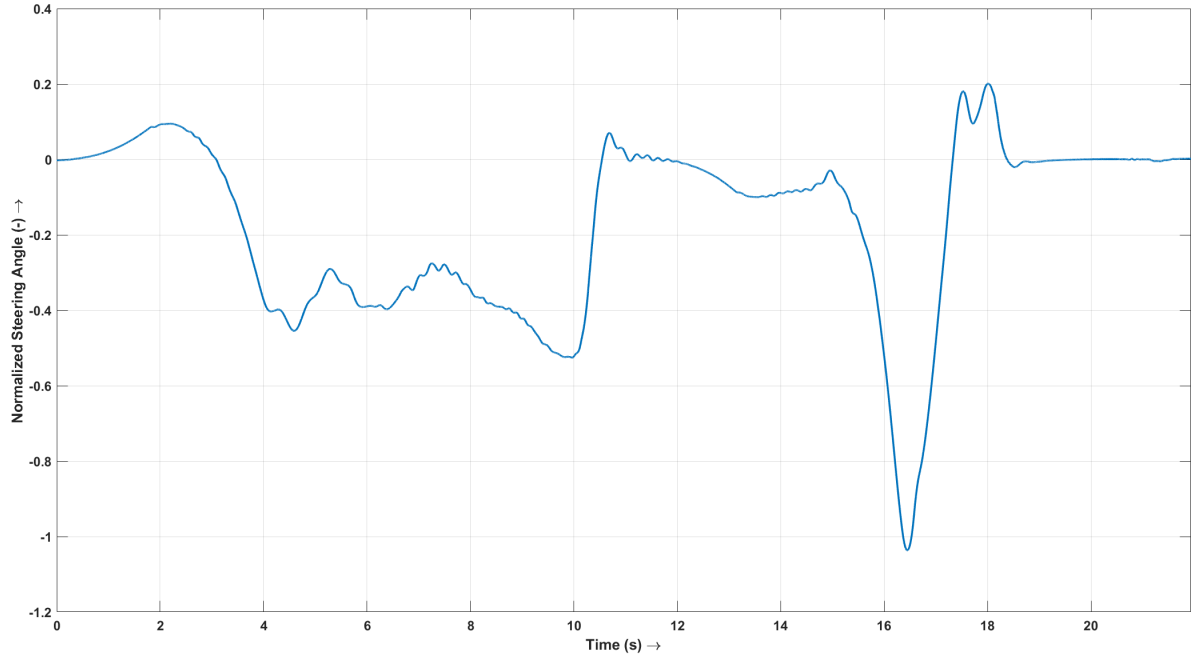


**Figure 6.11:** Result of simulation - steering angle

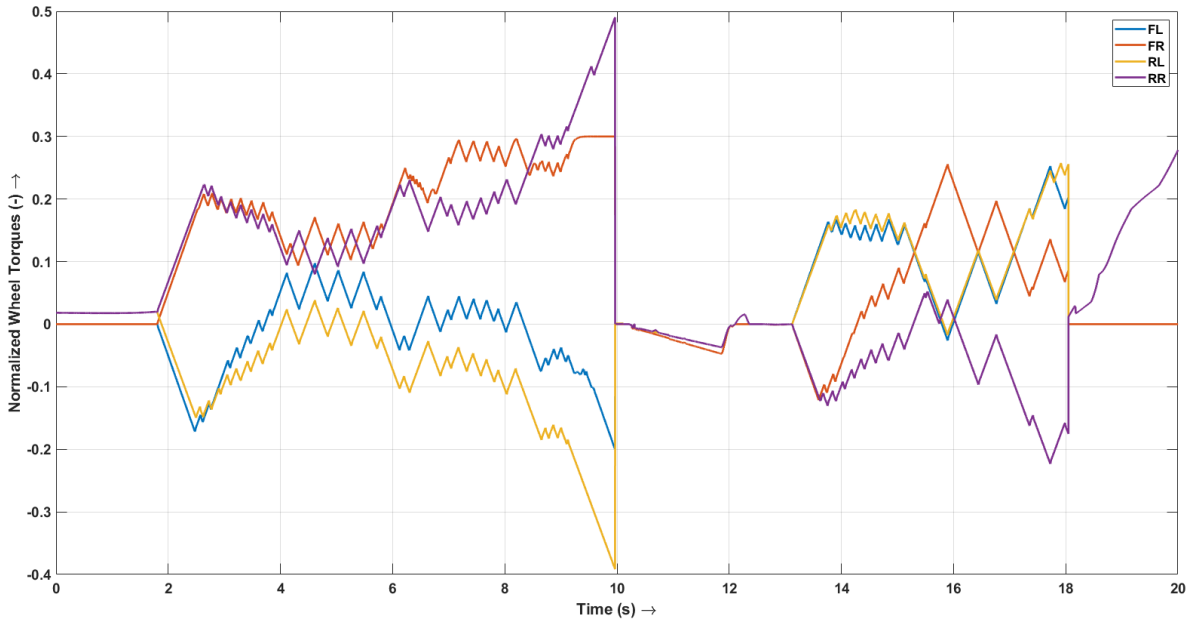


**Figure 6.12:** Result of simulation - wheel torques

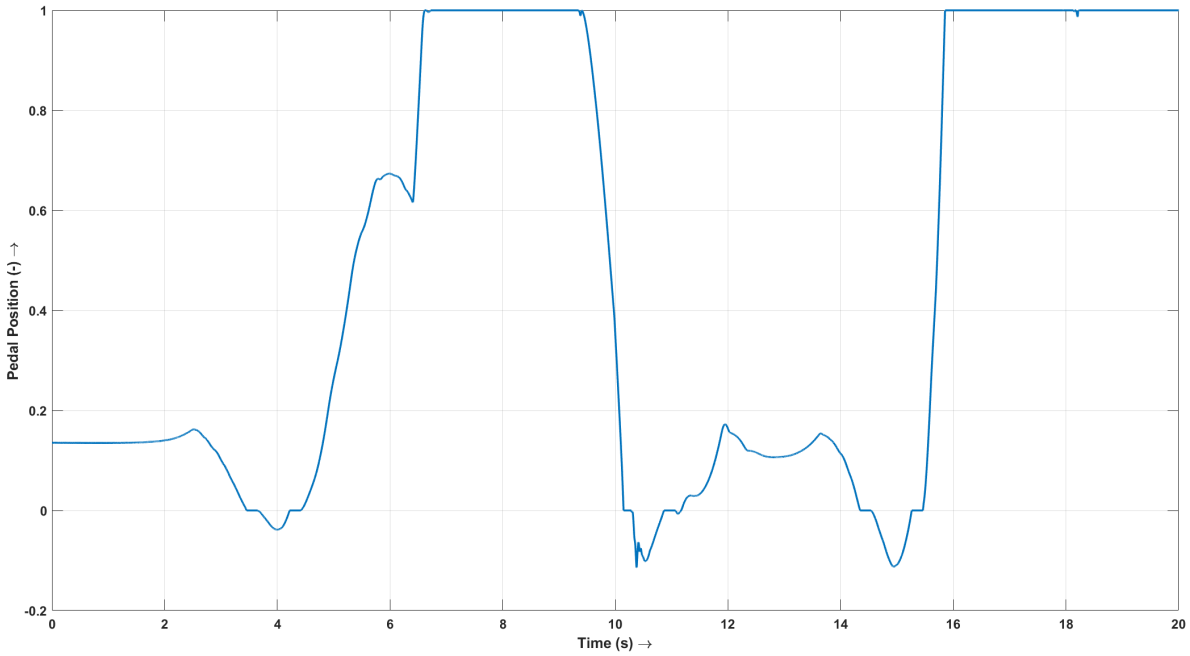


**Figure 6.13:** Result of simulation - pedal position

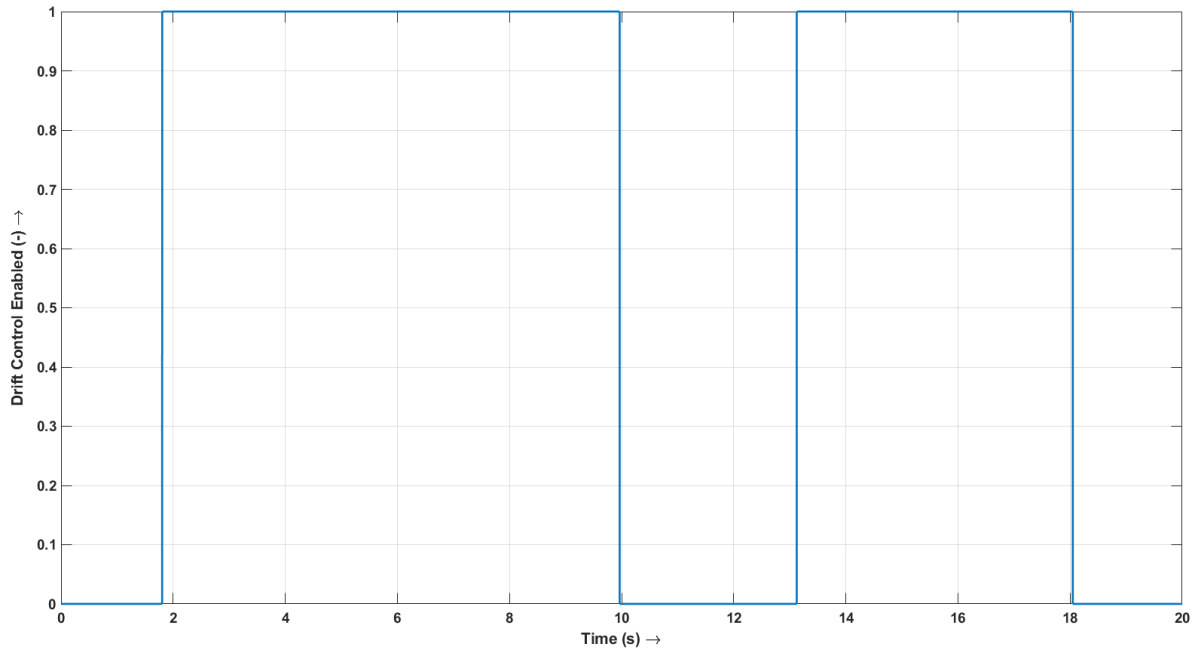


**Figure 6.14:** Result of simulation - drift enable

## 6.2. Discussion

The results from both scenarios show that the drift control system effectively initiates and maintains the vehicle's drift as per the driver's intentions. In the constant radius drift scenario, drift control is enabled at approximately $t = 2.5s$, when the driver starts to steer in the direction of the turn, to the left (positive) in this case, and the vehicle starts to develop yaw rate. Once the drift control is enabled, the torque vectoring system generates yaw moment in the direction of the turn, resulting in the vehicle sliding and developing sideslip. The vehicle maintains an approximate 20° sideslip throughout the simulation, with minimal steering interventions required from the driver to prevent the vehicle from spinning out. Furthermore, the standard deviation of the road wheel angle remains low at 1° once the vehicle reaches steady state, highlighting the effectiveness of the control strategy.

In the track drift simulation, the vehicle successfully drifts through both corners. It drifts along a left-hand corner, exits the drift, and drives straight. Then, it drifts along a right-hand corner, exits the drift, and returns to normal driving. Throughout both corners, the vehicle achieves a sideslip angle of approximately 20°, while enabling the simulation driver to precisely control the desired vehicle path. The drift mode is activated at around $t = 2s$ when the driver starts steering towards the left-hand corner. It is deactivated at approximately $t = 10s$ when the driver indicates the intention to accelerate onto the straight with a high throttle position (see figure 6.13). Later, the drift mode is reactivated around $t = 13s$ for the right-hand corner and then deactivated again at $t = 16s$ when the driver accelerates out of the corner. This showcases the effectiveness of the enable/disable mechanism, accurately capturing the driver's intent and allowing the torque vectoring system to control the vehicle accordingly during the drifts.

Overall, the IPG CarMaker simulations validate the proposed control algorithm's robustness and performance, making significant contributions to the refinement and validation of the control system.

# 7

# Conclusion

## 7.1. Summary

In this study, a comprehensive vehicle sideslip control system for driver-involved drifting scenarios was developed and evaluated. A seven-degree-of-freedom vehicle model was formulated to accurately capture the dynamics relevant to drift and wheel torque control. Real on-track data from drift maneuvers were utilized to identify essential tire parameters required to effectively represent the intricate drift dynamics.

Phase portrait analysis was conducted using the newly derived tire model, yielding valuable insights into the impact of different parameters and vehicle states on drift behavior. These insights, coupled with data from actual drift maneuvers, played a pivotal role in informing the generation of state targets. Furthermore, a module capable of detecting the driver's intent to drift and facilitating the enable/disable mechanism for the controller was implemented.

For the controller design, a model-based optimization scheme was employed. By utilizing PID controllers, target state derivatives were computed, which were subsequently utilized by the optimizer to allocate the four-wheel torques, aimed at achieving the desired targets. Through extensive simulations, successful demonstrations were made to show the controller's capability in initiating and stabilizing the vehicle in a drift state without requiring steering corrections from the driver. The controller's robustness to parameter uncertainties and noise was also thoroughly assessed.

Subsequently, the entire drift control system was subjected to evaluation in IPG CarMaker, a commercial vehicle dynamic simulation environment with a high fidelity vehicle model. The reference generator and the controller were assessed using two maneuvers: drifting along a constant radius circle and drifting along a section of a track. The system effectively identified the driver's intent to drift, initiated the drift, and subsequently stabilized the vehicle at the desired equilibrium.

## 7.2. Conclusions

This thesis aimed to develop an All-Wheel Torque Vectoring system for Driver-in-the-Loop Drifting, enabling drivers to safely and effectively perform drifting maneuvers while fully exploiting their vehicle's capabilities. The research objective was to design and evaluate a vehicle sideslip control system that incorporates driver inputs and intentions into the control process, achieving stable and controllable drift behavior.

The proposed control system utilized a reference generator to translate driver inputs into target vehicle states, and a controller that optimized torque allocation to each wheel to achieve the desired state during drifting. Through simulation-based assessments, the system's performance was evaluated in terms of maintaining target values for sideslip, velocity, and yaw rate during drift maneuvers, and its ability to track a specified trajectory using driver inputs while maintaining desired sideslip.

The research contributions can be summarized as follows:

1. The development of a robust reference generation methodology based on phase plane and logged data analysis, effectively translating driver inputs into meaningful state targets for the controller and ensuring precise control system activation.
2. The design of a controller using an optimization-based approach for all-wheel torque vectoring, which enabled the vehicle to maintain desired drift behavior while following specified trajectories accurately. This optimization-based approach also allows a similar problem formulation to be used for different vehicle architectures, such as front-wheel drive, rear-wheel drive and vehicles with differentials. By modifying the desired states within the Reference Generator, the controller can also serve as a stability control system, effectively preventing scenarios where the driver might lose control of the vehicle.
3. The demonstration of the controller's robustness to parameter uncertainties and noise, ensuring stable and reliable performance even under extreme conditions.
4. The successful integration of the driver into the control loop, allowing for a driver-involved drift control system that prioritizes driver experience and vehicle performance.

## 7.3. Future Work

Several promising avenues for future research and enhancements to the driver-involved drift control system can be explored to further improve its performance and expand its capabilities:

1. **Smooth Transition from Drift to Normal Driving**: One area of improvement involves addressing the abrupt vehicle movement observed when the drift control is disabled. To mitigate this issue, a smoother transition can be achieved by incorporating a mechanism to seamlessly switch from the drift controller to a conventional torque vectoring system when the driver disables drift control. This would ensure a more seamless and controlled shift in vehicle behavior, preventing sudden movements and enhancing overall safety.
2. **Transient Profile for Target Yaw Rate**: Instead of relying solely on steady-state targets for the controller, incorporating a transient profile for the target yaw rate based on driver inputs, such as a throttle blip, may offer a more natural and intuitive driving experience.
3. **Reducing Computational Complexity**: While the current optimization-based approach yields effective results, there is room for improving computational efficiency. Exploring faster optimization techniques or simplifying the vehicle and tire models could reduce the controller's computational complexity, making it more suitable for real-time implementation in practical driving scenarios.
4. **Real-world Testing and Validation**: Executing practical experiments involving skilled drivers executing drifting maneuvers would provide substantial empirical validation for the control system's performance. Real-world testing would enable the system to be evaluated under a broader range of conditions, further refining its performance and robustness.
5. **Advanced Human-Machine Interaction**: Investigating advanced human-machine interaction methodologies, such as haptic feedback or driver intention prediction using machine learning algorithms, could further enhance the driver's engagement and experience during drifting. By enabling seamless communication between the driver and the control system, the overall control experience can be elevated, resulting in more precise and intuitive vehicle behavior.

Exploring these future research directions will contribute to the continuous improvement and evolution of the driver-involved drift control system, paving the way for safer, more engaging, and highly controllable drifting experiences for performance vehicle enthusiasts.

# References


[1] Marco Baur and Luca Bascetta. “An experimentally validated lqr approach to autonomous drifting stabilization”. In: *2019 18th European Control Conference (ECC)* (2019), pp. 732–737.

[2] Ronnapee Chaichaowarat and Witaya Wannasuphoprasit. “Optimal control for steady state drifting of RWD vehicle”. In: *IFAC Proceedings Volumes* 46.21 (2013), pp. 824–830.

[3] Tim Cotgrove. *Vehicle motion control apparatus and method*. US Patent 9,296,424. March 29 2016.

[4] Kakan C Dey et al. “A review of communication, driver characteristics, and controls aspects of cooperative adaptive cruise control (CACC)”. In: *IEEE Transactions on Intelligent Transportation Systems* 17.2 (2015), pp. 491–509.

[5] Ziya Ercan et al. “Modeling, identification, and predictive control of a driver steering assistance system”. In: *IEEE Transactions on Human-Machine Systems* 47.5 (2017), pp. 700–710.

[6] Stephen M Erlien, Susumu Fujita, and Joseph Christian Gerdes. “Shared steering control using safe envelopes for obstacle avoidance and vehicle stability”. In: *IEEE Transactions on Intelligent Transportation Systems* 17.2 (2015), pp. 441–451.

[7] Tushar Goel, Jonathan Y Goh, and J Christian Gerdes. “Opening new dimensions: Vehicle motion planning and control using brakes while drifting”. In: *2020 IEEE Intelligent Vehicles Symposium (IV)* (2020), pp. 560–565.

[8] Jonathan Y Goh and J Christian Gerdes. “Simultaneous stabilization and tracking of basic automobile drifting trajectories”. In: *2016 IEEE Intelligent Vehicles Symposium (IV)* (2016), pp. 597–602.

[9] Jonathan Y Goh, T Goel, and J Christian Gerdes. “A controller for automated drifting along complex trajectories”. In: *14th International Symposium on Advanced Vehicle Control (AVEC 2018)* 7 (2018), pp. 1–6.

[10] Rami Y Hindiyeh and J Christian Gerdes. “A controller framework for autonomous drifting: Design, stability, and experimental validation”. In: *Journal of Dynamic Systems, Measurement, and Control* 136.5 (2014), p. 051015.

[11] Saeid Khosravani et al. “Development of a robust vehicle control with driver in the loop”. In: *2014 American Control Conference* (2014), pp. 3482–3487.

[12] Saeid Khosravani et al. “Torque-vectoring-based vehicle control robust to driver uncertainties”. In: *IEEE Transactions on Vehicular Technology* 64.8 (2014), pp. 3359–3367.

[13] Mauricio Marcano et al. “A review of shared control for automated vehicles: Theory and applications”. In: *IEEE Transactions on Human-Machine Systems* 50.6 (2020), pp. 475–491.

[14] Sina Milani, Hormoz Marzbani, and Reza N Jazar. “Vehicle drifting dynamics: discovery of new equilibria”. In: *Vehicle system dynamics* 60.6 (2022), pp. 1933–1958.

[15] Seungwuk Moon and Kyongsu Yi. “Human driving data-based design of a vehicle adaptive cruise control algorithm”. In: *Vehicle System Dynamics* 46.8 (2008), pp. 661–690.

[16] Hans Pacejka. *Tire and vehicle dynamics*. Elsevier, 2005.

[17] R. Rajamani. *Vehicle dynamics and control*. 2nd ed. Springer, 2012.

[18] Chouki Sentouh et al. “Toward a shared lateral control between driver and steering assist controller”. In: *IFAC Proceedings Volumes* 43.13 (2010), pp. 404–409.

[19] Efstathios Velenis. “FWD vehicle drifting control: The handbrake-cornering technique”. In: *2011 50th IEEE Conference on Decision and Control and European Control Conference* (2011), pp. 3258–3263.

[20] Efstathios Velenis, Emilio Frazzoli, and Panagiotis Tsiotras. “On steady-state cornering equilibria for wheeled vehicles with drift”. In: *Proceedings of the 48th IEEE Conference on Decision and Control (CDC) held jointly with 2009 28th Chinese Control Conference* (2009), pp. 3545–3550.

[21] Efstathios Velenis et al. “Steady-state drifting stabilization of RWD vehicles”. In: *Control Engineering Practice* 19.11 (2011), pp. 1363–1376.

[22] Michele Vignati, Edoardo Sabbioni, and Federico Cheli. “A torque vectoring control for enhancing vehicle performance in drifting”. In: *Electronics* 7.12 (2018), p. 394.

[23] Amedeo Visconti and Martino Cavanna. *Method for controlling the side slip angle of a rear-wheel drive vehicle when turning*. US Patent 8,463,498. June 11 2013.

[24] Christoph Voser, Rami Y Hindiyeh, and J Christian Gerdes. “Analysis and control of high sideslip manoeuvres”. In: *Vehicle System Dynamics* 48.S1 (2010), pp. 317–336.

[25] Jianqiang Wang et al. “An adaptive longitudinal driving assistance system based on driver characteristics”. In: *IEEE Transactions on Intelligent Transportation Systems* 14.1 (2012), pp. 1–12.

[26] Qiguang Wang et al. “A driver model–based direct yaw moment controller for in-wheel motor electric vehicles”. In: *Advances in Mechanical Engineering* 11.9 (2019), p. 1687814019877319.